UNIVERSIDADE FEDERAL DO CEARÁ

CENTRO DE TECNOLOGIA

DEPARTAMENTO DE ENGENHARIA DE TELEINFORMÁTICA

PROGRAMA DE PÓS-GRADUAÇÃO EM ENGENHARIA DE TELEINFORMÁTICA

CHRISTOPH ENNEKING

INTRA- AND INTERSYSTEM INTERFERENCE IN GNSS: PERFORMANCE MODELS AND SIGNAL DESIGN

FORTALEZA

2020

CHRISTOPH ENNEKING

INTRA- AND INTERSYSTEM INTERFERENCE IN GNSS: PERFORMANCE MODELS AND SIGNAL DESIGN

Tese apresentada ao Curso de Doutorado em Engenharia de Teleinformática do Programa de Pós-Graduação em Engenharia de Teleinformática do Centro de Tecnologia da Universidade Federal do Ceará, como requisito parcial à obtenção do título de doutor em Engenharia de Teleinformática. Área de Concentração: Sinais e Sistemas

Orientador: Prof. Felix Dieter Antreich
Coorientador: Prof. André Lima Férrer de Almeida

FORTALEZA

2020

CHRISTOPH ENNEKING

INTRA- AND INTERSYSTEM INTERFERENCE IN GNSS: PERFORMANCE MODELS AND SIGNAL DESIGN

Thesis defended at the Teleinformatics Engineering Doctorate Program at the Teleinformatics Engineering Post-Graduate Program of the Technology Center at the Federal University of Ceará, as a requirement to obtain the doctor degree in Teleinformatics Engineering. Concentration Area: Signals and Systems.

Approved on: December 22, 2020

EXAMINING COMMITTEE

Prof. Felix Dieter Antreich (Advisor)
Aeronautics Institute of Technology (ITA), Brazil

Prof. André Lima Férrer de Almeida (Co-Advisor)
Federal University of Ceará (UFC), Brazil

Prof. Renato Machado
Aeronautics Institute of Technology (ITA), Brazil

Prof. Dr.-Ing. habil. Michael Meurer
RWTH Aachen University, Germany

Prof. Rafael Timóteo de Sousa Júnior
University of Brasilia (UnB), Brazil

Prof. Charles Casimiro Cavalcante
Federal University of Ceará (UFC), Brazil

To my parents, Kornelia and Ludger

ACKNOWLEDGEMENTS

I would like to express my deepest gratitude to Prof. Felix Antreich. Our collaboration began almost ten years ago during my undergraduate studies at TU Munich, and continued at DLR. He has been (alternately) mentor, supervisor and colleague for me. He now lives in distant Brazil, but I can still count on his advice, hospitality and friendship anytime. This dissertation project was on the brink more than once (not least because of my inability to meet deadlines), but Felix has always given me confidence.

I would also like to thank my co-supervisor Prof. André Lima Férrer de Almeida for his help with my studies and for being an extremely helpful contact person on the part of the UFC.

Moreover, I would like to thank Prof. Michael Meurer, Steffen Thölert, and Andriy Konovaltsev very much for supporting me in my doctoral project over the years from DLR side. In particular, they kept my back free from arduous project work during important phases of my doctorate. I am also very grateful to all my colleagues at DLR (including those who have long gone elsewhere) for their team spirit, their friendship, coffee capsules, and for teaching me so much.

The guest semester at UFC Fortaleza was a very special personal experience for me. To Thiago, Gil, Rafael, and all of my dear Brazilian friends, who have helped me so much to find my way there: Obrigado por tudo!

Writing a doctoral thesis is nerve-wracking and sometimes makes you an uncomfortable fellow - especially on the last few meters. So I'm all the more grateful for my friends in Munich, who show me that there are other things in life than work. I would particularly like to thank my flatmate Lukas (for all the meat and mead we've shared, and for his help with unruly LaTeX templates) and my girlfriend Tabea (for her incredible patience that I have strained so much). Finally the stress is over!

Above all, I thank my parents Kornelia and Ludger, and my brother Florian. When things sometimes got over my head, they have always been my support and refuge.

RESUMO

O sistema Europeu Galileo, o sistema de Posicionamento Global Americano (GPS, do inglês Global Positioning System) e outros sistemas globais de navegação por satélite (GNSS, do inglês global navigation satellite systems) transmitem sinais de espectro de difusão de sequência direta do espaço, permitindo que os receptores na Terra calculem sua posição, velocidade e tempo (PVT) com base no princípio da trilateração em pseudo-faixa. No entanto, como vários satélites e sistemas transmitem sinais simultaneamente dentro de bandas de frequência compartilhadas, a interferência de acesso múltiplo (MAI, do inglês multiple access interference) na forma de interferência intra- e intersistema pode afetar o processamento do sinal no receptor. Para computar uma pseudo-faixa, o receptor deve estimar os parâmetros de sincronização do respectivo sinal com alta resolução. Esta sincronização é realizada em uma abordagem de duas etapas, consistindo na aquisição de sinal (detecção) e estimação fina de parâmetros. A maioria dos GNSS depende de acesso múltiplo por divisão de código de sequência direta assíncrona (DS-CDMA), atribuindo diferentes códigos de ruído pseudo-aleatório (PRN, do inglês pseudorandom noise) a cada satélite. O esquema de acesso múltiplo mantém um nível controlado de MAI e de desempenho de estimativa de parâmetro, que precisa ser cuidadosamente modelado antes de lançar novos sinais ou aumentar os níveis de potência de transmissão. A International Telecommunications Union (ITU) regulamenta que a compatibilidade de radiofrequência (RFC, do inglês radio frequency compatibility) de sistemas, satélites e sinais dentro das bandas de radionavegação deve ser garantida, o que significa que o desempenho do receptor não deve ser prejudicado significativamente. Os modelos convencionais de desempenho do receptor são baseados no coeficiente de separação espectral entre o sinal desejado e o de interferência, e principalmente se baseiam na idealização de que os sinais GNSS são estacionários no sentido amplo (WSS), processos aleatórios gaussianos circularmente simétricos. Neste trabalho, propomos modelos aperfeiçoados de desempenho de estimativa grossa e fina de parâmetros de sincronização, levando em consideração a propriedade cicloestacionária de sentido amplo dos sinais e sua não circularidade. Isso é de particular interesse em relação à recente tendência de projeto de sinal para novos sinais coarse/acquisition (C/A) com códigos PRN curtos, que são especialmente vulneráveis à MAI, mas muito atraentes para o grupo de dispositivos eletrônicos habilitados para GNSS do mercado de massa. Em última análise, nosso modelo de desempenho permite que o designer de sinal C/A minimize o comprimento do código PRN enquanto garante uma determinada restrição de desempenho de aquisição. Além disso, no que diz respeito ao RFC de um número crescente de sistemas de navegação, satélites

e sinais, nossos modelos detalhados para efeitos de interferência em equipamentos de uso em massa permitirão um uso mais eficiente do espectro de radiofrequência disponível.

Palavras-chave: Sistema Global de Navegação por Satélite. Ruído pseudo-aleatório. Interferência de acesso múltiplo. Sincronização. Compatibilidade de radiofrequência.

ABSTRACT

The European Galileo, the American Global Positioning System (GPS), and other global navigation satellite systems (GNSSs) transmit direct-sequence spread spectrum (DSSS) signals from space, allowing receivers on Earth to compute their position, velocity, and time (PVT) based on the principle of pseudorange trilateration. However, as multiple satellites and systems transmit signals simultaneously within shared frequency bands, multiple access interference (MAI) in the form of intra- and intersystem interference can affect signal processing at the receiver. To compute a pseudorange, the receiver must estimate synchronization parameters of the respective signal with high resolution. This synchronization is performed in a two-step approach, consisting of signal acquisition (detection) and fine parameter estimation. Most GNSSs rely on asynchronous direct-sequence code-division multiple access (DS-CDMA), assigning different pseudorandom noise (PRN) code to each satellite. This multiple access scheme involves a controlled level of MAI degrading acquisition and parameter estimation performance, which needs to be carefully modeled before launching new signals or raising transmit power levels. The International Telecommunications Union (ITU) regulates that radio frequency compatibility (RFC) of systems, satellites and signals within the radionavigation frequency bands must be ensured, meaning that receiver performance must not be harmed significantly. Conventional receiver performance models are based on the spectral separation coefficient (SSC) between desired and interfering signal, and mostly rely on the idealization that GNSS signals are wide-sense stationary (WSS), circularly-symmetric Gaussian (CSG) random processes. In this work, we propose refined models for performance of coarse and fine estimation of synchronization parameters, taking into account the signals' wide-sense cyclostationary (WSCS) property and their non-circularity. This is of particular interest in light of the recent signal design trend towards novel coarse/acquisition (C/A) signals with short PRN codes, which are especially vulnerable to MAI but very attractive for the group of mass-market GNSS-enabled electronic devices. Ultimately, our performance model enables the C/A signal designer to minimize the PRN code length while ensuring a given acquisition performance constraint. Moreover, with regard to RFC of an increasing number of navigation systems, satellites, and signals, our detailed models for interference effects on user equipment will allow to make more efficient use of the available radio frequency spectrum.

Keywords: Global Navigation Satellite Systems. Pseudorandom Noise. Multiple Access Interference. Synchronization. Radio Frequency Compatibility.

LIST OF FIGURES

LIST OF TABLES

LIST OF ABBREVIATIONS AND ACRONYMS

C/N_0	carrier-to-noise density ratio
A-GNSS	assisted GNSS
AltBOC	alternative BOC
AWGN	additive white Gaussian noise
BOC	binary offset carrier
BPF	bin probability of false alarm
BPSK	binary phase-shift keying
C/A	coarse/acquisition
CBOC	composite BOC
CDF	cumulative distribution function
CGA	conditional Gaussian approximation
CS	Commercial Service
CSG	circularly-symmetric Gaussian
DS-CDMA	direct-sequence code-division multiple access
DSSS	direct-sequence spread spectrum
FDMA	frequency-division multiple access
FEC	forward error correction
GLONASS	Globalnaya Navigatsionnaya Sputnikovaya Sistema
GNSS	global navigation satellite system
GPD	global probability of detection
GPF	global probability of false alarm
GPS	Global Positioning System
i.i.d.	independent and identically distributed
IC	integrated circuit
IGA	improved Gaussian approximation
IoT	internet of things
ITU	International Telecommunications Union
L1 C/A	Link One Coarse/Acquisition
L1C	Link One (New) Civil
L1OF	Link One OS FDMA
LDPC	low-density parity check codes

MAI	multiple access interference
MAI-A	intrasystem MAI, self-interference
MBOC	multiplexed BOC
MEO	medium earth orbit
NTS-2	Navigation Technology Satellite Two
OBPSK	offset BPSK
OS	Open Service
PDF	probability density function
PRN	pseudorandom noise
PRS	Public Regulated Service
PSD	power spectral density
PSWF	prolate spheroidal wave functions
PVT	position, velocity, and time
QPSK	quaternary phase-shift keying
R&D	research and development
REC	rectangular
RFC	radio frequency compatibility
RMSE	root mean squared error
RNSS	radionavigation-satellite system
ROC	receiver operating characteristic
RRC	root raised cosine
SA	Selective Availability
SGA	standard Gaussian approximation
SINR	signal-to-interference-pluse-noise ratio
SIR	signal-to-interference ratio
SNR	signal-to-noise ratio
SOI	signal of interest
SSC	spectral separation coefficient
SSC-D	deterministic refined SSC
SSC-R	randomized refined SSC
TTFF	time-to-first-fix
WSCS	wide-sense cyclostationary
WSS	wide-sense stationary

NOTATION

x	scalar
$\boldsymbol{x}$	vector
$\mathbb{R}$	set of real numbers
$\mathbb{C}$	set of complex numbers
$(\cdot)^*$	complex conjugate
$(\cdot)^T$	transpose
$\mathrm{E}[\,\cdot\,]$	statistical expectation
$\mathrm{Var}[\,\cdot\,]$	statistical variance
$\lfloor \cdot \rfloor$	floor operation
$\mathcal{O}(\cdot)$	big-O notation
j	imaginary unit $\sqrt{-1}$
$\delta(\cdot)$	Dirac delta distribution
$\delta[\,\cdot\,]$	discrete unit sample function (Kronecker delta)
$Q(\cdot)$	Marcum Q-function

CONTENTS

1 INTRODUCTION

1.1 Overview of GNSS signals: a brief history

We begin with an introduction to global navigation satellite system (GNSS) signals. It is instructive to do this in the form of a historic overview, distinguishing between signal generations.

1.1.1 First-generation signals (1977-2000)

On June 23, 1977, an American satellite with the plain name Navigation Technology Satellite Two (NTS-2) reached medium earth orbit (MEO) at 20200 km above the Earth's surface and began broadcasting pseudorandom noise (PRN) (EASTON; BUISSON; MCCASKILL, 1978; PARKINSON; POWERS, 2010) at a radio frequency. This event marks a milestone for more than one success story. NTS-2 was the prototype satellite of the Global Positioning System (GPS), a system which today is used by an estimated 4 billion devices for commercial, scientific, and military applications (COLBURN, 2020) − its success story is well-known. By contrast, the success story of the PRN signal itself is less known and perhaps even more surprising.

The name of the signal is Link One Coarse/Acquisition (L1 C/A)[1]. Since that first transmission in 1977, it has been continuously serving as an interface between the *GPS space segment* and the *GPS user segment*, and has been broadcast by several successive generations of GPS satellites. Unlike the satellites, it has remained virtually unchanged from its original design (SPILKER; NATALI; FITZGERALD, 1974; SPILKER, 1978), and is still unarguably the most used GPS signal (VAN DIGGELEN, 2014). It is a direct-sequence spread spectrum (DSSS) signal and can be described as the product of three components, as illustrated in Fig. 1.1:

1. a 50 Hz data stream, providing a reference for time and satellite orbit;
2. a PRN spreading code of 1023 chips, repeating every 1 ms;
3. a sinusoid at the carrier frequency 1575.42 MHz.

In the terminology of (PROAKIS, 2001), this signal uses a binary phase-shift keying (BPSK) alphabet for data and spreading code, and a rectangular chip pulse. Choosing the class of DSSS signals for GPS had a number of reasons:

- Radio signals can be used to estimate the satellite-to-user propagation delay. The tiered DSSS signal structure allows various degrees of estimation accuracy (time reference,

[1] Originally, C/A also referred to "clear/acquisition," indicating that this signal was transmitted "in the clear," i.e., unencrypted (SPILKER, 1978).

Figure 1.1 – Signal structure of GPS L1 C/A (data, code, carrier).

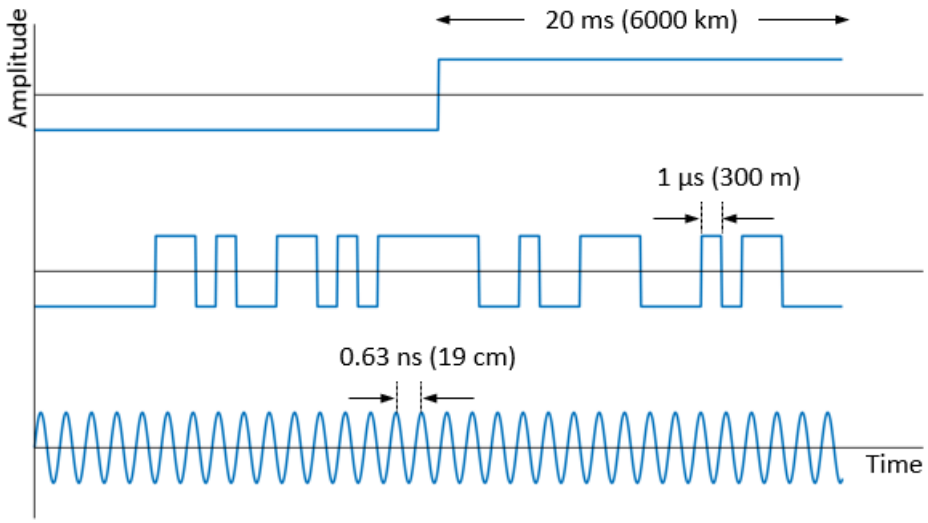

code-phase, carrier-phase), remotely comparable to a ruler with scales of finer and finer granularity to measure distances. Estimating the delay of signals from at least four in-view satellites (and having the satellites equipped with very accurate clocks), the principle of *pseudorange trilateration/multilateration* can be exploited to calculate the user's position, velocity, and time (PVT) (MISRA; ENGE, 2011).

- A different PRN code can be assigned to each satellite, so that simultaneous and asynchronous reception of multiple satellite signals centered around the same carrier frequency does not lead to intolerable levels of multiple access interference (MAI). This form of sharing the same transmission medium is called direct-sequence code-division multiple access (DS-CDMA). L1 C/A uses a set of Gold codes with fair cross-correlation properties (GOLD, 1967).
- As the PRN code is transmitted with a chipping rate of 1.023 Mchips per second, signal power is spread over the frequency domain. Therefore, the signal is (to a certain degree) robust to other kinds of radio frequency interference.

Another GPS signal transmitted from the very beginning is the P-code signal on the L1 and L2 carrier frequencies (1575.42 MHz and 1227.6 MHz, respectively) (SPILKER, 1978). While this is also a DS-CDMA signal, it uses a ten times higher chipping rate and considerably longer PRN code than L1 C/A. It is an encrypted signal and has been reserved for authorized/military use. L1 C/A, originally intended to facilitate acquisition of the P-code, was made available for civilian use in 1983, but the US military insisted on the signal being artificially degraded by Selective Availability (SA) for national security reasons (BONNOR, 2012).

During the 1970s, the Soviet Union conceived the Globalnaya Navigatsionnaya

Sputnikovaya Sistema (GLONASS), whose first satellites were launched on October 12, 1982 (BONNOR, 2012). Similarly to GPS, albeit with discontinuities in the 1990s, GLONASS has been offering an unencrpyted signal known as L1OF (TEUNISSEN; MONTENBRUCK, 2017) (in addition to its military signals). Like L1 C/A, L1OF is a DSSS signal with a 50 Hz data link, but all satellites use the same PRN code consisting of 511 chips. Rather than DS-CDMA, L1OF uses frequency-division multiple access (FDMA) with 15 channels spanning either side from 1602.0 MHz. The generic term GNSS established itself for satellite systems which provide autonomous geolocation and timing services anywhere on Earth at any time.

As both GPS and GLONASS declared full operational capability in 1995 (BONNOR, 2012), official performance standards were released to commit to the signal structure, received power levels, and other parameters of L1 C/A (GLOBAL..., 1993) and L1OF (GLONASS..., 1995), respectively. In 2000, the United States government discontinued SA, acknowledging the important role of GPS in many applications such as air traffic management, land surveying, mining, or transportation.

1.1.2 Second-generation signals (2000-2020)

The following decade saw an unprecedented surge of research and development (R&D) in GNSS signal design (SCHWEIKERT; WOERZ, 1998; SPILKER; ORR, 1998; SCHWEIKERT *et al.*, 2000; BETZ, 2001a; HEIN *et al.*, 2001; FONTANA *et al.*, 2001; RIES *et al.*, 2003; HUDNUT; TITUS, 2004; QUINLAN *et al.*, 2004; HEIN *et al.*, 2006; WALLNER *et al.*, 2007; SHANMUGAM *et al.*, 2008; WALLNER *et al.*, 2008; DAFESH; CAHN, 2009; YAO; LU; FENG, 2010b; ANTREICH; NOSSEK, 2011; YAO; ZHANG; LU, 2016). This was due to modernization plans for GPS and GLONASS, and due to Europe's and China's plans to launch their own GNSS *Galileo* and *Beidou* (BONNOR, 2012), targeting prominent applications such as aircraft guidance, remote farming, or the synchronization of power grids. The R&D activities, along with multilateral negotiations (AGREEMENT..., 2004) and new frequency allocations for radionavigation (ITU, 2000), paved the way for a series of modernized (or second-generation) signals (EUROPEAN..., 2016; BeiDou..., 2017a; BeiDou..., 2017b; BeiDou..., 2018; BeiDou..., 2020; NAVSTAR..., 2020b; NAVSTAR..., 2020a; NAVSTAR..., 2020c). Satellites capable of transmitting modernized signals were launched from 2005 onwards, and are still being inserted into the constellations today. Beidou and Galileo reached full operational capability with 24 MEO satellites in 2020. All GPS and GLONASS satellites continue to broadcast L1 C/A and

Figure 1.2 – Overview of GNSS signals in space as of 2020. The power spectral density (PSD) is shown qualitatively as a function of frequency, where in-phase and quadrature components are shown separately for the sake of clarity. Legacy signals: L1 C/A; L1OF, L2OF. Modernized signals: L1C, L2C, L5; L1OC, L2OC, L3OC; E1 OS, E6 CS, E5a, E5b; B1C, B3I, B2a, B2b. Authorized/military signals: M-Code, P-Code; L1SF, L1SC, L2SF, L2SC; E1 PRS, E6 PRS; B3, B3-A. (Courtesy of Orolia)

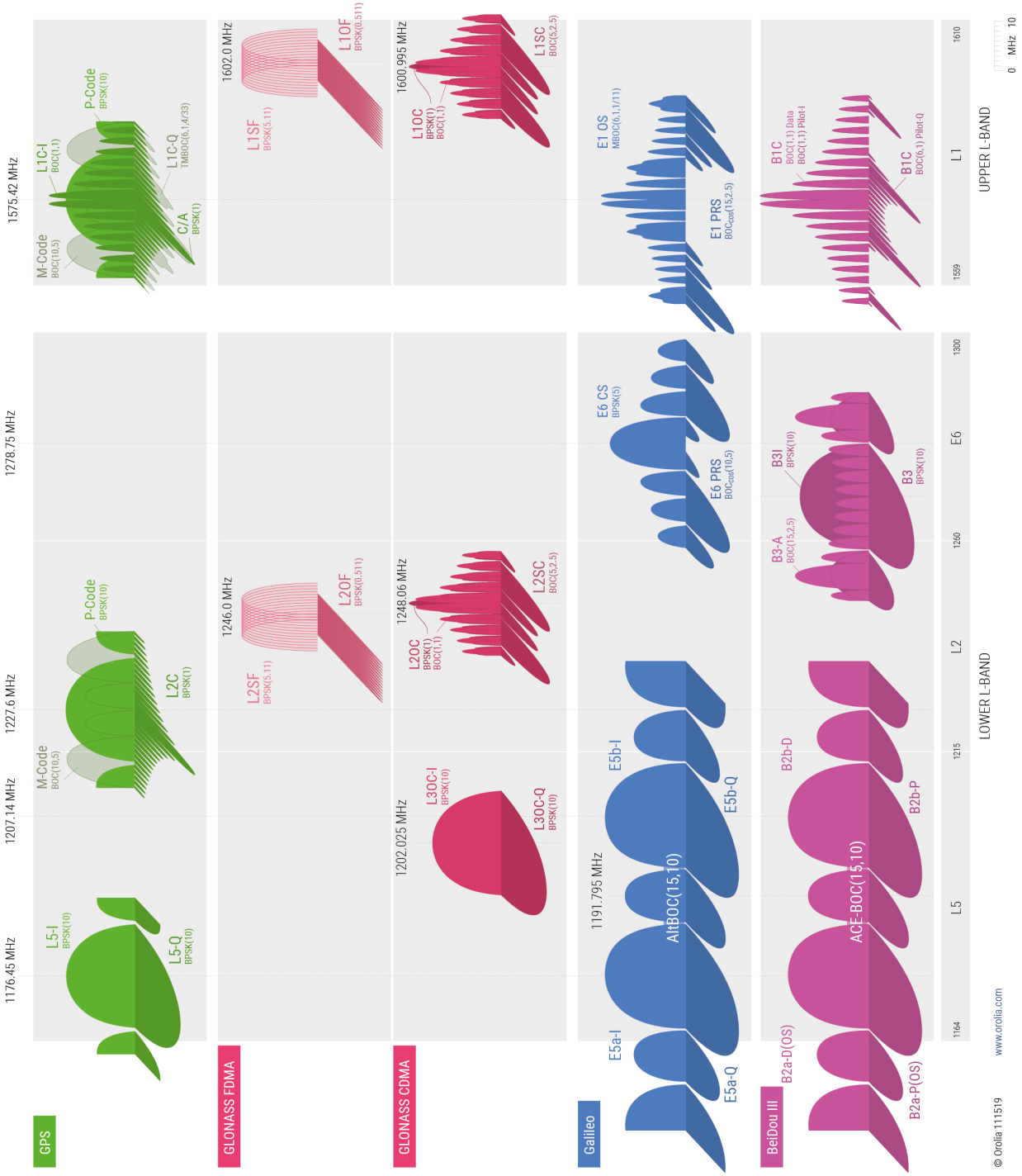

L1OF, which became known as legacy signals. However, L1 C/A was believed by some to be taken out of service in the long run (HUDNUT; TITUS, 2004).

An overview of all currently transmitted GNSS signals and their frequency assignments is given in Fig. 1.2. Across all four GNSSs, the portfolios of modernized signals show many characteristic communalities:

- All systems provide modernized signals for civil use on two or more carrier frequencies, including at least one "narrowband" signal (1.023 MHz chipping rate) in the upper L-band and one "wideband" signal (10.23 MHz chipping rate) in the lower L-band, as illustrated in Fig. 1.2. *Dual-frequency* receivers can compensate the frequency-dependent ionospheric signal propagation delay (TEUNISSEN; MONTENBRUCK, 2017). In addition, various authorized signals, such as the Public Regulated Service (PRS), are provided.
- All system operators (eventually also GLONASS (GLONASS…, 2016)) decided to use DS-CDMA as a means to share the same frequency bands among satellites and systems. This multiple access strategy moderates the MAI not only among satellites of the same system (*intrasystem interference*) but also among satellites of different systems (*intersystem interference*).
- PRN code lengths have increased significantly as compared with L1 C/A and L1OF. Among all signals in Fig. 1.2, the Galileo E1 Open Service (OS) uses the shortest code of length 4092, which is four times the L1 C/A code length. The intention behind such long codes was to achieve lower cross-correlation between signals, such that intra- and intersystem interference would be perceived as more noise-like (WALLNER *et al.*, 2007; WALLNER *et al.*, 2008).
- Binary offset carrier (BOC) modulation (BETZ, 2001a) is widely used to split power in the frequency domain, away from the carrier frequency. It can be viewed as the multiplication of the signal by a squarewave subcarrier. Variants with more than one subcarrier have been conceived, such as alternative BOC (AltBOC) (RIES *et al.*, 2003; YAO; ZHANG; LU, 2016) or multiplexed BOC (MBOC) (HEIN *et al.*, 2006; YAO; LU; FENG, 2010b). The purpose of BOC is twofold: to enhance the synchronization accuracy offered by the signal, and to shape its PSD so as to coordinate intra-/intersystem interference in the frequency domain (TEUNISSEN; MONTENBRUCK, 2017).
- All signals use squarewave/rectangular pulse shapes. Their bandwidth is − in theory − unlimited, and in practice limited only by the satellite transfer function (THOELERT *et al.*, 2015). Pulse shapes derived from strictly band-limited functions (such as the root raised

cosine (RRC)(SCHWEIKERT *et al.*, 2000) or prolate spheroidal wave functions (PSWF) (ANTREICH; NOSSEK, 2011)) have been considered but not implemented by any GNSS.

- Navigation data bits (system time, satellite ephemerides, integrity information, etc.) are encoded into BPSK symbols, using forward error correction (FEC) or low-density parity check codes (LDPC) to add redundancy. Therefore, a signal's symbol rate (typically 50-1000 Hz) is higher than its data rate (typically 25-500 Hz) (TEUNISSEN; MONTENBRUCK, 2017).
- The modernized signals come in pairs, consisting of a *data* component and a dataless *pilot* component (TEUNISSEN; MONTENBRUCK, 2017), which are combined to a single *interplex* signal. The former carries symbols with encoded navigation data, while the latter carries predictable symbols (known as *secondary code* (SHANMUGAM *et al.*, 2008)).[2] Both components use BPSK alphabets for symbols and spreading code. Often, data and pilot components are phase-offset against one another by $\pi/2$ and appear like a single quaternary phase-shift keying (QPSK) interplex signal (e.g., L5-I/L5-Q, E5a-I/E5a-Q, E5b-I/E5b-Q).

From these points, we can observe that there are now numerous signal components centered around the same carrier frequency (e.g., 5 GPS, 3 Galileo, and 3 Beidou components in the upper L-band). Clearly, to ensure radio frequency compatibility (RFC) of these many signals, there was a need to assess and coordinate intra- and intersystem interference. A methodology to do this has been recommended by the International Telecommunications Union (ITU) (ITU-R, 2015), based on research such as (BETZ, 2001b; TITUS *et al.*, 2003).

Furthermore, there was also a shift towards signals with higher complexity, as is illustrated at the example of some complexity measures in Fig. 1.3: nearly all modernized signals have longer PRN code, higher symbol rate, and larger bandwidth[3] when compared with the legacy signals. There has been little or no R&D in the low-complexity signal segment, which is indicated on the left hand side of the figure.

1.2 Motivation: towards interference-limited satellite navigation

At the present time, the overwhelming majority of GNSS receivers is integrated into mobile phones and other mass-market electronics (EUROPEAN GNSS SUPERVISORY

[2] For the sake of completeness, we mention here that some data components carry secondary code, too.

[3] As the bandwidth of rectangular/squarewave pulses is infinite in the strict sense, we refer to the mainlobe bandwidth, where most of the signal power is concentrated (SUNDARARAJAN, 2008).

Figure 1.3 – First- and second-generation civil GNSS signals and their complexity in terms of mainlobe bandwidth, symbol rate (encoded data or secondary code), and PRN code length. The low-complexity segment is indicated in blue on the left.

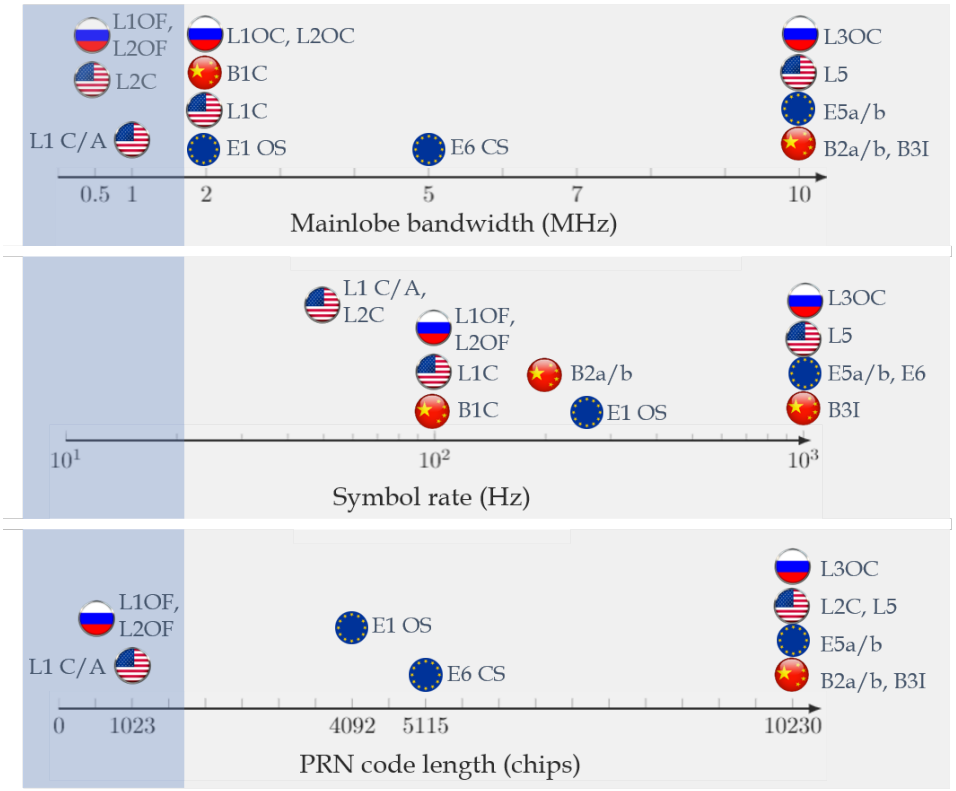

AUTHORITY, 2019). There is also a rapid advance of the internet of things (IoT) with its plethora of small low-power devices relying on GNSS for localization and timing (GSA, 2020). Clearly, receivers built on integrated circuits (ICs) face tighter constraints on cost, energy consumption and physical dimension than, e.g., an aeronautical receiver. Another change can be observed in the demand for performance. Mass-market users expect a faster time-to-first-fix (TTFF), as they only occasionally prompt their receiver for positioning in order to save battery (VAN DIGGELEN, 2009). This means that the receiver will not track the GNSS signal continuously, but rather acquire the signal, compute PVT, and go back to sleep mode. This may even be expected at low signal-to-noise ratio (SNR), e.g., in indoor scenarios.

Signal acquisition, however, is one of the most resource-hungry stages of a GNSS receiver, especially if second-generation GNSS signals are acquired. As mentioned before, these were developed with a focus on synchronization accuracy and data throughput, addressing high-performance industrial receivers. They turned out to be anything but well-tailored to the requirements of the consumer electronics mass-market (VAN DIGGELEN, 2014). To put it simply, the more complex a signal, the more hypotheses have to be tested by the receiver to acquire it. Research interest in low-complexity signals has intensified over the last few years,

with a focus on rapid, energy-efficient acquisition (PAONNI *et al.*, 2011; PAONNI; BAVARO, 2013; STANSELL *et al.*, 2015; WALLNER, 2017; ANGHILERI *et al.*, 2018; ESPLUGA *et al.*, 2018; ENNEKING *et al.*, 2019a; ENNEKING; ANTREICH; ALMEIDA, 2020; WALLNER *et al.*, 2020; VAN DIGGELEN, 2020). Most of these works argue that **a signal for mass-market users** should have some or all of the following five characeristics:

1. Use a **short PRN code** of length 1023 or even less. The shorter a signal's PRN code, the less energy, time, and memory are necessary to acquire it, because less hypotheses have to be generated and tested (VAN DIGGELEN, 2014; STANSELL *et al.*, 2015; WALLNER, 2017; ENNEKING *et al.*, 2019a; ENNEKING; ANTREICH; ALMEIDA, 2020; WALLNER *et al.*, 2020).
2. Use a **data symbol duration longer or much longer than the PRN code period**. This allows to integrate coherently over multiple successive periods of the PRN code to accumulate signal energy and compensate for low input SNR. While this leads to a reduction of data rate, most data except for the absolutely necessary GNSS time reference on the signal could be broadcast by terrestrial networks (VAN DIGGELEN, 2009; PAONNI *et al.*, 2011).
3. Closely related to the previous point, use **no secondary code** or virtually no secondary code with symbol duration much longer than the PRN code period (PAONNI; BAVARO, 2013; STANSELL *et al.*, 2015; ENNEKING *et al.*, 2019a). During the acquisition, the secondary code-phase is unknown to the receiver and must be treated as an additional unknown. If the receiver cannot afford this additional search effort, secondary code symbol transitions will have the same effect as data symbol transitions and will lead to less accumulated energy (PAONNI *et al.*, 2011; PAONNI; BAVARO, 2013; FOUCRAS *et al.*, 2016).
4. Use a **low mainlobe bandwidth** to allow for the use of low receiver front-end bandwidths. *Snapshot receivers* can even record such a narrowband signal with relatively low sampling rate, and then offload the digital signal processing and PVT computation to an external server (KANIUTH *et al.*, 2005; YAO; LU; FENG, 2010a; WALES; TARAZONA; BAVARO, 2010; SHAFRAN; GIZATULOVA; KUDRYAVTSEV, 2018). In this context, it may be worth reconsidering strictly band-limited pulse shapes (ANTREICH; NOSSEK, 2011).
5. Some have recommended to dedicate **higher transmit power** to low-complexity signals for faster and more reliable acquisition, if necessary at the cost of power reduction or discontinuation of other signal components (VAN DIGGELEN, 2020).

The features 1-4 correspond to the low-complexity signal segment indicated on the left hand side of Fig. 1.3. For simplicity, we will refer to signals with these features as coarse/acquisition (C/A) signals, indicating that their objective is acquisition (detection) performance rather than synchronization (estimation) accuracy. Notably, the first-generation signals already fulfill the above features 1-5 reasonably well. The L1 C/A PRN code of length 1023 repeats every 1 ms, while a phase change of its BPSK symbols can occur at most every 20 ms (on average every 40 ms) (STANSELL *et al.*, 2015). Moreover, it is one of the GNSS signals with the highest transmit power, most of it (90%) concentrated at ± 1 MHz (NAVSTAR…, 2020b). Indeed, L1 C/A has turned out to be well-suited to the needs of mass-market GNSS users, so much so that many use only this one signal (VAN DIGGELEN, 2014; STANSELL *et al.*, 2015). Therefore, GPS and also GLONASS (albeit to a lesser extent[4]) have a competitive edge in consumer GNSS thanks to their legacy signals (VAN DIGGELEN, 2014).

Clearly, discontinuing the L1 C/A signal in the near future is now out of the question, and only slight changes to its structure are contemplated: the authors of (STANSELL *et al.*, 2015) suggest to remove the navigation data stream from L1 C/A and replace it by secondary code symbols of an even lower rate (10 Hz). Presumably, Galileo and Beidou will soon provide similar signals. Users could acquire these C/A signals first and then (with less hypotheses to be considered) perform a handover to other signal components (PAONNI; BAVARO, 2013). A first version of a Galileo low-complexity signal called E1-D might be introduced with the transition satellite batch in 2025 (WALLNER *et al.*, 2020). However, these future prospects raise the problem of MAI. A signal with the above features 1-4 is particularly susceptible to MAI, and at the same time also causes significant MAI to other signals: while the short PRN code is a more obvious driver of MAI, the influence of features 2-4 will be discussed in more detail in Chapters 2 and 3. Finally, increasing the transmit power of a signal (feature 5) may be beneficial only for receivers of that particular signal, but detrimental otherwise.

In the following, and with regard to the existing and (presumably) forthcoming GNSS signals, we will formulate **two important research questions**, concerning the design of C/A signals as well as the RFC of these and other signals in a multi-GNSS scenario. Technically, the former question is more related to intrasystem interference, and the latter more to intersystem interference.

[4] The FDMA scheme on L1OF requires a relatively large receiver front-end bandwidth; additionally, symbol transitions are encountered twice as often due to Manchester encoding of the data (GLONASS…, 1995).

1.3 Research questions

The research in this thesis is split into two parts. The following two main research questions will be addressed in Chapters 2 and 3, respectively.

1.3.1 Q1: How to design C/A signals with short PRN codes?

Intrasystem interference is an important aspect to consider during the conception of a C/A signal. Since the number of in-view satellites of a nominal GNSS constellation is typically 7-9 (and as high as 14 in polar regions) (TEUNISSEN; MONTENBRUCK, 2017), the signals need to have an inherent robustness against mutual MAI, even when there are no other interfering signals from the same or other GNSS. This intrasystem interference in the slightly narrower sense[5] has also been referred to as *self-interference* (HEGARTY, 2020). For brevity, we will use the term MAI-A.

The vulnerability of L1 C/A to MAI-A was already known to be a problem in the 1970s, and has most likely been considered during its design (SPILKER, 1978). In the following decades, there has been some debate and research on the topic of C/A-on-C/A interference, and even about whether it was a significant problem or not (NAGLE; VAN DIERENDONCK; HUA, 1992; VAN DIERENDONCK *et al.*, 1999; VAN DIERENDONCK *et al.*, 2002; ENNEKING *et al.*, 2012; QAISAR; DEMPSTER, 2011; GOLSHAN *et al.*, 2014; VAN DIGGELEN, 2014; STANSELL *et al.*, 2015; VAN DIERENDONCK *et al.*, 2017). It is now widely agreed that the vulnerability of L1 C/A signals to MAI-A results from the combination of its short PRN code and low symbol rate (VAN DIERENDONCK *et al.*, 2017; HEGARTY, 2020): this combination leads to spectral lines in the signals' PSD and occasionally leads to a lower signal-to-interference-pluse-noise ratio (SINR) for adverse relative Doppler frequencies among the signals.

That being said, all of these works investigated explicitly L1 C/A or signals with fixed PRN code length 1023. A systematic treatment of MAI-A from a signal design perspective is not to be found in the literature to our best knowledge. In particular, there is no work on the effect of MAI-A on the global probability of false alarm (GPF) and global probability of detection (GPD). These performance measures indicate the reliability of the acquisition in case of the absence or presence of the signal, respectively; together, they form the receiver operating characteristic (ROC) curve (BORIO, 2008). Since a reduction of the PRN code length below 1023 would also

[5] In the wider sense, intrasystem interference includes also, for instance, the mutual MAI of the L1 C/A signal from one GPS satellite and the P-code signal from another one.

further reduce the number of acquisition hypotheses to be searched, it is obvious to ask:

- **Q1: How to design C/A signals with short PRN codes?**
  - Can we choose the PRN code shorter and shorter, or will MAI-A at some point degrade the ROC excessively?
  - What is a reasonable code length?
  - Moreover, how does the low symbol rate affect the ROC, and what happens if data and secondary code symbols are entirely removed from the signal (symbol rate equal to zero)?

1.3.2 Q2: How to assess RFC in interference-limited multi-constellation satellite navigation?

According to ITU regulations, GNSS operators have to ensure RFC of newly launched signals with the existing GNSS services in the relevant frequency band, meaning that MAI which could impair GNSS receiver functionalities has to be prevented. Introducing more signals in addition to those shown in Fig. 1.2, especially if they are C/A-type and/or have high transmit power, may lead to a situation where the signals' performance is not anymore limited by the SNR, but rather by a form of SINR or even signal-to-interference ratio (SIR). In a multi-constellation GNSS, MAI occurs in the form of both intra- and intersystem interference. While the SINR is a good indicator for RFC, other more specific measures for RFC are the accuracies of the receiver's fine code- and carrier-phase estimation in the presence of MAI.

For second-generation GNSS signals, RFC has been assessed using the simple analytical theory of spectral separation coefficients (SSCs) (BETZ, 2001b). Usage of this model has been recommended by the standard ITU-R M.1831 (ITU-R, 2015) to calculate the SINR (or closely related measures, such as the *aggregate interference PSD*). However, this model relies heavily on the assumption that MAI can be treated as "noise-like". More specifically, it is assumed that each GNSS signal can be approximated as a *proper* (SCHREIER; SCHARF, 2010) and wide-sense stationary (WSS) random process, and that MAI at the output of a signal-matched correlator can be treated as circularly-symmetric Gaussian (CSG) distributed (BETZ, 2000). While it is well-known that C/A-type signals do not fully match these assumptions, it remains an open question how well the proper/WSS/CSG approximations are matched to GNSS signals in general.

With the future prospect of more signals, higher transmit powers, and more C/A-type

signals, interference may become the dominant performance-limiting factor rather than noise. In such a case, it would be all the more important to model MAI with a high degree of detail when assessing RFC. Therefore, we raise the following research question:

- **Q2: How to assess RFC in interference-limited multi-constellation satellite navigation?**
  - In state-of-the-art RFC modeling, are the assumptions on signal statistics matched to GNSS signals, or should they be refined?
  - How would such refined assumptions change the CSG distribution of MAI after correlation?
  - How would such refined assumptions affect the SINR, code-phase and carrier-phase estimation accuracy?

1.4 Outline and contributions

The above research questions Q1 and Q2 are addressed in Chapters 2 and 3, respectively. A detailed description of the technical contributions of this thesis, as well as a clear delineation with respect to the state of the art, are provided in Sections 2.2 and 3.2. Eventually, future research directions and conclusions are presented in Chapter 4.

In the following, we give a short summary of the contributions of this thesis.

- **Chapter 2: Performance and design of coarse/acquisition signals**
  - We propose a simple and accurate acquisition performance model for the L1 C/A signal, where performance is measured in terms of the GPF and GPD as a function of the detection threshold. The model's simplicity is due to a novel randomized version of the well-known SSC (BETZ, 2001b).
  - The proposed acquisition performance model is not limited to the L1 C/A signal or a given receive scenario. It is given in a form general enough to investigate the impact of pulse shape (e.g., band-limited pulses), PRN code length, symbol rate, as well as search resolution, coherent/noncoherent integration time, or near-far power ratio.
  - As the acquisition performance is simple enough to be used for system optimization, we propose a systematic approach to minimize the PRN code length. On receiver side, this reduces the dimension of the acquisition search grid. Code length minimization is performed under constraints on acquisition sensitivity and symbol throughput, and leads to practical lengths as short as 300-700 chips.

  - As an application example, we discuss the design of a C/A signal for Galileo.
- **Chapter 3: Improved models for radio frequency compatibility**
  - To assess RFC in interference-limited multi-constellation GNSS, we refine existing models for the SINR in the presence of intra- and intersystem interference. We take into account the non-stationary effects of deterministic periodic PRN codes, pulse shape, and symbol modulation.
  - As GNSS signals are neither WSS nor white CSG, the statistics of the receiver's correlator outputs (early, late, and prompt) are not fully characterized by the SINR. We derive a full second-order characterization of the correlator outputs in the presence of non-WSS and non-CSG intra- and intersystem interference. This second-order characterization is used to model the root mean squared error (RMSE) and error probability density function (PDF) of coherent code- and carrier-phase estimators.
  - Furthermore, as an application example, we discuss the RFC of a hypothetical E1 C/A signal in the upper L-band with the existing GLONASS Link One OS FDMA (L1OF) signal at 1602 MHz.

1.5 Publications

Parts of the work presented in Chapters 2 and 3 appear in the following publications:

1. **ENNEKING, C.**; ANTREICH, F.; KRIEGER, L.; DE ALMEIDA, A. L. F. Gaussian Approximations for Intra- and Intersystem Interference in RNSS. **IEEE Communications Letters**, v. 23, n. 7, pp. 1198–1201, Jul. 2019;
2. **ENNEKING, C.**; ANTREICH, F.; APPEL, M.; DE ALMEIDA, A. L. F. Pure Pilot Signals: How Short Can We Choose GNSS Spreading Codes? **Proceedings of the 2019 International Technical Meeting of The Institute of Navigation**, pp. 1198–1201, Reston, Virginia, Feb. 2019;
3. **ENNEKING, C.**; ANTREICH, F.; DE ALMEIDA, A. L. F. GNSS Acquisition Performance of Short Spreading Codes. **Proceedings of the 33rd International Technical Meeting of the Satellite Division of The Institute of Navigation (ION GNSS+ 2020)**, pp. 1238–1260, St. Louis, Missouri, Sep. 2020;
4. **ENNEKING, C.**; ANTREICH, F.; DE ALMEIDA, A. L. F. Early-Late DiscriminatorPerformance of CDMA: Limitations of the Spectral Separation Coefficient. NAVITEC 2018 Signal Workshop, Noordwijk, The Netherlands, Dec. 2018;

5. **ENNEKING, C.**; ANTREICH, DE ALMEIDA, A. L. F. Design of GNSS Coarse/Acquisition Signals With Short Codes. *Submitted to:* **IEEE Transactions on Aerospace and Electronic Systems**, 11 pages, Nov. 2020.

2 PERFORMANCE AND DESIGN OF COARSE/ACQUISITION SIGNALS

We begin with a general overview on GNSS signal acquisition in Section 2.1, where we identify the potential benefits and pitfalls (in terms of intrasystem MAI, self-interference (MAI-A)) of a dedicated C/A signal with short PRN code. In Section 2.2, we compare the state of the art with our contributions. In Section 2.3, we define the acquisition system, consisting of the received signal, the generation of decision statistics, and the search strategy. In Sections 2.4 and 2.5, we introduce the GPF and GPD, respectively, as the central performance measures of an acquisition system. In the same sections, we also discuss state of the art models as well as a novel simple and accurate model. Numerical results are presented and discussed in Section 2.6, and a Galileo signal design application is given in Section 2.7.

2.1 Overview

For users on Earth, GNSS signals have very low received power[1], unknown carrier-phase, unknown PRN code-phase, and unknown Doppler frequency; in addition, they occasionally exhibit phase changes due to their BPSK modulation with secondary code or data symbols. We say that acquisition of such a signal is achieved if the receiver correctly detects the signal, and correctly estimates code-phase and Doppler frequency with coarse resolution (KAPLAN; HEGARTY, 2005). Having synchronized to code-phase and Doppler frequency, the receiver can initiate fine estimation of code-phase and carrier-phase (or *tracking*).

To acquire the signal, a 2-D search space of code-phases and Doppler frequencies is subdivided into search bins. For each bin, the received signal is converted to the respective frequency, correlated with a code-phase-shifted local copy of the signal of interest (SOI), and integrated to obtain a decision statistic. The resulting 2-D grid of decision statistics is a measure of correlation, and is illustrated qualitatively in Fig. 2.1a. The modulating symbol sequence is usually treated as a nuisance, which occasionally leads to a correlation loss and an outcome as shown in Fig. 2.1b. An exception are high-sensitivity receivers which generate local signal copies with all possible symbol transitions (ZIEDAN, 2006) − these are not considered here.

Generating and storing the correlation values requires considerable time (if bins are searched sequentially), memory (if bins are searched in parallel), and in any case energy (CHENG; HURD; STATMAN, 1990; VAN DIGGELEN, 2009; CHEN *et al.*, 2020). Besides these complexity measures, the GPF and the GPD indicate the reliability of the acquisition in case

[1] about -155 dBW at the output of a 0 dBi user antenna with unobstructed line-of-sight (EUROPEAN…, 2016)

Figure 2.1 – Illustration of 2-D acquisition search for correlation over code-phase and Doppler frequency. a) nominal case, b) correlation loss due to symbol transition.

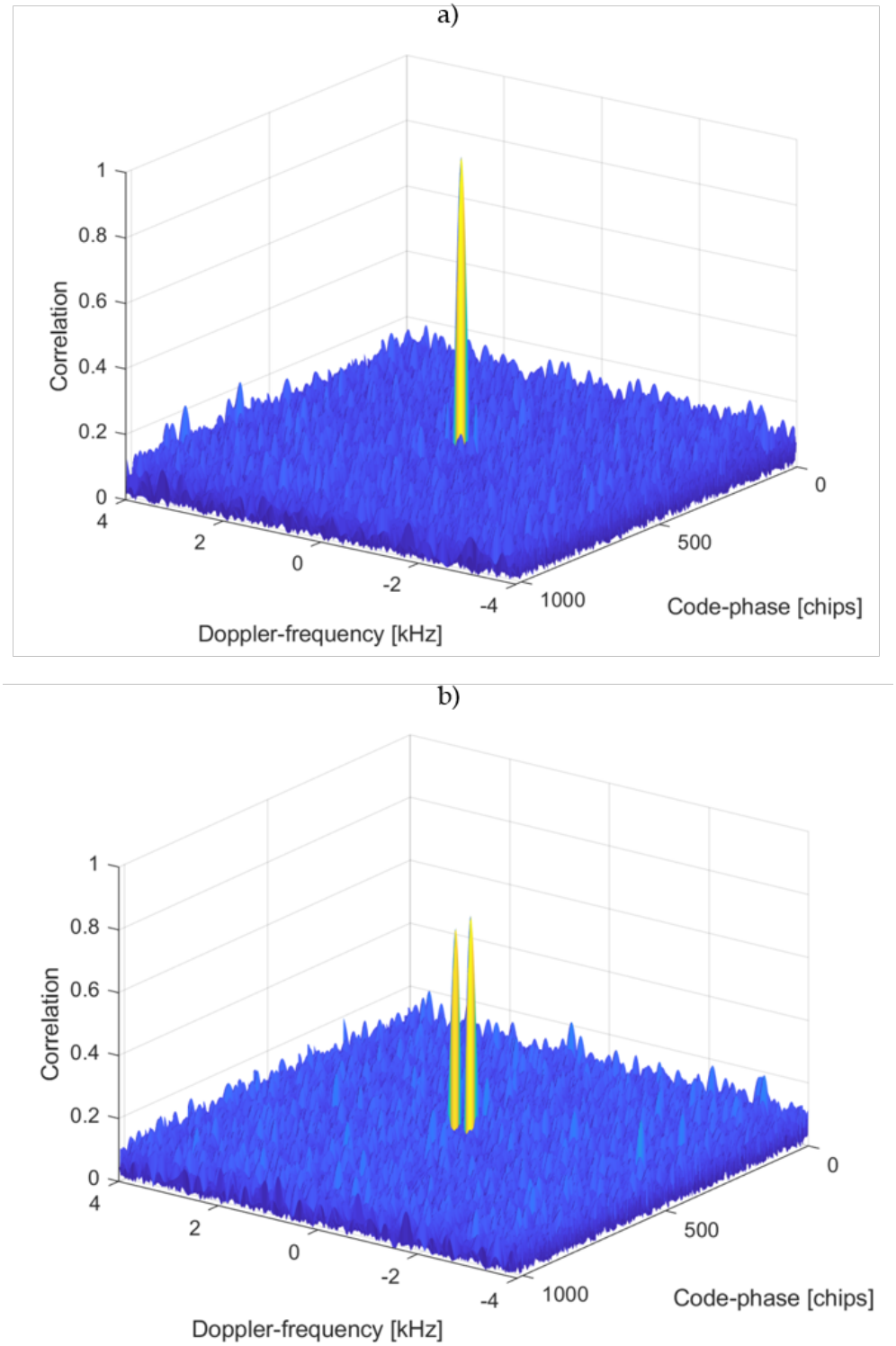

of the absence or presence of the signal, respectively (BORIO; CAMORIANO; PRESTI, 2008; O'DRISCOLL, 2007). Together, GPF and GPD form the ROC curve, which we will define later on as the central performance figure of signal acquisition. In the case of false alarm or missed detection, even more receiver resources are consumed (new acquisition, false initialization of

tracking loops) (POLYDOROS; WEBER, 1984a; POLYDOROS; WEBER, 1984b).

Signal acquisition with low complexity and high reliability would be beneficial especially to the consumer electronics mass-market (VAN DIGGELEN, 2009; GSA, 2020): as mentioned earlier, such receivers spend much of their duty cycle in acquisition mode. Moreover, they are built on very small ICs with limited memory, but are expected to acquire several signals within a few seconds and to economize the precious battery energy. A compromise between memory and computation time can be achieved, using serial, parallel, or hybrid search techniques (CORAZZA, 1996; COENEN; VAN NEE, 1992). The consumed energy, however, is essentially a constant proportional to the number of bins and cannot be traded off at the cost of time or memory. Therefore, the number of bins can be viewed as a single measure representative of acquisition complexity, and reducing it would be beneficial to all kinds of GNSS receivers.

The number of Doppler bins can relatively easily be reduced by using prior knowledge. While the receiver is still in a warm start or hot start mode, it can assume that the in-view satellites and their Doppler frequencies have not changed considerably. Another form or prior knowledge is assisted GNSS (A-GNSS) (VAN DIGGELEN, 2009), where cellular networks provide the list of in-view satellites along with their approximate Doppler frequency. Even without any prior knowledge or assistance data, the number of Doppler bins is typically on the order of 10-50, i.e., not excessively large. By contrast, the number of code-phase bins is proportional to the PRN code length, and it cannot usually be reduced by using A-GNSS or other forms of prior knowledge: the time-accuracy that cellular networks offer is too coarse ($\pm$2s) to be useful for synchronization on PRN code chip level (about 1μs), so that the full code-phase search dimension is left to the receiver (VAN DIGGELEN, 2014; STANSELL *et al.*, 2015).

To reduce the number of code bins, transmitter side solutions should be explored. The successful GPS L1 C/A signal can be considered as a blueprint. Its simple rectangular (REC) pulse shape has an autocorrelation function which does not have sidelobes; this requires less code bins per PRN code chip than a BOC pulse, for instance. However, an even simpler and more effective solution to achieve a small number of code bins could be to keep PRN codes short, with a length of 1023 chips or even less. Besides having short PRN code, C/A signals should also have a low symbol rate to avoid correlation loss due to symbol transitions. The problem of providing a system time reference at very low symbol rates is addressed in great detail in (PAONNI *et al.*, 2011; PAONNI; BAVARO, 2013). As the authors of (STANSELL *et al.*, 2015; HEGARTY, 2020) point out, this combination of short PRN period and long symbol duration (more precisely, the repetition of more than one PRN code during the transmission of a single

symbol) has inconvenient implications. It causes the C/A signals to be wide-sense cyclostationary (WSCS) rather than WSS, and leads to spectral lines of the PSD. Both these features make it considerably more difficult to model MAI-A correctly: first, because a PSD with fine spectral features is computationally costly to evaluate; second, because even if one would take this effort, the PSD alone does not describe WSCS signals accurately (for a short example, consider the cyclic spectrum analysis in Fig. 3.4).

2.2 State of the art and contributions

The impact of MAI in general, and MAI-A more specifically, has been modeled using the theory of SSCs. This is a powerful tool to model the MAI between any two signals, e.g., between a local copy of a signal to be acquired and another interfering signal. While the standard SSC as originally proposed by Betz (BETZ, 2000; BETZ, 2001b) is only accurate as long as the signals are uncorrelated, more accurate versions (referred to as deterministic refined SSC (SSC-D) hereafter) have been proposed which also work well with C/A signals (HEGARTY, 2020; O'DRISCOLL; FORTUNY-GUASCH, 2012; ENNEKING *et al.*, 2019b). The SSC-D takes into account fine features of the signals' PSD, and therefore depends on the instantaneous relative Doppler offset between the SOI and the interfering signal.

Applying the SSC-D, it has been demonstrated that cyclostationary MAI-A occasionally leads to a decrease of the SINR by several dB or can even create a detectable false correlation peak in near-far scenarios (HEGARTY, 2020; QAISAR; DEMPSTER, 2011). If the spectral lines of the interfering signal and the local copy of the SOI align, the loss of SINR is most severe. This lead to 2-D decision statistics resembling those shown in Fig. 2.2.

However, the effect of cyclostationary MAI-A on the GPF and GPD remains unknown. A straightforward application of the SSC-D to assess the mutual MAI-A between a set of interfering satellites and *each* local replica of the 2-D search space, would simply require considerable processing. Beyond that, it would be absolutely computationally prohibitive during a system optimization process, in which the PRN code length and possibly other signal features are design parameters.

In the following, we will develop a methodology to model the impact of cyclostationary MAI-A on the ROC for any given PRN code length. Our approach is based on work on the SSC-D, but a randomized version thereof, which we call randomized refined SSC (SSC-R). A key assumption is that MAI-A can be approximated as independent random variables over all bins.

Figure 2.2 – Illustration of 2-D decision statistics, generated for random PRN code of length 341, symbol rate equal to zero, and MAI-A from 7 satellites.

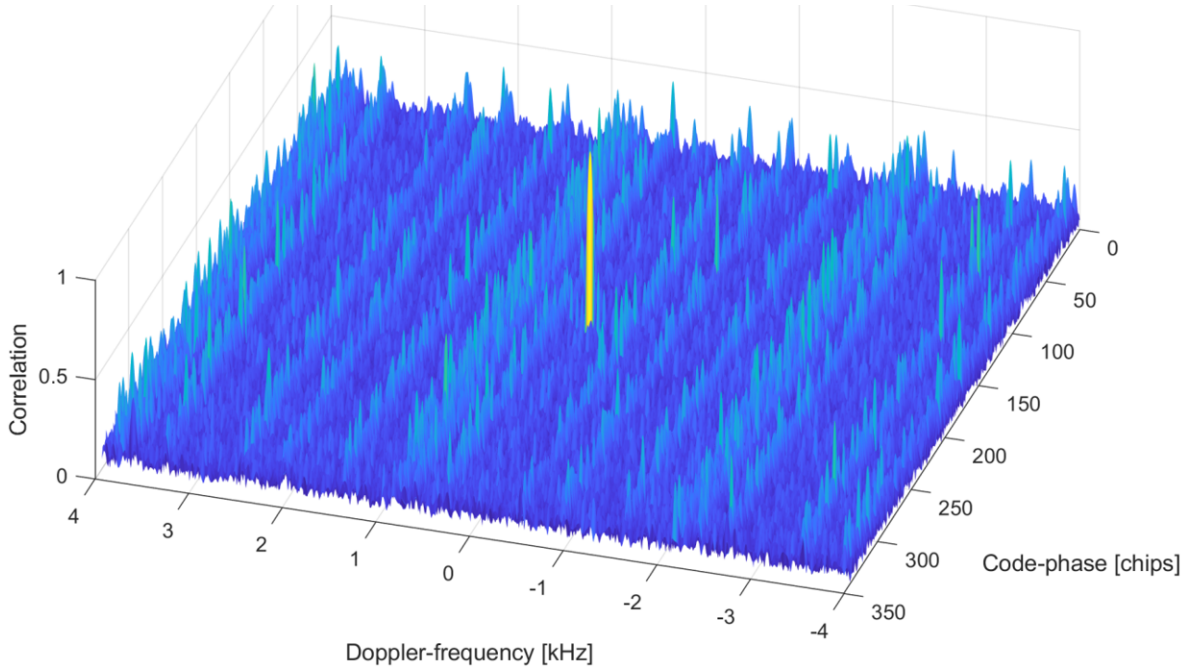

This approximation obviates the need to compute the SSC-D explicitly for each bin, but allows to work with one representative PDF of MAI-A instead. Our approach is a trade-off between the accuracy of the SSC-D (HEGARTY, 2020; O'DRISCOLL; FORTUNY-GUASCH, 2012; ENNEKING *et al.*, 2019b) and the simplicity of the (standard) SSC (BETZ, 2000; BETZ, 2001b), simple enough to use for optimization of system parameters such as the PRN code length, symbol rate, and other parameters of a novel C/A signal. As an application example, we demonstrate how the proposed methodology can be used to minimize the PRN code length, while ensuring constraints on the ROC and received power.

2.3 System model

In the following, we consider K satellite signals received over an additive white Gaussian noise (AWGN) channel, where one signal is to be acquired and the remaining $K-1$ signals are interference. We describe the processing steps for the generation of decision statistics from a baseband signal snapshot (recorded over a certain *dwell time*). An arbitrary but fixed number of coherent and noncoherent summations is considered. Subsequently, we briefly describe the search strategy for serial and parallel search.

2.3.1 Received signal

The received signal in complex baseband notation is given as

$$r(t) = \sum_{k=1}^{K} \sqrt{P_k} x_k(t) + w(t), \tag{2.1}$$

where the kth satellite contributes the signal $x_k(t)$ with power P_k, while the real and imaginary part of $w(t)$ are two independent white Gaussian noise processes each with two-sided PSD $N_0/2$. For $k = 1, \ldots, K$, the satellite signals are given as

$$x_k(t) = e^{\mathrm{j}2\pi\nu_k t + \mathrm{j}\varphi_k} \sum_{m=-\infty}^{\infty} s_k(t - mT_0 - \tau_k) b_k[m]. \tag{2.2}$$

The parameters τ_k, ν_k, and φ_k denote to the unknown code-phase, Doppler frequency, and carrier-phase, respectively. The signal $s_k(t)$ is a known spreading (code) waveform, which repeats with code rate $1/T_0$ and is modulated by a binary symbol sequence $b_k[m]$. Since we consider only DS-CDMA waveforms, we can write

$$s_k(t) = \sum_{j=0}^{N_c-1} c_k[j] h(t - jT_c), \tag{2.3}$$

where $c_k[j]$ is the known PRN code, and $h(t)$ is any real-valued analog pulse shape. The code period is equal to $T_0 = N_c T_c$.

For $k = 1, \ldots, K$, the code-phase, Doppler frequency, and carrier-phase are assumed to be independent random variables on the intervals $(-T_0/2, T_0/2)$, $(-\pi, \pi)$, and $(-F_0/2, F_0/2)$, respectively, with some Doppler span $F_0 \geqslant 0$ (typically on the order of several kHz).

In the following, we will have a closer look at some important features of the satellite signals.

2.3.1.1 PRN code and symbol sequence model

The statistical properties of the PRN code $c_k[j]$ and the symbol sequence $b_k[m]$ deserve special attention, as they can have a fundamental impact on the distribution of MAI-A. We model the PRN code $c_k[0], \ldots, c_k[N_c - 1]$ as a "coin-flip" sequence of length N_c (i.e., N_c i.i.d. binary random variables which assume values $\{-1, +1\}$ with equal probability). The symbol sequence $b_k[m]$ is *not*, in general, a coin-flip sequence of infinite length. Instead, we use the slightly more general model $b_k[m] = d_k[\lceil (m - \vartheta_k)/M \rceil]$, where $d_k[m]$ is an infinite coin-flip sequence, $\vartheta_k \in \{1, \ldots, M\}$ is a uniformly random initial symbol-phase, and $M \in \mathbb{N}$.

Thus, a symbol transition may only occur every M elements of $b_k[m]$. PRN code and symbol sequences are mutually independent, and also independent for $k = 1, \ldots, K$. Note that we model both as truly random, although in fact PRN codes will always and symbols (in case they are secondary code) may sometimes be pseudorandom. Note that we restrict ourselves to binary symbol and code alphabets $\{-1, +1\}$ in this chapter. A signal model including arbitrary alphabets is formulated in Chapter 3.

It is important to distinguish between the symbol rate $1/(MT_0)$ and the code rate $1/T_0$. A few typical setups are worth mentioning:

(i) *balanced:* $M = 1$ (e.g., L1C, E1 OS, L5, E5);

(ii) *quasi-pilot:* $M \gg 1$ (e.g., L1 C/A);[2]

(iii) *pure pilot:* $M \to \infty$;

(iv) *aperiodic:* M arbitrary, but $T_0 \to \infty$ (e.g., P-code, PRS).

The balanced configuration (i) is typical for second-generation (civil) GNSS signals. In the remainder of this chapter, we will focus on (ii) and (iii), as they are the most attractive options for C/A signals (and the most prone to MAI-A).

2.3.1.2 Pulse shape model

Let the pulse's Fourier transform be denoted by $H(\nu) \triangleq \int_{\mathbb{R}} h(t) e^{-\mathrm{j}2\pi\nu t}\,\mathrm{d}t$, and its autocorrelation function by $\rho_h(t) \triangleq \int_{\mathbb{R}} h(\tau)h(\tau + t)\,\mathrm{d}\tau$, with normalization $\rho_h(0) = T_c$. For simplicity, we consider only Nyquist pulses. These have an autocorrelation function that satisfies $\rho_h(nT_c) = 0$ for all $n = \pm 1, \pm 2, \ldots$ (G. Zang; C. Ling, 2003). In the following, we give three examples of Nyquist pulse shapes which will be used in the remainder of this chapter:

- The REC pulse can be found on many first- and second-generation GNSS signals, e.g., L1 C/A, E5a/b, L5.

$$h(t) = \begin{cases} 1, & |t/T_c| \leq 1/2 \\ 0, & \text{otherwise.} \end{cases} \tag{2.4}$$

- A BOC pulse (the simple BOC(1,1)-variant) can be given by

$$h(t) = \begin{cases} \operatorname{sgn}(t/T_c), & |t/T_c| \leq 1/2 \\ 0, & \text{otherwise.} \end{cases} \tag{2.5}$$

[2] The term quasi-pilot has also been used in a narrower sense for signals whose symbols do not only have a long duration, but are also entirely predictable after time synchronization is achieved (PAONNI *et al.*, 2011).

This pulse can be used to represent sine-phased BOC with subcarrier rate equal to the chipping rate, which is used by many second-generation signals, e.g., L1C (Data), B1C (Data).

- The RRC with zero roll-off factor is given by

$$h(t) = \begin{cases} 1, & t = 0 \\ \frac{\sin(\pi t/T_c)}{\pi t/T_c}, & \text{otherwise.} \end{cases} \tag{2.6}$$

This pulse is also known as the sinc-pulse or flat-spectrum pulse.

Note that the first two pulses do not only satisfy the Nyquist criterion, but are also strictly time-limited, since $h(t) = 0$ for $|t| > T_c/2$. The third pulse is an example for a band-limited Nyquist pulse.

2.3.2 Search grid, correlators, and decision statistics

Without loss of generality, we consider $k = 1$ as the SOI. Then the acquisition task is specified as follows. Decide for either of the following hypotheses:

- H_0: the SOI is absent $(P_1 = 0)$;
- H_1: the SOI is present $(P_1 > 0)$;

additionally, if the decision is taken for H_1, select a coarse estimate for τ_1 from a set of code-phase candidates $\mathcal{X}_\tau$, and a coarse estimate for ν_1 from a set of Doppler candidates $\mathcal{X}_\nu$.

These candidate sets form a 2-D grid of bins with P code-phases and Q Doppler frequencies, distributed uniformly over the uncertainty intervals $[-T_0/2, T_0/2)$ and $[-F_0/2, F_0/2)$, respectively. Thus, we have

$$\mathcal{X}_\tau = \left\{ -\frac{T_0 + \Delta\tau}{2}, -\frac{T_0 + 3\Delta\tau}{2}, \ldots, \frac{T_0 - \Delta\tau}{2} \right\}, \tag{2.7}$$

$$\mathcal{X}_\nu = \left\{ \frac{-F_0 + \Delta\nu}{2}, \frac{-F_0 + 3\Delta\nu}{2}, \ldots, \frac{F_0 - \Delta\nu}{2} \right\}, \tag{2.8}$$

with code-phase spacing $\Delta\tau = T_0/P$ and frequency spacing $\Delta\nu = F_0/Q$. We use a linear index $i \in \{1, \ldots, PQ\}$ to refer to the 2-D bin $(\tau^{(i)}, \nu^{(i)}) \in (\mathcal{X}_\tau \times \mathcal{X}_\nu)$. We define the *correct bin* with index $i = 1$ as the bin that deviates the least from the true parameters in the sense that

$$|\tau^{(1)} - \tau_1| \leqslant \Delta\tau/2 \text{ and } |\nu^{(1)} - \nu_1| \leqslant \Delta\nu/2. \tag{2.9}$$

It is easily checked that this assignment is unique, i.e., there is always one correct bin with probability one.[3] The remaining bins $i = 2, \ldots, PQ$ are in no particular order yet.

[3] Special cases, where the true code-phase and/or Doppler frequency lie exactly at a bin boundary, have probability measure zero.

Figure 2.3 – Generation of statistics and threshold comparison.

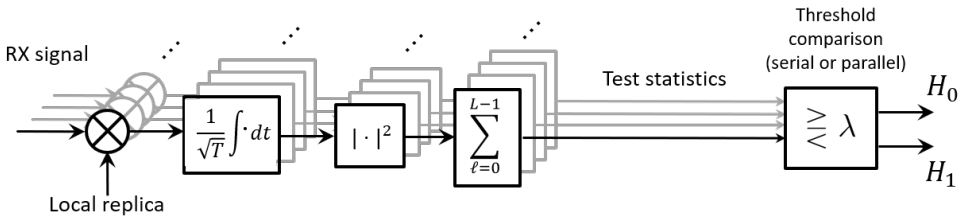

As shown in Fig. 2.3, a decision statistic

$$Z^{(i)} = \sum_{\ell=0}^{L-1} \left| Y^{(i)}[\ell] \right|^2 \tag{2.10}$$

is generated for each bin i, where $Y^{(i)}[0], \ldots, Y^{(i)}[L-1]$ is a sequence of L correlator outputs. The correlator outputs are obtained via correlation of the received signal $r(t)$ with a *local replica* of the spreading waveform delayed by $\tau^{(i)}$ and shifted in frequency by $\nu^{(i)}$,

$$x_\ell^{(i)}(t) \triangleq e^{\mathrm{j}2\pi\nu^{(i)}t} \sum_{n=\ell N}^{\ell N+N-1} s_1\big(t - nT_0 - \tau^{(i)}\big). \tag{2.11}$$

The structure of $x^{(i)}(t)$ resembles the structure of the satellite signal $x_1(t)$. However, it is not modulated by a symbol sequence, since this is an unknown nuisance to the receiver. Moreover, it is an "energy" signal, meaning that the integral

$$\begin{aligned}
&\int_{-\infty}^{\infty} \left| x_\ell^{(i)}(t) \right|^2 \mathrm{d}t \\
&= \sum_{n=\ell N}^{\ell N+N-1} \sum_{'=\ell N}^{\ell N+N-1} \sum_{j=0}^{N_c-1} \sum_{j'=0}^{N_c-1} \\
&\qquad \times c_1[j] c_1[j'] \int_{-\infty}^{\infty} h(t - jT_c - nT_0 - \tau^{(i)}) h(t - j'T_c - n'T_0 - \tau^{(i)}) \, \mathrm{d}t \\
&= \sum_{n=\ell N}^{\ell N+N-1} \sum_{'=\ell N}^{\ell N+N-1} \sum_{j=0}^{N_c-1} \sum_{j'=0}^{N_c-1} c_1[j] c_1[j'] \rho_h\big((j-j')T_c + (n-n')T_0\big) \\
&= \sum_{n=\ell N}^{\ell N+N-1} \sum_{j=0}^{N_c-1} \rho_h(0) \\
&= NN_cT_c \triangleq T
\end{aligned} \tag{2.12}$$

is finite. We call T the *coherent integration time*, and require that it is a multiple of the code-phase $T_0 = N_cT_c$. Correlation with the received signal leads to

$$Y^{(i)}[\ell] = \frac{1}{\sqrt{T}} \int_{-\infty}^{\infty} \big(x_\ell^{(i)}(t)\big)^* r(t) \, \mathrm{d}t \tag{2.13}$$

for coherent subintervals $\ell = 0, \ldots, L-1$. For the further analyses, it is useful to express the correlator output as the superposition of K signal contributions and noise

$$Y^{(i)}[\ell] = \sum_{k=1}^{K} \sqrt{P_k}\, X_k^{(i)}[\ell] + W^{(i)}[\ell] \tag{2.14}$$

$$X_k^{(i)}[\ell] = \frac{1}{\sqrt{T}} \int_{-\infty}^{\infty} \left(x_\ell^{(i)}(t)\right)^* x_k(t)\, \mathrm{d}t \tag{2.15}$$

$$W^{(i)}[\ell] = \frac{1}{\sqrt{T}} \int_{-\infty}^{\infty} \left(x_\ell^{(i)}(t)\right)^* w(t)\, \mathrm{d}t. \tag{2.16}$$

Finally, we define the *dwell time* for the generation of $Z^{(i)}$ as LT.

2.3.3 Decision strategy

We consider only decision strategies based on threshold comparison, implemented either as serial or parallel search. Other techniques based on ratio detection have been proposed for GNSS, but were shown to have higher computational complexity and often inferior performance (GEIGER; VOGEL; SOUDAN, 2012). Moreover, we limit our considerations to single-dwell strategies, while more sophisticated approaches include the use of multiple dwell times, search resolutions, or verification stages (VITERBI, 1995; DICARLO; WEBER, 1983; POLYDOROS; WEBER, 1984b; POLYDOROS; WEBER, 1984a).

- **Serial search**: Determine the starting index $j \in \{1, \ldots, PQ\}$ (uniformly random or according to prior knowledge). Serially for $i = j, j-1, \ldots, 1, PQ, PQ-1, \ldots, j+1$, compare the statistic $Z^{(i)}$ to a fixed threshold $\lambda \geqslant 0$. As soon as $Z^{(i)} > \lambda$, immediately accept H_1, return the bin i, and terminate the search. If no statistic has exceeded the threshold after PQ comparisons, accept H_0.
- **Parallel search**: Compare all statistics to the threshold in parallel. Determine the subset $\mathcal{J}$ of all bins $j \in \{1, \ldots, PQ\}$ for which $Z^{(j)} > \lambda$. If $\mathcal{J}$ is non-empty, accept H_1 and return the bin $i = \arg\max_{j \in \mathcal{J}} Z^{(j)}$ as code-phase/Doppler estimate. Otherwise, accept H_0.

2.4 Probability of False Alarm

Let H_0 be the true hypothesis. We say that a *bin false alarm* occurs in the ith bin if $Z^{(i)} > \lambda$ for some $i \in \{1, \ldots, PQ\}$ (regardless of whether the actual search is terminated before reaching the ith bin). Let the probability of this event be given by $P_f^{(i)}(\lambda)$. Moreover, a *system false alarm* is raised if at least one bin false alarm occurs (in that case, the receiver erroneously

decides for H_1). We refer to $P_f^{(i)}(\lambda)$ as bin probability of false alarm (BPF), and to $P_F(\lambda)$ as GPF.

In the following, we discuss various models for BPF/GPF, including existing approaches and the novel model based on the SSC-R. All of them are based on the notion of an *effective noise floor*, which means that they account for MAI-A by a noise-equivalent model. The defining feature of each approach is the model for the effective noise floor $\mathcal{N}_0^{(i)}$ for each bin $i = 1, \ldots, PQ$. Once $\mathcal{N}_0^{(i)}$ is specified, the ith statistic is assumed to follow the cumulative distribution function (CDF)

$$F_Z(z; \mathcal{N}_0^{(i)}) \triangleq 1 - e^{-\frac{z}{\mathcal{N}_0^{(i)}}} \sum_{\ell=0}^{L-1} \frac{1}{\ell\,!} \left(\frac{z}{\mathcal{N}_0^{(i)}} \right)^{\ell}, \; z \geqslant 0, \tag{2.17}$$

independent for $i = 1, \ldots, PQ$. This is a scaled version of the CDF of a central χ^2-distribution with $2L$ degrees of freedom. Given the effective noise floor for each bin, BPF and GPF are given by

$$P_f^{(i)}(\lambda) \approx 1 - F_Z(\lambda; \mathcal{N}_0^{(i)}), \quad i = 1, \ldots, PQ, \tag{2.18}$$

$$P_F(\lambda) \approx 1 - \prod_{i=1}^{PQ} F_Z(\lambda; \mathcal{N}_0^{(i)}). \tag{2.19}$$

Clearly, $P_F(\lambda)$ is the same for serial and parallel search (BORIO, 2008).

2.4.1 Neglecting Interference

The simplest approximation is to ignore MAI-A and consider only the contribution of noise, i.e., to choose

$$\mathcal{N}_0^{(i)} = N_0, \quad i = 1, \ldots, PQ. \tag{2.20}$$

This model is in fact exact for a pure AWGN channel and a Nyquist pulse, as the following calculation shows. Clearly, $\mathrm{E}\left[W^{(i)}[\ell]\right] \equiv 0$, as local replica and AWGN are uncorrelated, and

$$\begin{aligned}
&\mathrm{E}\left[(W^{(i)}[\ell])^* W^{(i)}[\ell']\right] \\
&= \frac{1}{T}\int_{-\infty}^{\infty}\int_{-\infty}^{\infty} \mathrm{E}\left[w^*(t)w(u)\right] \mathrm{E}\left[x_\ell^{(i)}(t)\big(x_{\ell'}^{(i)}(u)\big)^*\right] \mathrm{d}u\ \mathrm{d}t \\
&= \frac{1}{T}\sum_{n=\ell N}^{\ell N+N-1}\sum_{n'=\ell' N}^{\ell' N+N-1}\sum_{j=0}^{N_c-1}\sum_{j'=0}^{N_c-1}\int_{-\infty}^{\infty}\int_{-\infty}^{\infty} N_0\,\delta(t-u)e^{\mathrm{j}\,2\pi\nu^{(i)}(t-u)} \\
&\qquad \times \mathrm{E}\left[c_1[j]c_1[j']\right] h(t - jT_c - nT_0 - \tau^{(i)})h(u - j'T_c - n'T_0 - \tau^{(i)})\,\mathrm{d}u\ \mathrm{d}t \\
&= \frac{N_0}{T}\delta[\ell-\ell'] \sum_{n=\ell N}^{\ell N+N-1}\sum_{j=0}^{N_c-1} \rho_h(0) \\
&= \delta[\ell-\ell']N_0,
\end{aligned} \tag{2.21}$$

where we used the Nyquist property several times. Moreover, $\delta(t)$ and $\delta[\ell]$ denote the Dirac delta function and the discrete unit sample function, respectively (PROAKIS, 2001). For non-Nyquist pulses, the noise samples are actually correlated over successive coherent subintervals $\ell, \ell+1, \ldots$; moreover, even Nyquist pulses would lead to correlation across bins $i, i+1, \ldots$ in the code-phase domain unless the bin spacing is equal to T_c, as can be observed from (2.21). However, white noise and independent statistics across bins are a common approximation (BORIO, 2008).

The resulting approximation for the BPF can be expressed in terms of the generic CDF (2.17) as

$$P_f(\lambda) \approx 1 - F_Z(\lambda; N_0). \tag{2.22}$$

Importantly, this approximation does not depend on the bin index, so that (2.19) reduces to a simple exponentiation form $P_F(\lambda) \approx 1 - (F_Z(\lambda; N_0))^{PQ}$.

2.4.2 Spectral separation coefficient (SSC)

A common approximation is to calculate the MAI-A's noise-equivalent PSD I_0 in units of W/Hz, and then simply assume an increased effective noise floor for all bins

$$\mathcal{N}_0^{(i)} = N_0 + I_0, \quad i = 1, \ldots, PQ. \tag{2.23}$$

The convenience of this approach is that results for the pure AWGN channel can be reused, simply replacing N_0 by $N_0 + I_0$, to obtain the BPF

$$P_f(\lambda) \approx 1 - F_Z(\lambda; N_0 + I_0). \tag{2.24}$$

Table 2.1 – Spectral separation coefficient for common pulse shapes

$h(t)$	REC	BOC	RRC
SSC	$2/3$	$1/3$	1

Again, this model does not depend on the bin index i. The MAI-A's noise-equivalent PSD is given by

$$I_0 \triangleq \mathrm{Var}\left[\sum_{k=2}^{K} \sqrt{P_k}\, X_k^{(i)}[\ell]\right] = \frac{1}{T_c^3} \int_{-\infty}^{\infty} |H(\nu)|^4 \,\mathrm{d}\nu \sum_{k=2}^{K} E_k \tag{2.25}$$

where $E_k \triangleq P_k T_c$, and the derivation is given, for instance, in (VITERBI, 1995). In the context of satellite navigation, the pulse-dependent factor

$$\mathrm{SSC} = \frac{1}{T_c^3} \int_{-\infty}^{\infty} |H(\nu)|^4 \,\mathrm{d}\nu \tag{2.26}$$

has become known as the *self*-SSC. This term stems from the fact that the interfering signal and the SOI have the same pulse shape. The self-SSCs of some pulse shapes are stated in Table 2.1. Note that a different version of the SSC is used in Chapter 3, where interfering signal and SOI not necessarily have the same pulse shape[4]. In the remainder of Chapter 2, we will refer to various ways to refine the *self*-SSC only.

2.4.3 Deterministic refined SSC (SSC-D)

The SSC-D models MAI-A with a much higher level of detail than the standard SSC. While slight variations can be observed among the proposed versions (HEGARTY, 2020; ENNEKING *et al.*, 2019b; O'DRISCOLL; FORTUNY-GUASCH, 2012) in how they treat the dependency on code-phase, they are all essentially the same with regard to the (much more significant) Doppler dependency.

The initial approach is to calculate the MAI-A's noise-equivalent PSD conditioned on the constellation parameters of the interferers, $\boldsymbol{\nu} \triangleq [\nu_2, \ldots, \nu_K]^T$ and $\boldsymbol{\tau} \triangleq [\tau_2, \ldots, \tau_K]^T$. This leads to the conditional variance

$$\mathcal{I}_0^{(i)} \triangleq \mathrm{Var}\left[\sum_{k=2}^{K} \sqrt{P_k}\, X_k^{(i)}[\ell] \,\middle|\, \boldsymbol{\tau}, \boldsymbol{\nu}\right], \tag{2.27}$$

and an effective noise floor

$$\mathcal{N}_0^{(i)} = N_0 + \mathcal{I}_0^{(i)}, \quad i = 1, \ldots, PQ. \tag{2.28}$$

[4] Additionally, in the context of RFC, a scaling factor of T_c^{-2} rather than T_c^{-3} is used, so that the SSC has then the dimension of 1/Hz.

Figure 2.4 – Pulse interference function vs. relative delay for various pulse shapes: rectangular (REC), binary offset carrier (BOC), root raised cosine (RRC, with zero roll-off).

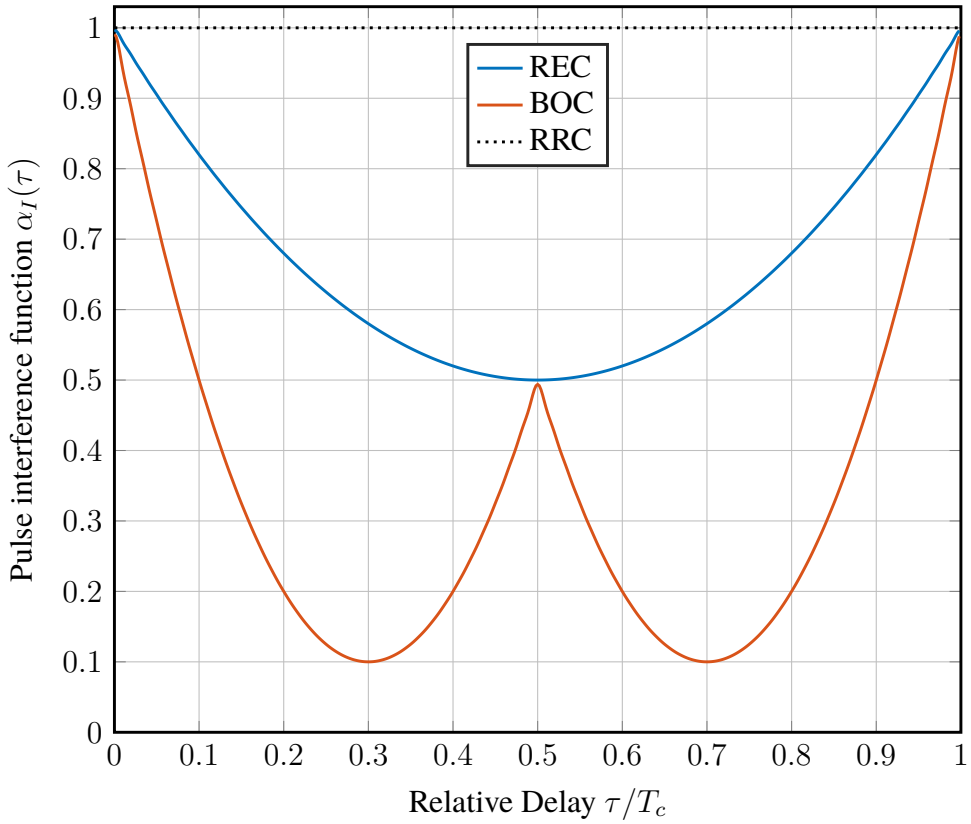

Note that this effective noise floor varies from bin to bin. Therefore, the following equations (2.29)-(2.33), which are results from (CHO; LEHNERT, 2002; O'DRISCOLL; FORTUNY-GUASCH, 2012; ENNEKING *et al.*, 2019b; HEGARTY, 2020) (and a particularization of the proof in Section 3.4.4), need to be evaluated PQ times per interferer. The conditional variance of the superposition of $K-1$ independent signals is the sum of conditional variances $\mathcal{I}_0^{(i)} = \sum_{k=2}^{K} \mathcal{I}_k^{(i)}$. For an interferer $k \neq 1$ affecting the ith bin, a weighted SSC-D is obtained

$$\begin{aligned}\mathcal{I}_k^{(i)} &\triangleq \operatorname{Var}\left[X_k^{(i)}[\ell] \middle| \tau_k, \nu_k\right] \\ &= \operatorname{SSC}\left(\tau^{(i)} - \tau_k, \nu^{(i)} - \nu_k\right) E_k. \end{aligned} \tag{2.29}$$

The SSC-D depends on the difference of the ith code-phase/Doppler candidate with respect to the kth interferer's code-phase/Doppler and factorizes as

$$\operatorname{SSC}(\tau, \nu) = \alpha_I(\tau)\beta_I(\nu), \tag{2.30}$$

Figure 2.5 – Code interference function vs. relative Doppler. N and M are the number of code repetitions per coherent correlation and per symbol, respectively. Shaded areas indicate the cases where $N < M < \infty$.

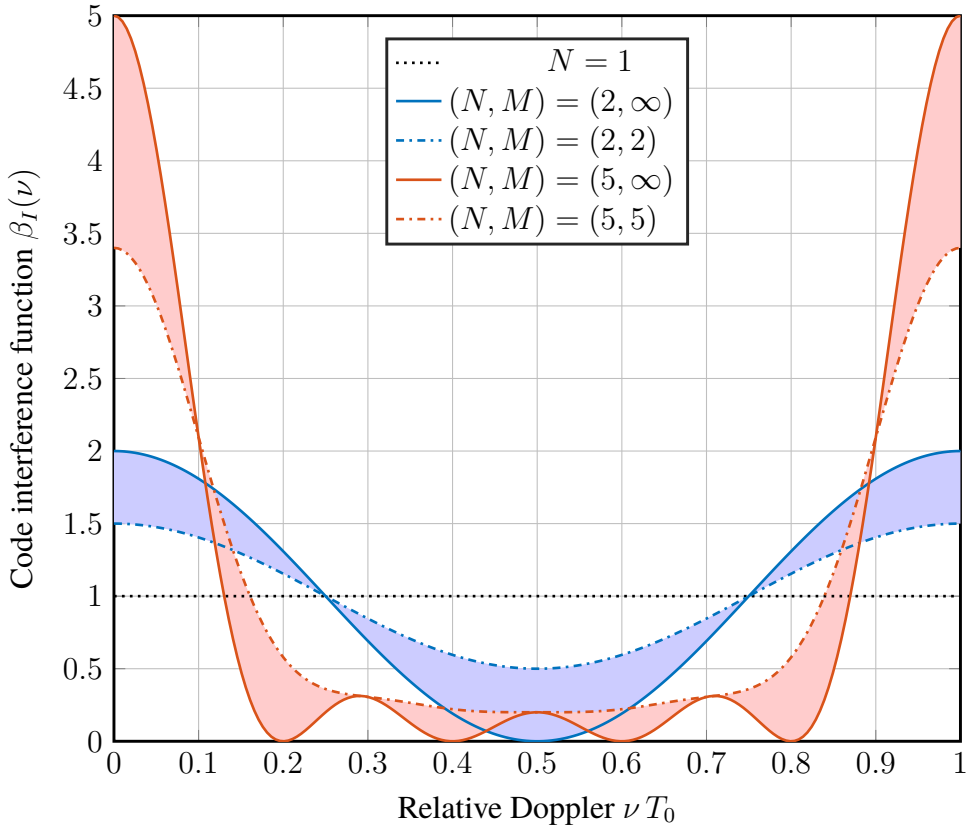

with two periodic interference functions as in Figs. 2.4 and 2.5

$$\alpha_I(\tau) = \sum_{m=-\infty}^{\infty} \frac{\rho_h^2(\tau - mT_c)}{T_c} \tag{2.31}$$

$$\beta_I(\nu) = \sum_{n=1-N}^{N-1} \left(1 - \frac{|n|}{M}\right)\left(1 - \frac{|n|}{N}\right) \cos(2\pi\nu n T_0). \tag{2.32}$$

The *pulse interference function* $\alpha_I(\tau)$ is determined solely by the pulse shape and the fractional part of τ/T_c. To facilitate the analysis a bit, one may choose to replace this function by its average over one period

$$\alpha_I(\tau) \approx \frac{1}{T_c} \int_0^{T_c} \sum_{m=-\infty}^{\infty} \frac{\rho_h^2(\tau - mT_c)}{T_c^2}\, \mathrm{d}\tau = \mathrm{SSC} = \text{const.}, \tag{2.33}$$

which, interestingly, leads to the standard SSC (2.26). For some band-limited pulses, this approximation is exact (G. Zang; C. Ling, 2003); even if not, the resulting error can be expected to be negligible, since τ_k is usually a fast-changing parameter and the deviation of $\alpha_I(\tau)$ from its average is moderate.

The *code interference function* $\beta_I(\nu)$ can cause much greater variations of the SSC-D. It depends on the fractional part of νT_0, as well as on the number of code repetitions per

Figure 2.6 – Left: structure of the satellite signal, modulated by a new symbol every M periods of the PRN code. Right: structure of the local replica, consisting of N repetitions of the PRN code.

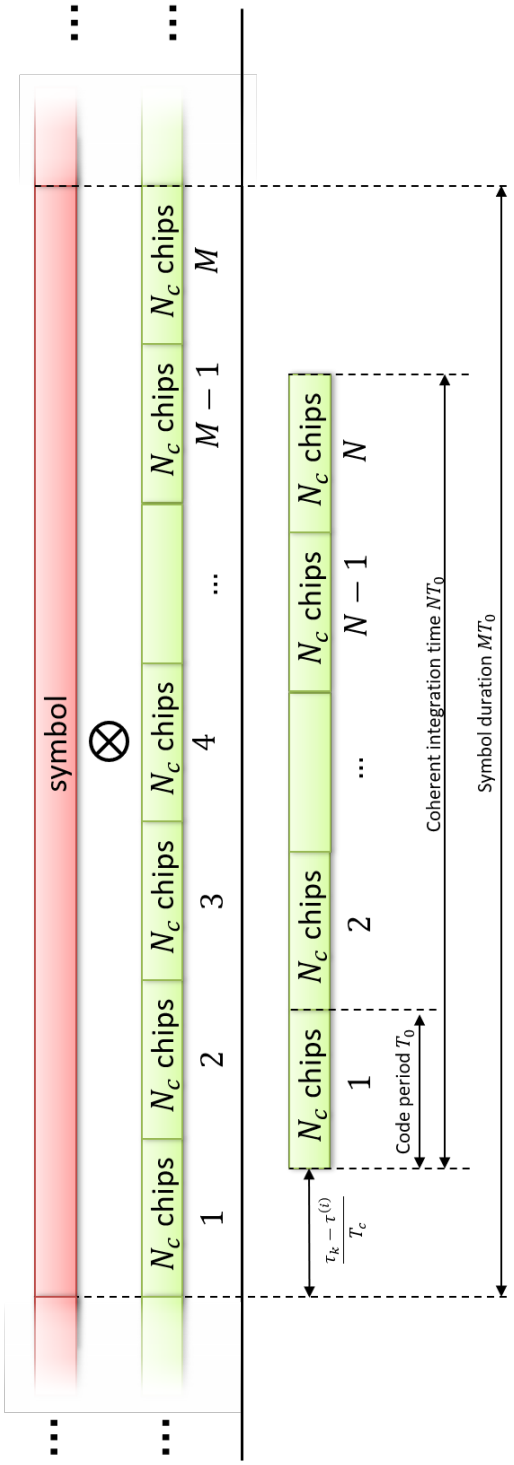

correlation (N) and per symbol (M). The difference between N and M is illustrated in Fig. 2.6. While works on MAI-A often assume that these two are the same for simplicity (O'DRISCOLL; FORTUNY-GUASCH, 2012; HEGARTY, 2020), this need not be the case, as the receiver may choose to integrate coherently over less than one full symbol period. Unlike an interferer's

code-phase, its Doppler frequency is slowly changing and its peak-to-average ratio can scale with N. Therefore, $\beta_I(\nu)$ should not simply be replaced by the average over one period (which is always unity (O'DRISCOLL; FORTUNY-GUASCH, 2012)). As is shown in Fig. 2.5, the code interference function assumes a maximum of $N + (1 - N^2)/(3M)$ times its average if its argument is a multiple of the code rate. We can observe that longer symbol duration (M large) can result in larger MAI-A. The trivial case occurs if the receiver performs correlation over only a single code period ($N = 1$), which leads to $\beta(\nu) \equiv 1$.

Figure 2.7 – Variation of the effective noise floor vs. Doppler bins during a satellite pass. The correct Doppler ν_1 of the SOI is indicated by the dotted line.

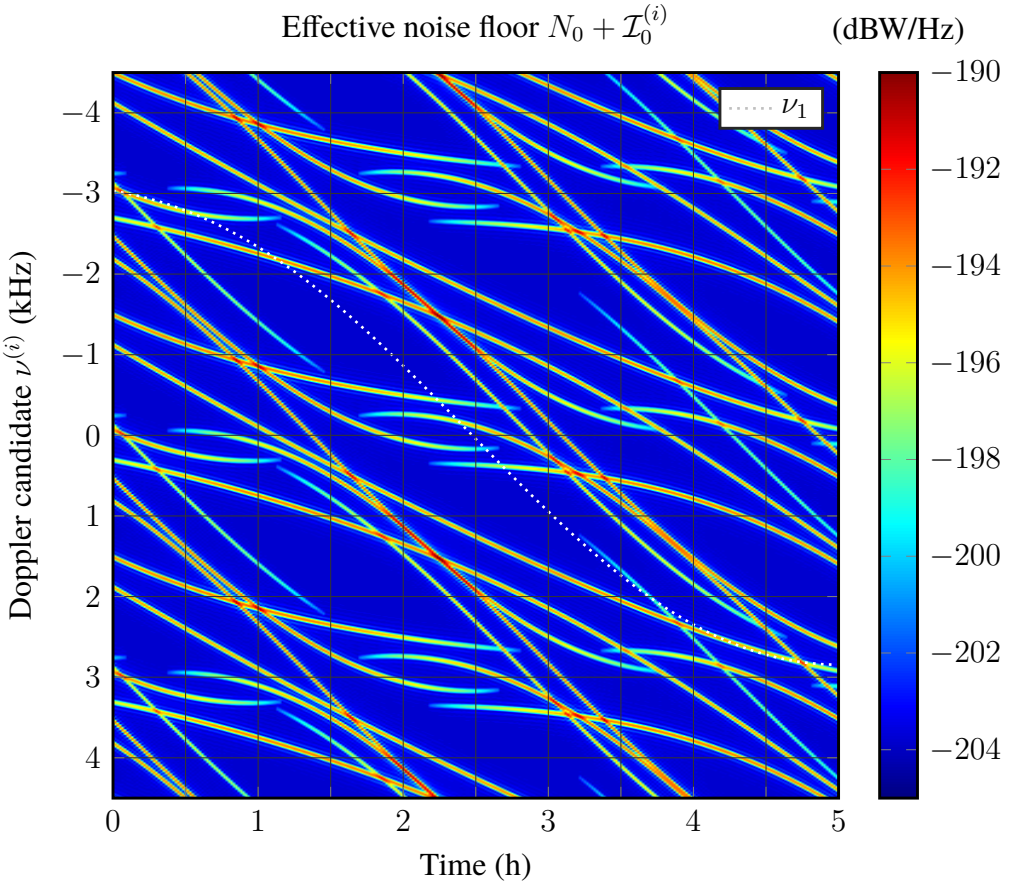

Example: A static receiver observes a Walker(24/3/1) constellation (EUROPEAN…, 2016). Each in-view satellite transmits a pure pilot signal with PRN code length $N_c = 341$, RRC pulse with zero roll-off, and chip duration $T_c = 1/1.023\,\mu$s. The noise floor N_0 is -204 dBW/Hz, and the received powers P_k are between -160 dBW and -152 dBW, using the elevation dependent model from (RTCA, Inc., 2008). The SOI is transmitted from satellite $k = 1$, whose pass takes about five hours. The coherent correlation period is 20 ms, hence we have $N = 60$ code periods per coherent correlation and $M \to \infty$ (pure pilot). In Fig. 2.7, the effective noise floor $N_0 + \mathcal{I}_0^{(i)}$

is shown as a function of a bin's Doppler candidate $\nu^{(i)}$ and time. The maximum contribution of interferer k to the effective noise floor is equal to $60E_k$, and occurs whenever the relative Doppler $\nu^{(i)} - \nu_k$ is approximately a multiple of $1/T_0 = 3\,\text{kHz}$. For this scenario, it can be observed that this can happen for up to three interferers at the same time for the same Doppler candidate. As Doppler frequencies change slowly over time, such "Doppler-collisions" can last for several minutes.

The difficulty with the SSC-D model is the necessity to calculate not one, but up to PQ effective noise floors. The BPF for bin i using the SSC-D is

$$P_f^{(i)}(\lambda) \approx 1 - F_Z(\lambda; N_0 + \mathcal{I}_0^{(i)}), \quad i = 1, \ldots, PQ. \tag{2.34}$$

which depends on the bin index. Calculating all PQ BPFs and the resulting GPF $P_F(\lambda)$ (2.19) is usually not practical for two reasons. First, it is extremely cumbersome to compute PQ effective noise floors, especially for a large number of bins. Second, $P_F(\lambda)$ and $P_f^{(i)}(\lambda)$ under the SSC-D are conditional probabilities, as they treat the random interferer parameters as deterministic (conditional). As such, they may be very accurate for an instantaneous satellite constellation, but not representative of all possible cases. Nevertheless, this model provides useful insights and can be used to develop another approximation superior to the standard SSC.

2.4.4 Randomized refined SSC (SSC-R)

Like in the previous section, we allow for a bin-dependent effective noise floor $\mathcal{N}_0^{(i)} = N_0 + \mathcal{I}_0^{(i)}$. However, instead of using the exact conditional formula (2.27) for the MAI-A variance $\mathcal{I}_0^{(i)}$, we assume that it is a random variable. Therefore, the CDF (2.17) becomes a compound probability distribution function. Furthermore, we assume that the PQ MAI-A variances are i.i.d.

$$\mathcal{I}_0^{(i)} \sim f_{\mathcal{I}_0}(\mathcal{I}_0),\ i = 1, \ldots, PQ, \tag{2.35}$$

sampled from a single representative model PDF $f_{\mathcal{I}_0}(\mathcal{I}_0)$. A trivial model would be $f_{\mathcal{I}_0}(\mathcal{I}_0) = \delta(\mathcal{I}_0 - I_0)$, which leads to the standard SSC model. Instead, we construct $f_{\mathcal{I}_0}(\mathcal{I}_0)$ by the following two-step approach.

- Compute the PDF of the periodic function $\mathrm{SSC}(\tau, \nu)$ for uniform relative delay $\tau \sim \mathcal{U}(0, T_c)$ and relative Doppler $\nu \sim \mathcal{U}(0, T_0^{-1})$. The result is the PDF of the SSC-R, which is shown in Fig. 2.8.

Figure 2.8 – PDF of the SSC-R and its two factors for an L1 C/A signal with coherent integration over $N = 20$ code periods, assuming independent uniformly distributed relative code-phase and relative Doppler (τ, ν).

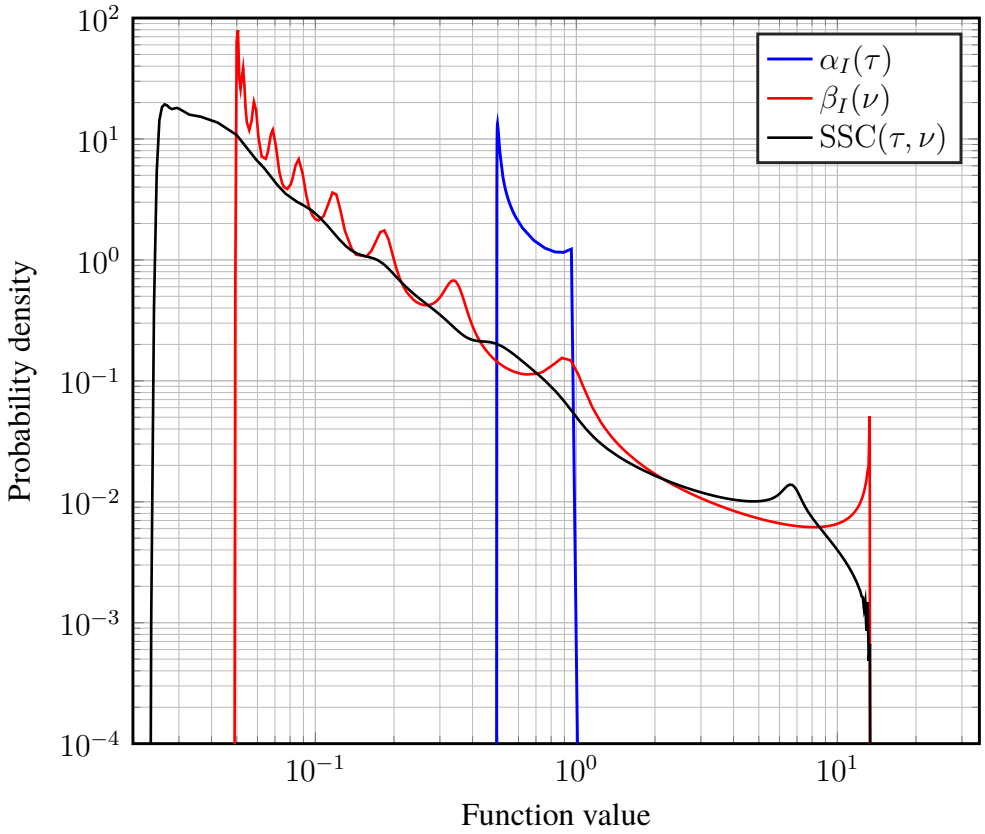

- Scale the obtained PDF by the energy E_k of interferer k to obtain the PDF $f_{\mathcal{I}_k}(\cdot)$ for $k = 2, \ldots, K$. For the superposition of MAI-A from $K - 1$ independent interferers, perform $K - 2$ convolutions

$$f_{\mathcal{I}_0}(\mathcal{I}_0) = \left(f_{\mathcal{I}_2} * \ldots * f_{\mathcal{I}_K}\right)(\mathcal{I}_0). \tag{2.36}$$

  The result is shown in Fig. 2.9.

With $f_{\mathcal{I}_0}(\mathcal{I}_0)$, the conditioning in (2.34) can be removed to obtain the unconditional BPF

$$P_f(\lambda) \approx 1 - \int_0^\infty F_Z(\lambda; N_0 + \mathcal{I}_0) f_{\mathcal{I}_0}(\mathcal{I}_0)\, \mathrm{d}\mathcal{I}_0. \tag{2.37}$$

This approximation does not depend on the bin index and only needs to be computed once per threshold λ. Note that this unconditional BPF is not representative for any particular bin, but for the ensemble of bins. Clearly, the assumption of i.i.d. MAI-A variances is an oversimplification of reality. For instance, the variances of two Doppler search bins which are separated by $1/T_0$ are not independent but highly correlated, as we observed using the SSC-D in Fig. 2.7. We argue to use this independence assumption nevertheless as a first-order approximation, because is at least more accurate than the standard SSC model, which the variances as having the same constant

Figure 2.9 – PDF of MAI-A variance for $K-1$ interferers ($E_2 = \cdots = E_K = 1\,\text{Ws}$) for an L1 C/A signal with coherent integration over $N = 20$ code periods. The PDF for a single interferer corresponds to the PDF of the SSC in Fig. 2.8.

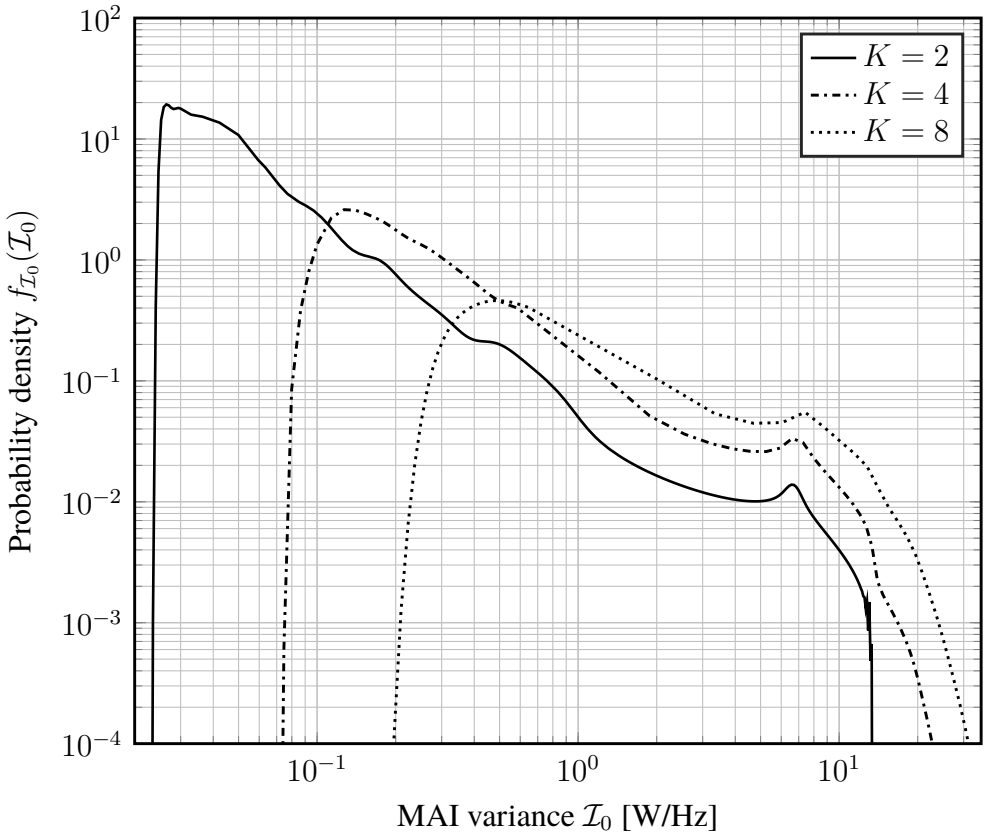

value across all search bins. Simulation results in Section 2.6 suggest that this assumption is reasonably accurate for our purposes.

2.5 Probability of Detection

Let H_1 be the true hypothesis, i.e., the SOI is present. We say that *global detection* occurs if the receiver decides for H_1 and returns the correct bin $i = 1$. The probability of this event is called global probability of detection (GPD). It is denoted by $P_D^{\downarrow}(\lambda)$ for serial search and by $P_D^{\parallel}(\lambda)$ for parallel search, respectively. For serial search, global detection is achieved if the statistics $Z^{(j)}, Z^{(j-1)}, \ldots, Z^{(2)}$ (j denoting the starting index) do not exceed the threshold λ, and $Z^{(1)}$ is greater than the threshold. For parallel search, global detection is achieved if the value of $Z^{(1)}$ is the largest among all statistics, and does exceed the threshold. In Section 2.5.1, we construct a conditional GPD, given the MAI and a set of parameters called noncentrality energies. In Section 2.5.2, the conditioning on these random variables is removed to obtain the overall GPD.

2.5.1 Conditional global probability of detection

We define the ith *noncentrality energy* as the energy that is delivered to the statistic $Z^{(i)}$ in the absence of MAI-A and noise

$$\mathcal{E}^{(i)} \triangleq \sum_{\ell=0}^{L-1} \left| X_1^{(i)}[\ell] \right|^2, \qquad i = 1, \ldots, PQ. \tag{2.38}$$

Ideally, $\mathcal{E}^{(1)} = P_1 LT$ and $\mathcal{E}^{(2)} = \cdots = \mathcal{E}^{(PQ)} = 0$. In practice, this is not the case: energy is lost in the correct bin and can leak into other bins due to various effects. In fact, the noncentrality energies are functions of τ_1, ν_1 and the states of the symbol sequence $\boldsymbol{b}_1 \triangleq [b_1[0], \ldots, b_1[LN]]^T$ during the observation time. Therefore, $\mathcal{E}^{(1)}, \ldots, \mathcal{E}^{(PQ)}$ are statistically dependent random variables. Exemplarily, we determined the marginal distribution of the noncentrality energy $\mathcal{E}^{(1)}$ numerically in Fig. 2.10. It can be shown that (O'DRISCOLL, 2007)

$$\mathcal{E}^{(i)} = \alpha_C\big(\tau^{(i)} - \tau_1\big)\, \beta_C\big(\nu^{(i)} - \nu_1; \vartheta_1 T_0 + \tau_1, \boldsymbol{b}_1\big) P_1 LT, \tag{2.39}$$

with a code-phase correlation function

$$\alpha_C(\tau) = \sum_{i=-\infty}^{\infty} \frac{\rho_h^2(\tau - iT_0)}{T_c^2} \tag{2.40}$$

and a Doppler correlation function

$$\beta_C(\nu; \theta, \boldsymbol{b}) = \frac{T_c^2}{T^2} \frac{\sin^2(\pi\nu T)}{\sin^2(\pi\nu T_c)} \left(1 - \frac{2X(\boldsymbol{b})}{L} \phi(\nu, \theta)\right), \tag{2.41}$$

with the number of symbol transitions $X(\boldsymbol{b}) \in \{0, \ldots, L\}$ and an auxiliary function[5] (O'DRISCOLL, 2007)

$$\phi(\nu, \theta) = \cot^2(\pi\nu T)\big(\tan(\pi\nu T)\sin(2\pi\nu\theta) - 2\sin^2(\pi\nu\theta)\big). \tag{2.42}$$

If a pure pilot signal is considered, we can simplify (2.41) to

$$\beta_C(\nu) \triangleq (T_c/T)^2 (\sin(\pi\nu T)/\sin(\pi\nu T_c))^2. \tag{2.43}$$

The energy loss and leakage effects are illustrated in Figs. 2.10, 2.11, and 2.12. We can see that if the search bin spacings $\Delta\tau, \Delta\nu$ are chosen wider, the peak of the respective correlation function can be missed more easily during the generation of decision statistics. On the other hand, choosing the spacings narrower will lead to a larger number of search bins. This tradeoff is analyzed in

[5] Note that the auxiliary function becomes more complicated if $L > 1$ and $N < M$, a case which is ommitted at this point for brevity but is treated in the thorough work of O'Driscoll (O'DRISCOLL, 2007).

more detail in (GEIGER; VOGEL, 2014). In this work, we leave the spacings as parameters. However, from a practical viewpoint, they should be selected such that tracking can be initiated in case the signal is declared present in bin $i = 1$ (i.e., if global detection occurs). More specifically, the intervals $(-\Delta\tau/2, \Delta\tau/2)$ and $(-\Delta\nu/2, \Delta\nu/2)$ should lie within the tracking loops' *pull-in range* (TEUNISSEN; MONTENBRUCK, 2017).

Figure 2.10 – PDF of the energy loss in the correct bin with code-phase spacing $\Delta\tau = T_c$ and Doppler spacing $\Delta\nu = 1/T$, for a REC pulse and pure pilot signaling ($\boldsymbol{b} = \mathbf{1}$).

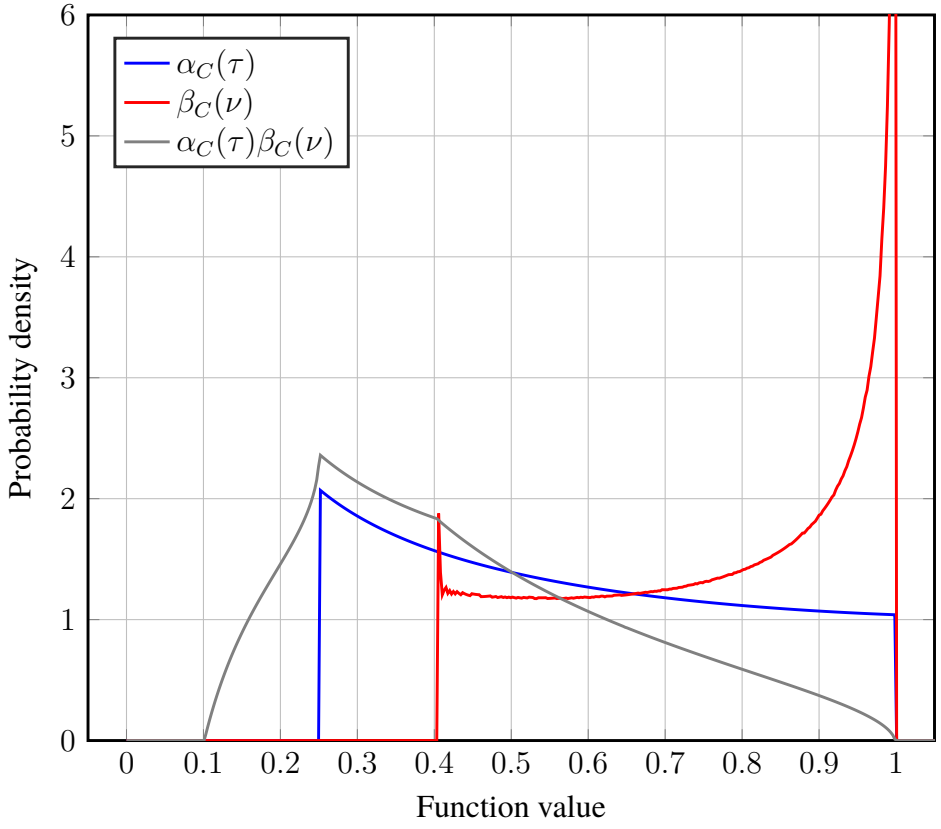

Unlike MAI-A and noise, the contribution of the SOI to the statistic $Z^{(i)}$ is not Gaussian distributed. As proposed by (O'DRISCOLL, 2007), we model this contribution by modifying the central χ^2-distribution from (2.17) to a noncentral χ^2-distribution with random noncentrality parameter (hence, a compound probability distribution). MAI-A and noise are the same as under H_0 and can be modeled by an effective noise floor $\mathcal{N}_0^{(i)}$, using one of the previously discussed interference models (2.20), (2.23), (2.28), or (2.35). Adding the noncentral component to (2.17) leads to the generic CDF of $Z^{(i)}$ under H_1, given $\mathcal{E}^{(i)}$ and $\mathcal{N}_0^{(i)}$,

$$F'_Z\left(z; \mathcal{E}^{(i)}, \mathcal{N}_0^{(i)}\right) \triangleq 1 - Q_L\left(\sqrt{2\frac{\mathcal{E}^{(i)}}{\mathcal{N}_0^{(i)}}}, \sqrt{2\frac{z}{\mathcal{N}_0^{(i)}}}\right), \; z \geqslant 0. \tag{2.44}$$

$Q_L(\cdot,\cdot)$ denotes the Lth order Marcum Q-function (MARCUM, 1960). This CDF is a scaled

Figure 2.11 – Correlation vs. code-phase for various pulse shapes: rectangular (REC), binary offset carrier (BOC), root raised cosine (RRC, with zero roll-off).

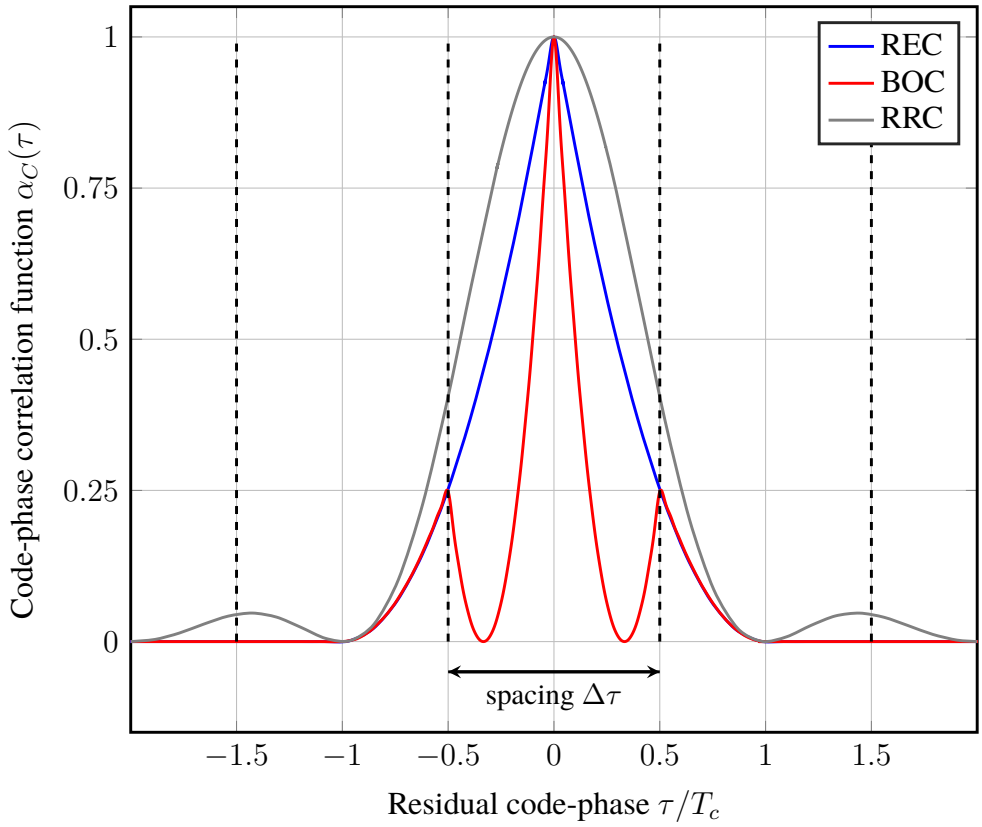

version of the CDF of a noncentral χ^2-distribution with $2L$ degrees of freedom and noncentrality parameter $2\mathcal{E}^{(i)}/\mathcal{N}_0^{(i)}$. The according conditional bin probability of detection (BPD) is

$$P_d^{(i)}(\lambda) \approx 1 - F_Z'\left(\lambda; \mathcal{E}^{(i)}, \mathcal{N}_0^{(i)}\right). \tag{2.45}$$

This probability can be viewed as a compound probability in $\mathcal{E}^{(i)}$ and, if the randomized SSC is used, in $\mathcal{N}_0^{(i)}$.

Next, we compute the conditional GPD, given the vector of all noncentrality energies $\boldsymbol{\mathcal{E}} \triangleq [\mathcal{E}^{(1)}, \ldots, \mathcal{E}^{(PQ)}]^T$ and the vector of effective noise floors $\boldsymbol{\mathcal{N}}_0 \triangleq [\mathcal{N}_0^{(1)}, \ldots, \mathcal{N}_0^{(PQ)}]^T$. Standard formulas (BORIO, 2008) lead to the following results for serial or parallel search

$$P_D^{\downarrow}\big|\boldsymbol{\mathcal{E}}, \boldsymbol{\mathcal{N}}_0 = \frac{1 - F_Z'\left(\lambda; \mathcal{E}^{(1)}, \mathcal{N}_0^{(1)}\right)}{PQ} \sum_{j=1}^{PQ} \prod_{i=2}^{j} F_Z'\left(\lambda; \mathcal{E}^{(i)}, \mathcal{N}_0^{(i)}\right) \tag{2.46}$$

$$P_D^{\shortparallel}\big|\boldsymbol{\mathcal{E}}, \boldsymbol{\mathcal{N}}_0 = \int_{\lambda}^{\infty} f_Z'\left(z; \mathcal{E}^{(1)}, \mathcal{N}_0^{(1)}\right) \prod_{i=2}^{PQ} F_Z'\left(z; \mathcal{E}^{(i)}, \mathcal{N}_0^{(i)}\right) \mathrm{d}z, \tag{2.47}$$

as long as we condition on $\boldsymbol{\mathcal{E}}$ and $\boldsymbol{\mathcal{N}}_0$. It remains to remove the conditioning on these parameters.

To simplify computation of the above equations, we assume $\mathcal{E}^{(i)} \approx 0$ if $|\tau^{(i)} - \tau_1| > T_c$ and $|\nu^{(i)} - \nu_1| > 3/(2T)$. Therefore, apart from the the correct bin and some few adjacent bins, most bins are treated as central χ^2-distributed.

Figure 2.12 – Correlation vs. Doppler, with symbol boundaries in the middle of L coherent subintervals ($\theta = T/2$). The number of symbol transitions is $X(\boldsymbol{b}) \in \{0, 1, \ldots, L\}$.

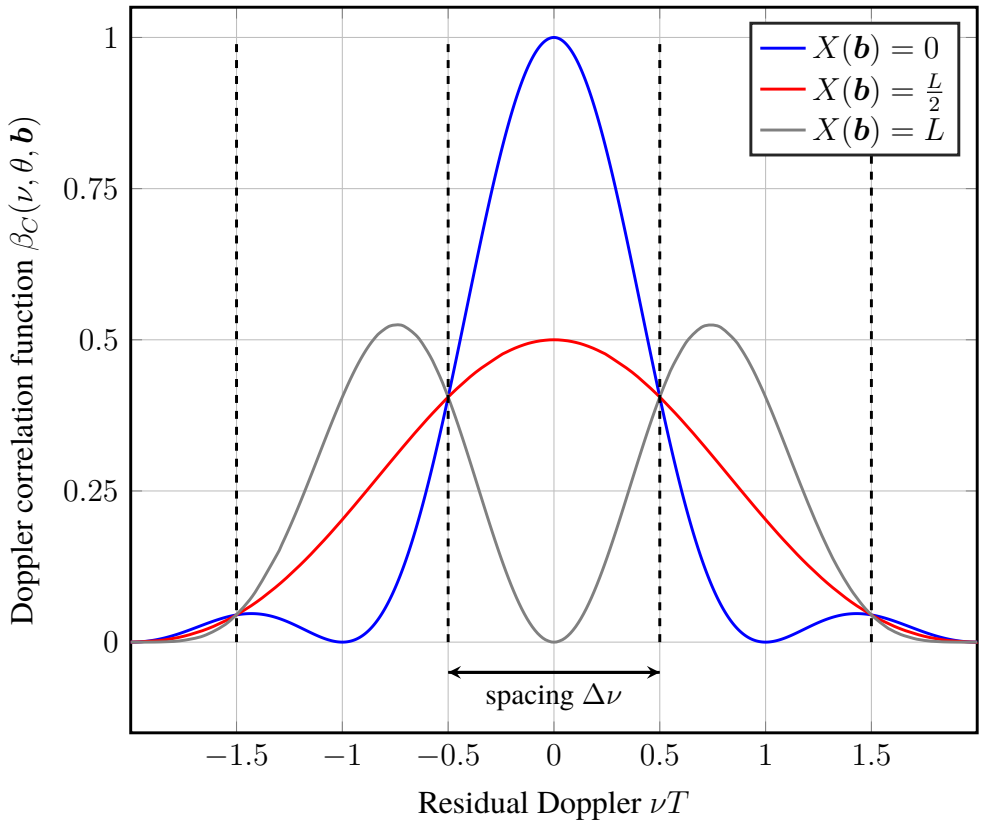

2.5.2 Removing the conditioning

Starting from the conditional GPD (2.46) or (2.47), respectively, we remove the conditioning as follows:

1. Apply a MAI-A model to remove the conditioning on $\boldsymbol{\mathcal{N}}_0$:
   - To neglect MAI-A (or use the standard SSC), simply set $\mathcal{N}_0^{(i)} = N_0(+I_0)$ for $i = 1, \ldots, PQ$.
   - To use the SSC-R, apply the law of total probability w.r.t. $\boldsymbol{\mathcal{N}}_0$: replace the conditional CDF $F'_Z\big(z; \mathcal{E}^{(i)}, \mathcal{N}_0^{(i)}\big)$ by the partly conditional CDF

$$F'_Z\big(z; \mathcal{E}^{(i)}\big) \triangleq \int_0^\infty F'_Z\big(z; \mathcal{E}^{(i)}, N_0 + \mathcal{I}_0\big) f_{\mathcal{I}_0}(\mathcal{I}_0)\, \mathrm{d}\mathcal{I}_0 \tag{2.48}$$

   for all bins. For parallel search and $i = 1$, replace the conditional PDF with $f'_Z\big(z; \mathcal{E}^{(1)}\big) \triangleq \frac{\mathrm{d}}{\mathrm{d}z} F'_Z\big(z; \mathcal{E}^{(1)}\big)$.
2. Remove the conditioning on $\boldsymbol{\mathcal{E}}$ directly by averaging over the random SOI parameters τ_1, ν_1 and all possible symbol sequences $\boldsymbol{b}_1$,[6] using (2.39) as in (O'DRISCOLL, 2007).

[6] There are $(L+1)M$ possible symbol sequences, as $\boldsymbol{b}$ can be parameterized in terms of the number of symbol

2.6 Numerical Results

Figure 2.13 – Bin probabilities vs. threshold for Scenarios 1 (balanced) and 2 (near-far) with baseline setup ($N_c = 341, T = 1$ ms). Markers represent simulation results.

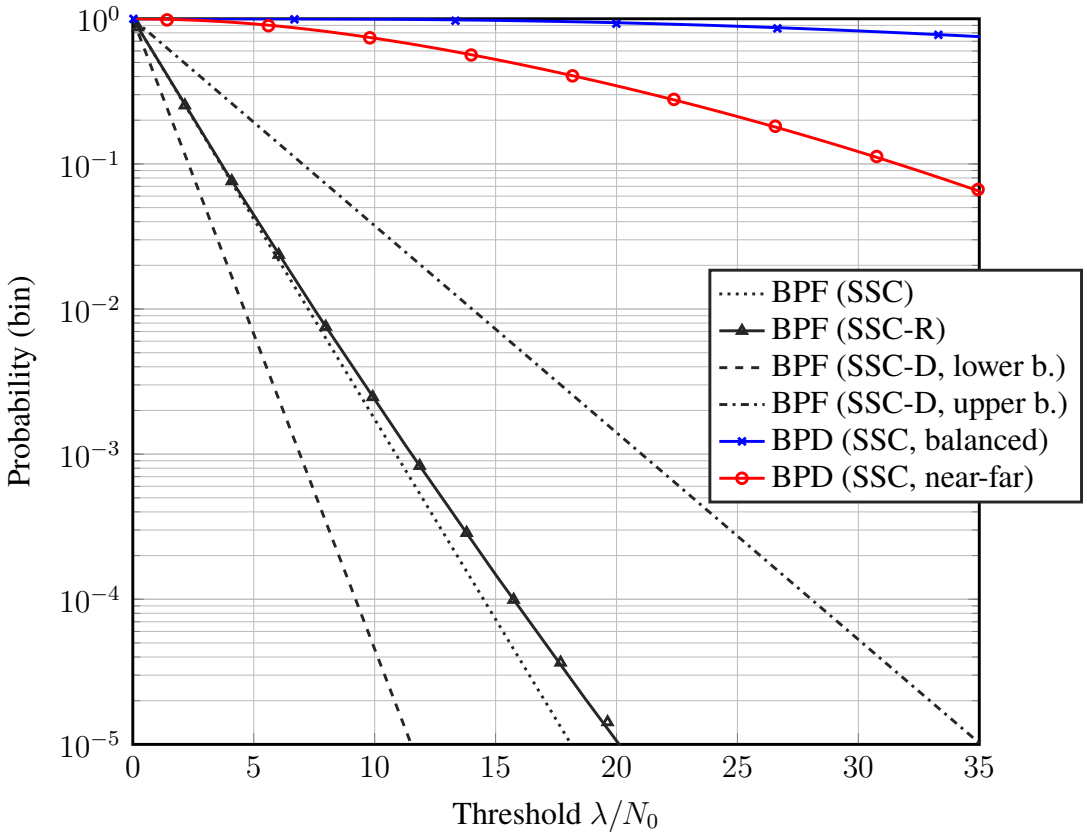

Unless stated otherwise, the following baseline setup is used for the simulations.

- REC pulse, chip rate $1/T_c = 1.023$ MHz;
- symbol rate $1/T_b = 0$ (pure pilot);
- code length $N_c = 341 \Rightarrow$ code period $T_0 = 0.33$ ms;
- coh. integration time $T = 1$ ms $\Rightarrow N = 3$ code periods;
- number of noncoherent summations $L = 1$;
- Doppler span $F_0 = 8$ kHz;
- number of satellites $K = 8$;
- noise floor $N_0 = -204$ dBW/Hz;
- code-phase spacing $\Delta\tau = T_c$;
- Doppler spacing $\Delta\nu = 1/T$.

This setup leads to $PQ = 341 \times 8 = 2728$ bins. Furthermore, we consider three characteristic

transitions $X(\boldsymbol{b}) \in \{0, \ldots, L\}$ and the uniformly random initial symbol-phase $\vartheta_1 \in \{1, \ldots, M\}$. If $L > 1$, $X(\boldsymbol{b})$ follows a binomial distribution with L trials and success probability $1/2$.

scenarios, which are represented by three different power profiles $(P_1, \ldots, P_K)$:

1. *Balanced scenario*: maximum received power (EUROPEAN..., 2016) for all satellites: $P_k = -153\,\text{dBW}$ for $k = 1, \ldots, K$.
2. *Near-far scenario*: maximum received power for $k = 2, \ldots, K$, minimum received power (EUROPEAN..., 2016) for the SOI: $P_1 = -158.5\,\text{dBW}$.
3. *Weak signals scenario*: typical indoor received power: $P_k = -180\,\text{dBW}$ for $k = 1, \ldots, K$.

As per definition, $P_1 = 0$ always under H_0. Note that the power profiles of Scenarios 1 and 2 are within system specifications (EUROPEAN..., 2016), while GNSS are usually not committed to service in weak signal conditions such as Scenario 3. However, C/A signals are of some interest for navigation indoors or even in space (WALLNER, 2017).

2.6.1 Baseline Setup

Figure 2.14 – Global probabilities vs. threshold for Scenarios 1 (balanced) and 2 (near-far) with baseline setup ($N_c = 341, T = 1\,\text{ms}$). Solid lines: SSC-R, dotted lines: SSC, markers: simulation results. $PQ = 341 \times 8$ bins.

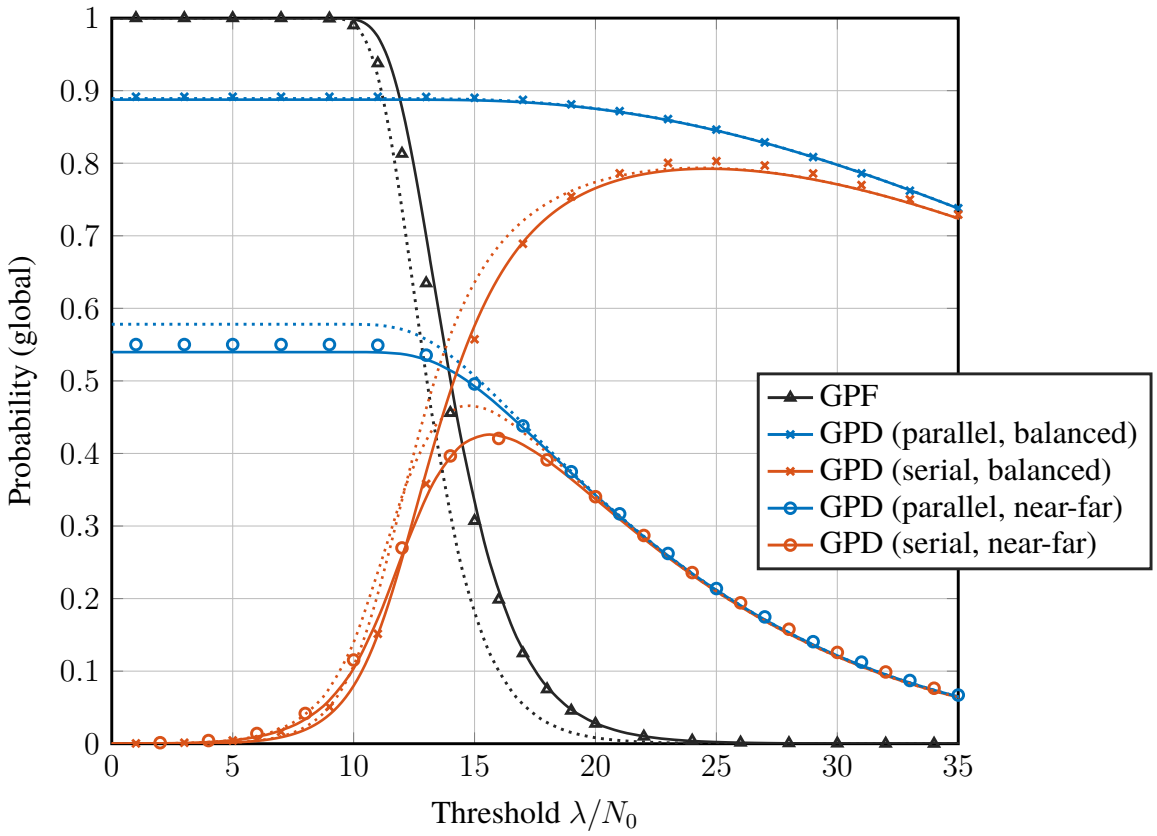

The BPF that is obtained with the baseline setup for Scenarios 1 and 2 is shown in Fig. 2.13. Note that there is not *one* BPF but many, depending on the bin's effective noise floor.

The simulation results (markers) were obtained by Monte-Carlo simulations, randomly selecting one of the PQ bins and determining its BPF. The BPF obtained with the SSC-R is representative not for any particular bin, but for the ensemble of bins, and matches well with the simulation results. The standard SSC leads to a slight underestimation of the BPF. For the SSC-D, only the BPF of the bin with the highest and lowest effective noise floor are shown. It is interesting to note that the BPFs under SSC and SSC-D appear as straight lines in a semilogarithmic plot, as the BPF for $L = 1$ is an exponential function (2.17) of the threshold. By contrast, the SSC-R leads to a compound (mixture) BPF and appears as a slightly curved line. For the BPD in bin $i = 1$, all SSC models lead to essentially the same results.

Figure 2.15 – ROC curve for Scenarios 1 (balanced) and 2 (near-far) with baseline setup ($N_c = 341, T = 1$ ms). Solid lines: SSC-R, dotted lines: SSC, markers: simulation results. $PQ = 341 \times 8$ bins.

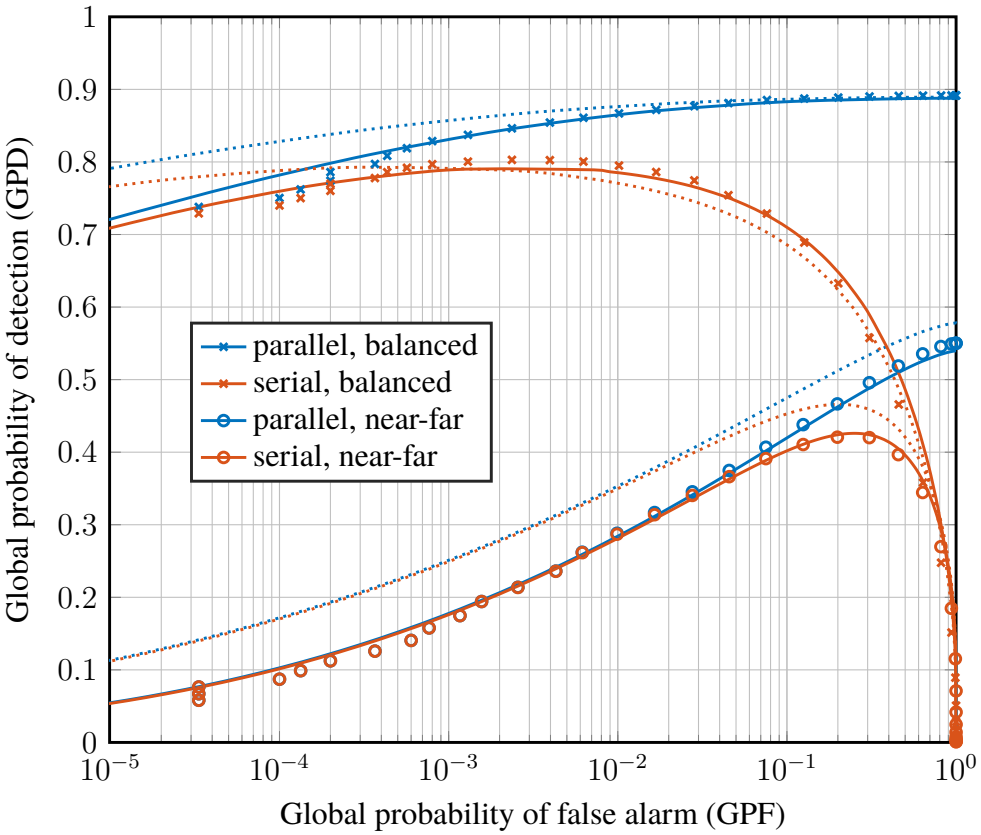

Fig. 2.14 shows the global probabilities $P_F(\lambda), P_D^{\parallel}(\lambda), P_D^{\downarrow}(\lambda)$ as a function of the threshold, for Scenarios 1 and 2. As these scenarios differ only in terms of the SOI power, $P_F(\lambda)$ is the same in either case, while detection is less likely in the near-far scenario. It can be observed that the standard SSC underestimates the GPF and slightly overestimates the GPD for all thresholds, while the SSC-R is in line with results from Monte-Carlo simulations. Plotting

Figure 2.16 – BPF vs. threshold for Scenarios 1 (balanced) and 2 (near-far) with varying number N of code periods per coherent integration. Markers represent simulation results.

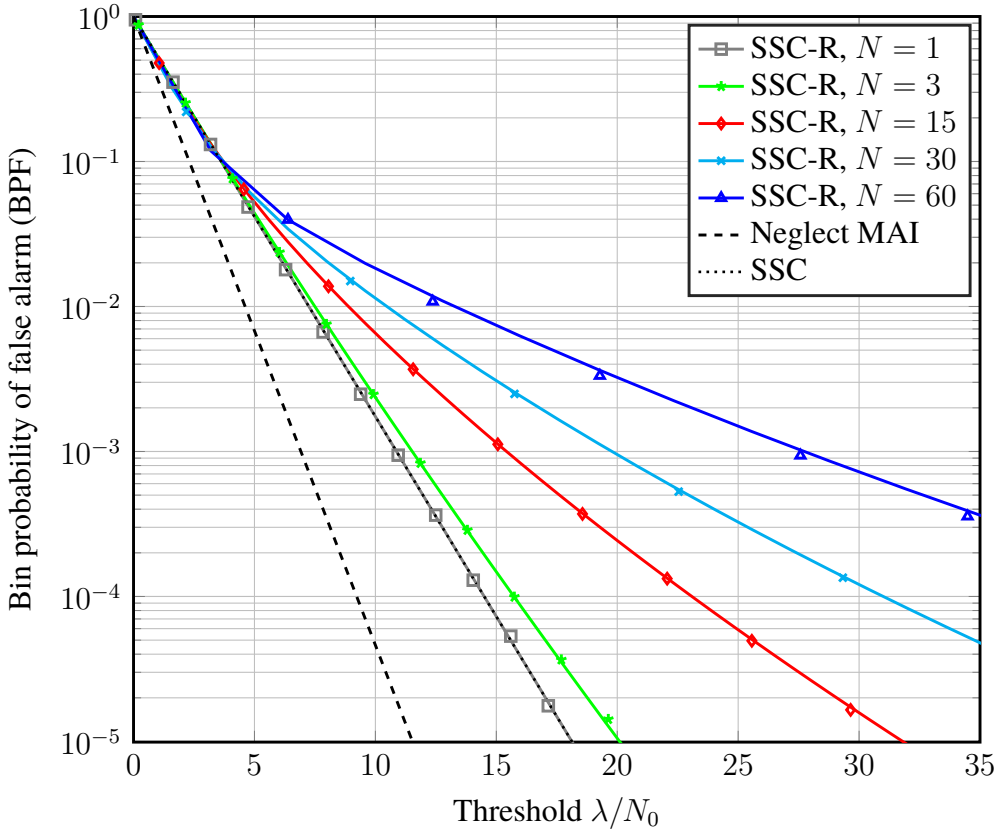

the GPD against the GPF, with the threshold $0 \leqslant \lambda < \infty$ as the varying parameter, leads to the *ROC curve* in Fig. 2.15. The receiver can operate at any point on the ROC curve by choosing the threshold accordingly.

2.6.2 Increasing the coherent integration time T

Increasing the coherent integration time is a good receiver side solution to enhance the acquisition reliability, especially in a near-far scenario. This leads to a proportional increase of the number of Doppler bins Q, while the number of code-phase bins P remains constant. As the code length N_c and code period T_0 remain fixed, the receiver performs coherent integration over multiple code periods N. Increasing N reveals the great weakness of the standard SSC: it depends only on T but not on $N = T/T_0$. Thus, for large values of N, the BPF is grossly underestimated by the standard SSC, but correctly modeled by the SSC-R, as is shown in Fig. 2.16. The standard SSC also leads to a very overoptimistic ROC for $T = 5\,\text{ms}$ and $N = 15$ in Fig. 2.17.

Figure 2.17 – ROC for Scenario 2 (near-far) with extended coherent integration time, $N_c = 341, T = 5\,\text{ms}, N = 15$. Solid lines: SSC-R, dotted lines: SSC, markers: simulation results. $PQ = 341 \times 40$ bins.

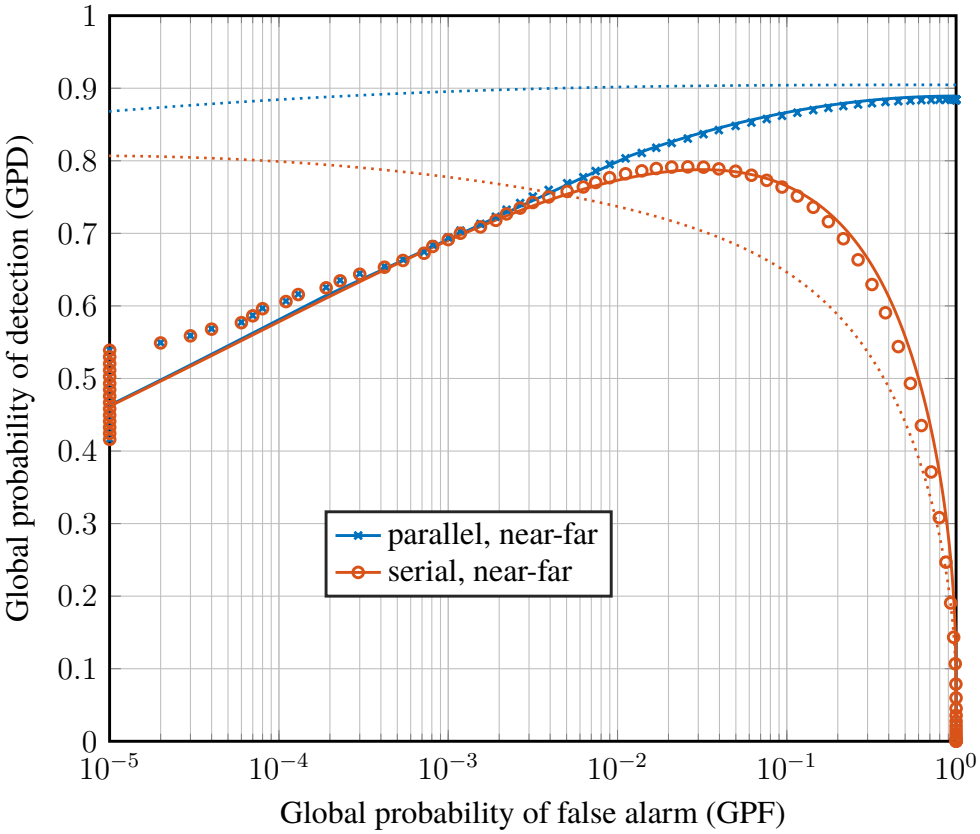

2.6.3 Increasing the number of noncoherent summations L

For weak signals such as in Scenario 3, a good option to enhance reliability further is to increase the number of noncoherent summations L. Increasing the coherent integration time T further and further would lead to an excessive number of Doppler bins, and is also difficult due to limitations of the receiver clock stability. Using more than $T = 20\,\text{ms}$ (hence $N = 60$ in this case) is usually not practical. In Fig. 2.18, we show the ROC for $N = 60$ and $L = 1, 5, 10, 20, 30$. It can be observed that despite the large value of N, the standard SSC is already accurate (and virtually coincides with the SSC-R). This is due to the very low relative threshold λ/N_0 at the relevant operating points. As could be observed from Fig. 2.16, SSC and SSC-R lead to similar results as long as the ratio λ/N_0 is small.

2.7 Application: Galileo C/A signal with minimum PRN code length

As an application example of the proposed methodology, we consider the design of a C/A signal for the European GNSS Galileo. This signal would complement the existing Galileo

Figure 2.18 – ROC for Scenario 3 (indoor) with $N = 60$ coherent integrations and L noncoherent summations. Solid lines: SSC, markers: simulation results. $PQ = 341 \times 160$ bins.

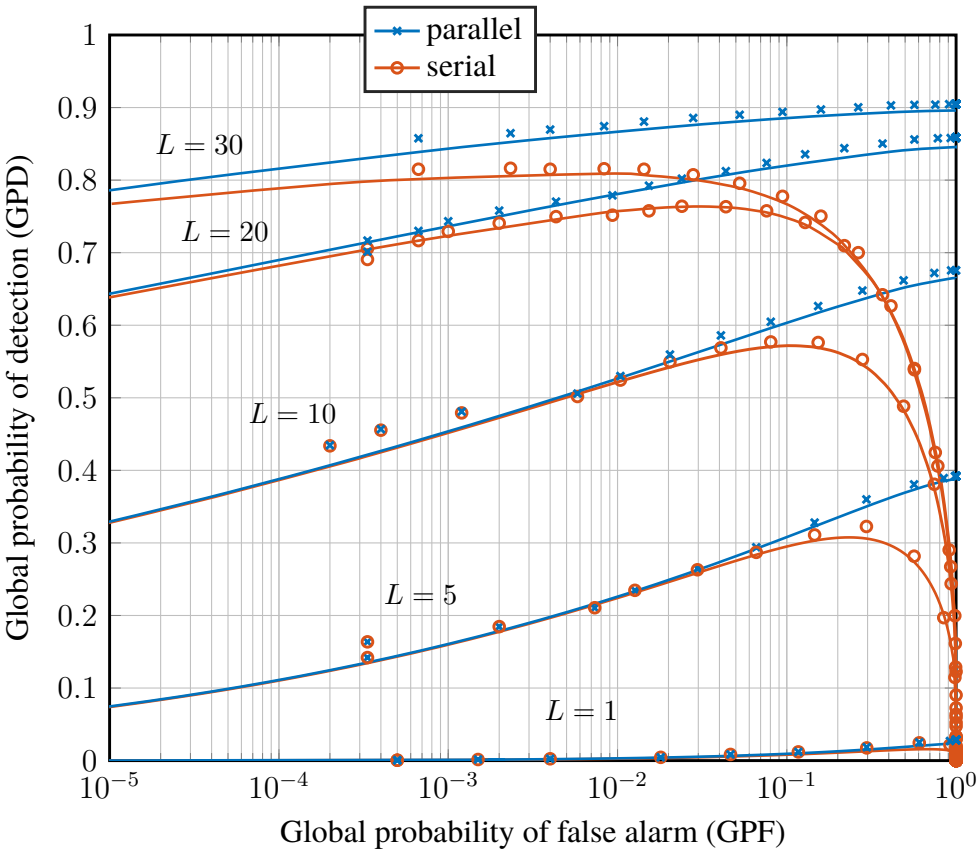

OS signals E1-B and E1-C transmitted at 1575.42 MHz and will be called E1-D in the following. E1-B and E1-C use a PRN code length of $N_c = 4092$, which is why we consider integer divisors $N_c = 2046, 1023, 682, 372, \ldots$ as possible E1-D code lengths: this would allow for an easier handover from the C/A signal to the signals with longer PRN code (WALLNER *et al.*, 2020). In terms of symbol rate, we consider the two options of a "pure pilot" signal with zero symbol rate, and a low-rate "quasi-pilot" signal with symbol duration $MT_0 = 20$ ms. The pulse shape is REC. We aim to minimize the PRN code length over the set of integer divisors of 4092, while ensuring that the target reliability of $P_D^{\|}(\lambda) > 80\%$, $P_F(\lambda) < 5\%$ can be achieved for some $\lambda \geq 0$. The coherent integration time is $T = 4$ ms with $L = 1$ and interferers $k = 2, \ldots, 8$ are received with maximum power $P_k = -153$ dBW.

In Fig. 2.19 (presented at (ENNEKING; ANTREICH; ALMEIDA, 2020)), we show the *sensitivity*, i.e., the necessary received power P_1 at which reliable acquisition is possible. We can observe that the standard SSC is accurate only if $T = T_0$ and is therefore of no use for this application. For a PRN code length to be feasible, the sensitivity should not be above the nominal minimum received power level of -158.5 dBW (EUROPEAN..., 2016). As a

result, we suggest the minimum code length of $N_c = 341$ for a pure pilot signal or, alternatively, $N_c = 682$ for a 50 Hz quasi-pilot signal. The slightly worse sensitivity of a 50 Hz quasi-pilot signal compared with a pure pilot is due to the symbol bit transititons that occasionally lead to an energy loss. Nevertheless, with regard to computation of a pseudorange or handover to other signal components, it may be reasonable to prefer a quasi-pilot signal as opposed to a pure pilot: the symbol sequence can serve as a means to resolve ambiguities arising from the short period of the PRN code.

The final design options for E1-D are presented in Table 2.2. We present the ROC performance, as well as the dimension of the search grid for a coherent integration time of $T = 4$ ms. The proposed options are compared to GPS L1 C/A and to the Galileo E1 OS, which is currently the Galileo signal with the "shortest" PRN code. E1-D would offer a complexity reduction by a factor of 18-36 as compared to E1 OS, and by a factor of 1.5-3 as compared to L1 C/A.

Figure 2.19 – Sensitivity (received power level at which reliable acquisition with $P_D^{\|}(\lambda) > 80\%$, $P_F(\lambda) < 5\%$ is still possible) for Galileo C/A signal candidates, shown as a function of PRN code length. The options of a quasi-pilot (50 Hz symbol rate) and a pure pilot (0 Hz symbol rate) are considered. The proposed signal designs and GPS L1 C/A are indicated. Solid lines: SSC-R, dotted lines: SSC, markers: simulation results.

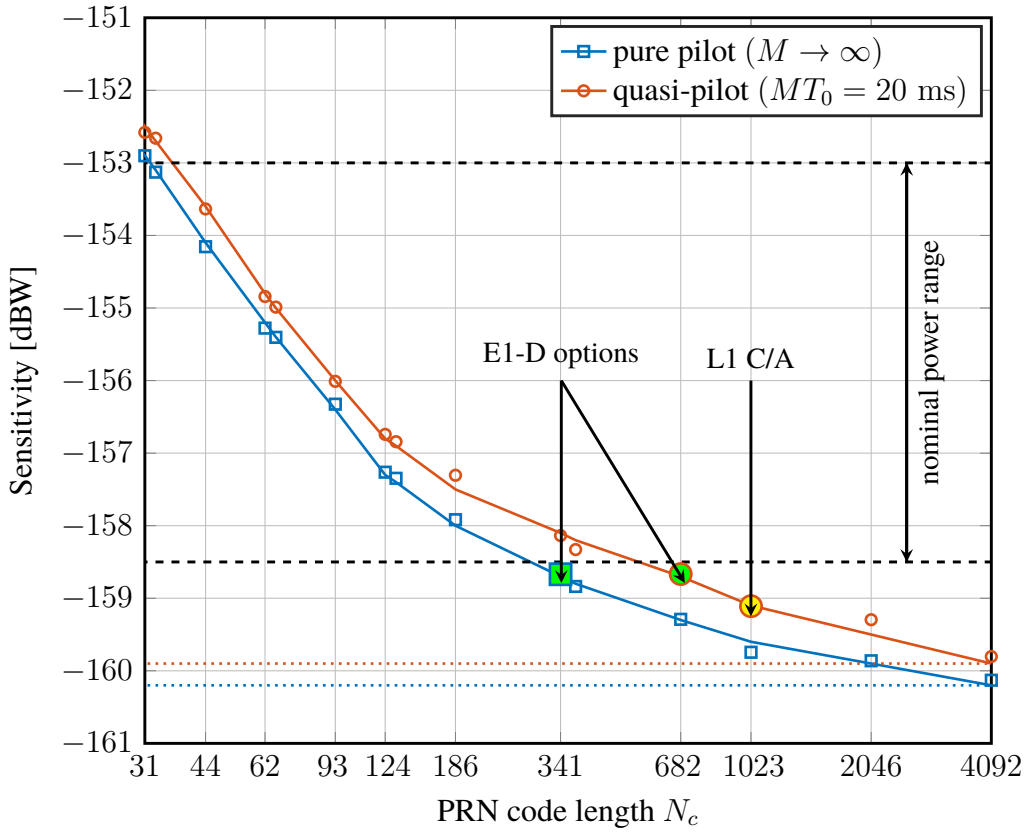

Table 2.2 – Final design options: E1-D pure pilot (PP), E1-D quasi-pilot (QP) compared with L1 C/A in terms of coherent integration time, number of Doppler (Q) and code-phase (P) bins, symbol rate, and GPD/GPF.

Signal	T	Q	P	PQ	$1/T_b$	GPD / GPF
L1 C/A	4 ms	32	1023	32 736	50 Hz	82% / 5%
E1-D PP	4 ms	32	341	10 912	0 Hz	82% / 5%
E1-D QP	4 ms	32	682	21 824	50 Hz	81% / 5%
E1 OS	4 ms	32	4092×3 [7]	392 832	250 Hz	66% / 5%

[7] The code-phase spacing $\Delta\tau$ should be reduced by a factor of 3 to reduce the probability of energy loss due to the narrower peak of the BOC-autocorrelation function (cf. Fig. 2.11).

3 IMPROVED MODELS FOR RADIO FREQUENCY COMPATIBILITY

We begin with a general overview on methodologies for RFC modeling and assessment in Section 3.1, where we identify the potential inaccuracies of the conventional methods. In Section 3.2, we compare the state of the art with our contributions. In Section 3.3, we define the system model, consisting of the received signal, the generation of complex correlator outputs, and the generation of fine code-/carrier-phase estimates. In Sections 3.4 and 3.5, we discuss the improved RFC assessment methodologies based on two Gaussian approximations. Numerical results are presented and discussed in Section 3.6.

3.1 Overview

GNSSs rely on DS-CDMA to allow simultaneous broadcast of multiple signals by multiple satellite constellations in a common frequency band. Inherently, this is a form of asynchronous DS-CDMA, because signals have different code-phases at the user antenna. Therefore, while they can be uncorrelated, they can never be fully orthogonal, such as in the case of synchronous DS-CDMA (PROAKIS, 2001). Instead, a controlled level of MAI is experienced by each user. As of today, the effect of MAI on GNSS receivers is much more subtle than perturbances caused by multipath propagation or the ionosphere, for which correction algorithms are commonly used (TEUNISSEN; MONTENBRUCK, 2017). By contrast, only very few receivers take the effort to cancel or suppress MAI (ENNEKING *et al.*, 2012), while most treat MAI as noise.

The ITU regulates that RFC must be ensured before the launch of a new GNSS signal, meaning that receiver functionalities must not be harmed significantly by the additonal MAI. Besides the signal acquisition (i.e., coarse synchronization with the SOI), important receiver functionalities include data demodulation and the fine synchronization to the SOI's code-phase and carrier-phase. These functionalities are essential to compute accurate pseudoranges. While the data demodulation and carrier-phase estimation is performed based on the output of a single ("prompt") correlator, code-phase estimation is based on two additional correlators (early, late) (KAPLAN; HEGARTY, 2005).

Assuming that transmit powers will be further raised by system operators or that more signals will be launched, these functionalities may be limited by MAI rather than noise. Therefore, it is worthwile to review and refine the models that have been used to ensure RFC. A conservative performance analysis of code-phase and carrier-phase estimation accuracy is of

particular interest for integrity modeling of safety-critical services such as space-based or ground-based augmentation systems (RTCA, Inc., 2008; DAUTERMANN *et al.*, 2012). Especially, new C/A-type signals such as discussed in Chapter 2 may not be radio frequency compatible with existing signals in the relevant frequency bands. For instance, there is currently discussion at which carrier frequency to transmit the forthcoming Galileo C/A signal E1-D (WALLNER *et al.*, 2020).

3.1.1 Conventional RFC modeling

In the following, we briefly explain the most common approach to model the effect of intra- and intersystem interference on RFC. While there do exist more accurate state of the art models, the following methodology is used in accordance with the ITU-Recommendation M.1831 (ITU-R, 2015). For the sake of a clearer presentation, we break M.1831 down to the essential mathematics on signal processing level, and neglect the more involved orbital propagation model and transmitter/receiver antenna gains.

In the presence of an interfering signal $k \neq 1$ with PSD $\Phi_k(f)$, the signal-to-interference ratio (SIR) observed at the correlator output of a desired signal $k = 1$ with PSD $\Phi_1(f)$ is computed as the product of three factors: the ratio of desired to interfering power

$$\frac{C_1}{C_k} = \frac{\int_{-\infty}^{\infty} \Phi_1(f)\,\mathrm{d}f}{\int_{-\infty}^{\infty} \Phi_k(f)\,\mathrm{d}f}, \tag{3.1}$$

the coherent integration time T, and the inverse of the SSC

$$\psi_k^{(1)} = \frac{\int_{-\infty}^{\infty} \Phi_1(f)\Phi_k(f)\,\mathrm{d}f}{\int_{-\infty}^{\infty} \Phi_1(f)\,\mathrm{d}f \int_{-\infty}^{\infty} \Phi_k(f)\,\mathrm{d}f}, \tag{3.2}$$

which is calculated as the inner product of the normalized PSDs of desired and interfering signal. It is a reciprocal measure for the MAI between the two signals 1 and k, so that subscript and superscript could be interchanged (whenever the signal of interest is clear from the context, we may choose to omit the superscript "1"). It is maximized for the case of matched-spectrum interference (TEUNISSEN; MONTENBRUCK, 2017), which would lead to the self-SSC as used in Chapter 2. Thus we have

$$\mathrm{SIR} = \frac{C_1\,T}{C_k\,\psi_k^{(1)}}. \tag{3.3}$$

In the additional presence of AWGN, we simply add the noise floor N_0 to the denominator of (3.3) to obtain the SINR

$$\mathrm{SINR} = \frac{C_1\,T}{N_0 + C_k\,\psi_k^{(1)}}. \tag{3.4}$$

For more than one interferer, all interferers are represented by a single AWGN-equivalent in units of W/Hz, given by the *aggregate interference PSD* $I_0 \triangleq \sum_{k \neq 1} C_k \psi_k^{(1)}$ (ITU-R, 2015). With the SIR or SINR (or effective carrier-to-noise density ratio (C/N_0) or other derivative parameters) as a single figure of merit, standard formulas for noise performance can then be used to calculate the code-/carrier-phase estimation accuracy or other performance measures (e.g., symbol/bit error rate).

3.1.2 Problems with the conventional model

The authors of ITU-R M.1831 are well aware that the above conventional model may not be accurate, especially for C/A-type signals. They describe this difficulty from a frequency domain perspective as follows (ITU-R, 2015):

The analytical model (…) approximates the spectrum of the received signals as an aggregate spectrum, where the fine structures of individual signal spectra are averaged together into an essentially continuous spectrum. This "continuous spectrum" modelling is valid for RNSS[1] *signals with long PRN codes. (…) However, this model is not appropriate for analysis of short PRN codes within an RNSS system, or between RNSS systems. In those cases, dynamic modelling is necessary to account for the detailed modulation properties of the signals, such as data rate and PRN code characteristics, as well as relative Doppler frequency shift and relative received signal power.*

We summarize the mismatched assumptions of the conventional approach in the following.

- Usually, perfectly aperiodic code is assumed for the PRN sequence (which is an idealization), so that the ***smooth* PSD** resulting from the pulse shape can be used: with aperiodic code and pulse shape Fourier transform $H(f)$, the PSD would be given simply by $\phi(f) \propto |H(f)|^2$. Examples for such smooth PSDs are given in Fig. 3.1. However, when the deterministic periodic PRN codes of the signals in space (EUROPEAN…, 2016; BeiDou…, 2017a; BeiDou…, 2017b; BeiDou…, 2018; BeiDou…, 2020; NAVSTAR…, 2020b; NAVSTAR…, 2020a; NAVSTAR…, 2020c) are taken into account, all GNSS signals show fine spectral features, as shown in Fig. 3.2. It is left unclear by (ITU-R, 2015) with which level of detail the PSDs should be modeled.

[1] The generic term used by the ITU for global or regional navigation satellite systems is radionavigation-satellite system (RNSS).

- It is assumed that GNSS signals are, like noise, **Gaussian** random processes. As a BPSK signal with squarewave pulse shape can essentially assume two values, this approximation is mismatched at least prior to correlation.
- It is assumed that GNSS signals, like complex baseband noise, are ***proper***, i.e., second-order circularly-symmetric (LAPIDOTH, 2017). The difference between proper and *improper* symbol modulations is illustrated in Fig. 3.3. A BPSK modulation with a real pulse shape is *maximally improper*, since its support reduces to a line in the complex plane. Interplexing schemes of multiple BPSK signal components do also not lead to a proper modulation, in general. However, the QPSK interplex signals mentioned in Section 1.1.2 are indeed proper.
- The conventional approach models each GNSS signal as a **WSS** random process. However, like most modulated signals, GNSS signals are actually WSCS owing to the repeating PRN code and due to the modulation with a pulse shape (GARDNER; NAPOLITANO; PAURA, 2006).
- It is implied that the SINR can be representative for the performance of all receiver functionalities. However, the SINR (or SIR) is defined at the output of a single correlator. While this correlator output is used for data demodulation and carrier-phase synchronization, the code-phase estimation is based on two correlator outputs (often narrowly spaced in the code-phase domain, hence correlated) (KAPLAN; HEGARTY, 2005).

The CSG assumption is often justified by the intuitive argument that for many asynchronous BPSK signals with random relative code- and carrier-phases, and with approximately the same power, can be approximated as CSG owing to the central limit theorem (BETZ, 2001b; TITUS *et al.*, 2003; ITU-R, 2015). The WSS model may be justified by the fact that spreading codes are very long or have additional secondary code. However, it is unclear just how long the codes should be, or how many satellites there should be, in order for these approximations to be valid. Also, the WSS/CSG model is not at all suited for performance analysis in near-far scenarios (LOPEZ-RISUENO; SECO-GRANADOS, 2005). For a thorough analysis of MAI, the wide-sense cyclostationarity and non-circularity of the GNSS signals should be taken into account.

Figure 3.1 – PSDs of L1 C/A (REC) and E1-C (MBOC) under the aperiodic PRN code assumption, and typical thermal noise floor of AWGN.

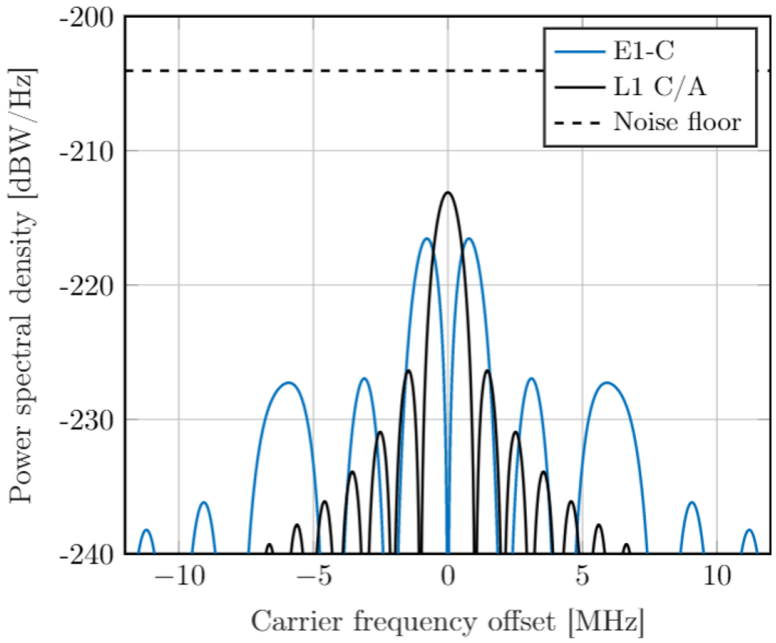

Figure 3.2 – Fine PSD features of Galileo and GPS civil signal components in the upper L-band, calculated with Eqs. (3.12)-(3.14). The displayed frequency range and PRN selection are exemplary.

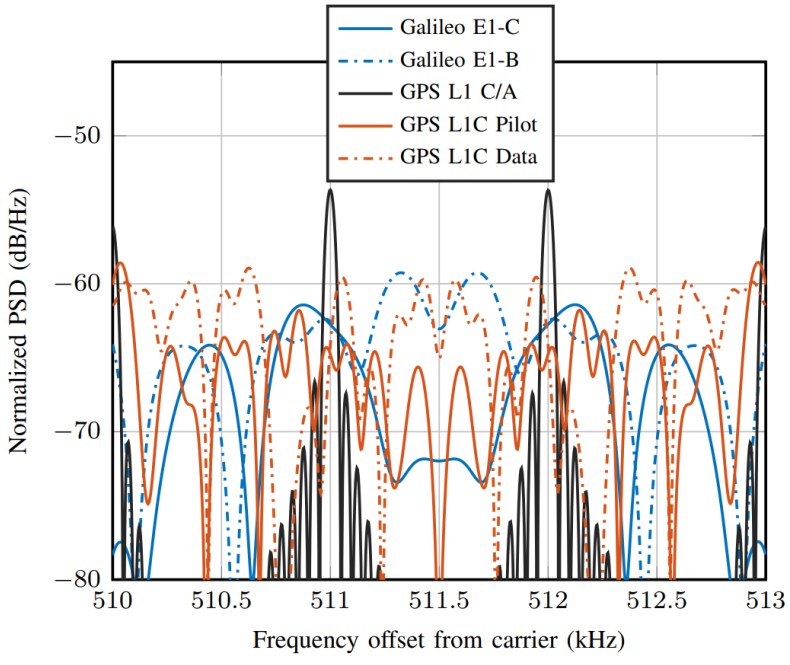

Figure 3.3 – Illustration of a proper and an improper symbol modulation.

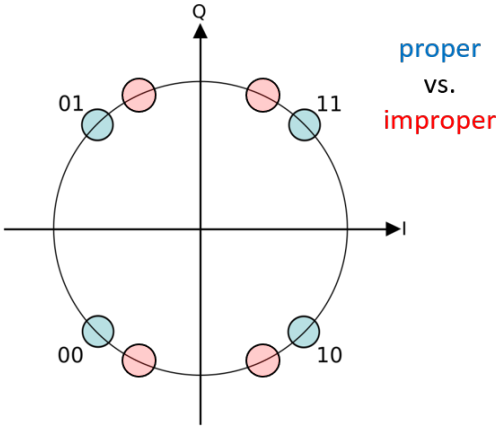

3.2 State of the art and contributions

It was pointed out by Betz (BETZ; KOLODZIEJSKI, 2009a; BETZ; KOLODZIEJSKI, 2009b) that the SSC in its basic form is not suited to assess RFC in terms of code-phase estimation accuracy, except if the interference is not only WSS/CSG but also white within the receiver front-end bandwidth. A more accurate analysis is obtained if, rather than the prompt correlator SIR, the joint early and late correlator statistics are taken into account: Betz provided expressions for the code-phase estimation variance for an arbitrary correlator spacing, as well as for infinitesimally small correlator spacing (*code-tracking SSC*).

So far, one of the most accurate models for the effect of intra-/intersystem interference, with one or more involved C/A-type signals, has been proposed by O'Driscoll and Fortuny-Guasch (O'DRISCOLL; FORTUNY-GUASCH, 2012). The authors propose a model for the SINR or derivative measures thereof, as well as for the code-phase estimation accuracy with infinitesimally small correlator spacing. Their model takes into account the WSCS PRN code, using the assumption of finite random codes (AVILA-RODRIGUEZ, 2008). Remarkably, based on their research the authors even suggested a short section to be added to ITU-R M.1831 (ITU-R, 2015). However, their results still rely on the CSG assumption and do not take into account the deterministic PRN code or the cyclostationarity induced by the analog pulse shape.

In the context of satellite navigation, performance models in the presence of MAI are not as sophisticated as they are in terrestrial communications (VITERBI, 1995; TANG; SIEGEL; MILSTEIN, 2001; PURSLEY, 1977; LOK; LEHNERT, 1998; G. Zang; C. Ling, 2003; YOON, 2002; CHO; LEHNERT, 2002; CHO; JEONG; LEHNERT, 2000), which are typically interference-limited. Performance of terrestrial DS-CDMA has been studied extensively for time-limited (PURSLEY, 1977; LOK; LEHNERT, 1998; VITERBI, 1995; TANG; SIEGEL;

MILSTEIN, 2001) or band-limited (VITERBI, 1995; CHO; LEHNERT, 2002; CHO; JEONG; LEHNERT, 2000; G. Zang; C. Ling, 2003; YOON, 2002) spreading waveforms. It is generally agreed that MAI at the output of a single correlator employing a matched filter (MF) is accurately modeled by the conditional Gaussian approximation (CGA) (LOK; LEHNERT, 1998; CHO; JEONG; LEHNERT, 2000), when conditioned on the channel parameters (code-phase and carrier-phase). The considerably simpler standard Gaussian approximation (SGA) (PURSLEY, 1977; VITERBI, 1995), which comes closer to the model proposed by O'Driscoll and Fortuny-Guasch (O'DRISCOLL; FORTUNY-GUASCH, 2012), is accurate only in special cases. In particular, SGA and CGA are identical for IS-95-type systems (G. Zang; C. Ling, 2003), which employ second-order circular spreading with random codes and a flat-spectrum pulse. However, GNSS signals do not use band-limited pulse shapes, and (with few exceptions) rely on binary (hence *improper*) symbol alphabets, so that the SGA must be considered mismatched here. The rather sophisticated CGA (LOK; LEHNERT, 1998; CHO; JEONG; LEHNERT, 2000) cannot readily be applied to the multiple access performance of GNSS signals. It was originally proposed with a focus on the performance of data transfer in terms of bit error rate, rather than on the accuracy of code-phase and carrier-phase estimation. Moreover, it was developed for terrestrial propagation channels, where the relative velocity between transmitter and receiver is usually not excessive and the resulting Doppler shift of radio frequencies is typically on the order of less than a few hundreds of Hertz; in comparison, L-band signals transmitted by MEO satellites are observed on Earth with Doppler shifts on the order of several Kilohertz (TEUNISSEN; MONTENBRUCK, 2017), which is on the order of fine features of the signals' PSD. Finally, in (LOK; LEHNERT, 1998; CHO; JEONG; LEHNERT, 2000), all users are assumed to have the same modulation in terms of pulse shape and keying rates, which is not usually the case in GNSS intersystem interference.

In this work, we assume WSCS, non-circular, and conditionally Gaussian GNSS signals, rather than relying on any WSS/CSG approximations. Based on this more general assumption, we derive refined expressions for the SINR and for the variance of code-/carrier-phase estimation, which will allow a more accurate assessment of RFC. We pick up the CGA from (LOK; LEHNERT, 1998; CHO; JEONG; LEHNERT, 2000) and generalize it from the case of a single terrestrial service to multiple satellite services. To obtain this generalized CGA, we formulate a signal model where pulse shapes, symbol rates, and chipping rates can vary from signal to signal, and take into account the signals' Doppler frequencies. Moreover, the deterministic PRN codes of the signals in space are taken into account by the proposed generalized

CGA. Our main contribution is a full second-order characterization of the receivers early, prompt, and late correlator outputs, in terms of (co-)variances and conjugate (co-)variances, which allows to assess the accuracy of widely linear estimators for code-phase and carrier-phase, such as the coherent early-late discriminator or the coherent phase discriminator (KAPLAN; HEGARTY, 2005). In a second step, we show how the conditioning of the CGA on channel parameters (satellite visibility, Doppler frequencies, code-phases, carrier-phases) can be removed over short-term (few milliseconds) or long-term (constellation period) periods of observation. After the conditioning is removed, it is possible that estimation errors are actually distributed according to a non-Gaussian PDF.

Monte Carlo simulations with the civil L1/E1 signals in space as defined in (EUROPEAN..., 2016; NAVSTAR..., 2020b; NAVSTAR..., 2020a; NAVSTAR..., 2020c) serve as a means of verification, where we also take into account the true PRN codes. We demonstrate that the CGA is already accurate for one single interfering satellite. This obviates the need to invoke the central limit theorem for many asynchronous, power-balanced interferers, when assessing RFC. One important result is that the classic WSS/CSG model generally tends to underestimate the tails of the code-phase estimation error PDF. As an application example of current relevance, we show how the refined performance models can be used to assess the RFC of a forthcoming Galileo C/A signal with the existing GLONASS L1OF in the upper L-band. The proposed model is also perfectly suitable for error analysis in near-far problems.

3.3 System Model

We consider K satellite signals received over an AWGN channel. Signals are processed independently, producing a code-phase estimate and a carrier-phase estimate per signal. These estimates, which are the crucial raw observables for satellite navigation, are obtained by widely linear (SCHREIER; SCHARF, 2010) combinations of an early, late and prompt MF output.

3.3.1 Received Signal

The receiver's pre-correlation baseband signal is the sum of K satellite signals and noise

$$y(t) = \sum_{k=1}^{K} \sqrt{C_k}\, s_k(t; \boldsymbol{\theta}_k) \; + \; \eta(t), \tag{3.5}$$

with

$$x_k(t;\boldsymbol{\theta}_k) = \sum_{n=-\infty}^{\infty} b_k^{(n)} e^{\mathrm{j}2\pi\nu_k t} e^{\mathrm{j}\phi_k} q_k(t - \tau_k - nT_k). \tag{3.6}$$

The term $\eta(t)$ represents complex baseband AWGN, which means that its real and imaginary part are independent AWGN processes each with two-sided PSD $N_0/2$ (LAPIDOTH, 2017). Each satellite signal is characterized by the respective received power C_k and synchronization parameter $\boldsymbol{\theta}_k = [\tau_k, \nu_k, \phi_k]^T$, including code-phase τ_k, Doppler shift ν_k and carrier-phase ϕ_k. The signal $x_k(t;\boldsymbol{\theta}_k)$ is modulated at rate $1/T_k$ by a sequence $\{b_k^{(n)}\}$ of independent and identically distributed (i.i.d.) random elements which are assumed to satisfy

$$\mathrm{E}[b_k^{(n)}] \triangleq \mu_k = 0 \tag{3.7}$$

$$\mathrm{E}[|b_k^{(n)}|^2] \triangleq \Sigma_{kk^*} = 1 \tag{3.8}$$

$$\mathrm{E}[(b_k^{(n)})^2] \triangleq \Sigma_{kk} \in \mathbb{C}. \tag{3.9}$$

We let the conjugate variance Σ_{kk} be an arbitrary complex number in the unit circle plane $|\Sigma_{kk}| \leq 1$. The modulation is proper if and only if $\Sigma_{kk} = 0$. It is easily verified that a QPSK alphabet with equiprobale elements $\{-1-\mathrm{j}, -1+\mathrm{j}, 1-\mathrm{j}, 1+\mathrm{j}\}$ is proper, while a BPSK alphabet with equiprobable elements $\{-1, +1\}$ leads to $\Sigma_{kk} = 1$ (or to $\Sigma_{kk} = -1$ for the alphabet $\{-\mathrm{j}, +\mathrm{j}\}$). Furthermore, let the sequences $\{b_k^{(n)}\}$ be independent for $k = 1, \ldots, K$.

The waveforms $q_k(t)$ are deterministic and normalized as

$$\int_{-\infty}^{\infty} |q_k(t)|^2 \,\mathrm{d}t = T_k. \tag{3.10}$$

Moreover, they are band-limited to a common receiver bandwidth B in the sense that the Fourier transforms

$$Q_k(f) \triangleq \int_{-\infty}^{\infty} q_k(t) e^{-\mathrm{j}2\pi f t} \,\mathrm{d}t \tag{3.11}$$

have compact frequency support $[-B, B]$ for $k = 1, \ldots, K$.

Signals of the form (3.6) are, in general, not WSS. While the sequence $b_k^{(n)}$ is WSS (in fact even stationary), the periodically recurring waveform $q_k(t)$ induces cyclostationarity. This is illustrated by the following example.

Example: For simplicity, consider (3.6) with zero Doppler frequency and zero carrier-phase. Let $\{b_k^{(n)}\}$ be an infinite sequence of pseudorandom code with chipping rate $1/T_k = 1.023\,\mathrm{MHz}$. The sequence elements are assumed as i.i.d. and to assume values from the code alphabet $\{-1-\mathrm{j}, -1+\mathrm{j}, 1-\mathrm{j}, 1+\mathrm{j}\}$ with equal probability. Furthermore, let $q_k(t)$

Figure 3.4 – Cyclic spectrum of a DS-CDMA signal with infinite, perfectly random spreading code, 1.023 MHz chipping rate, and REC pulse.

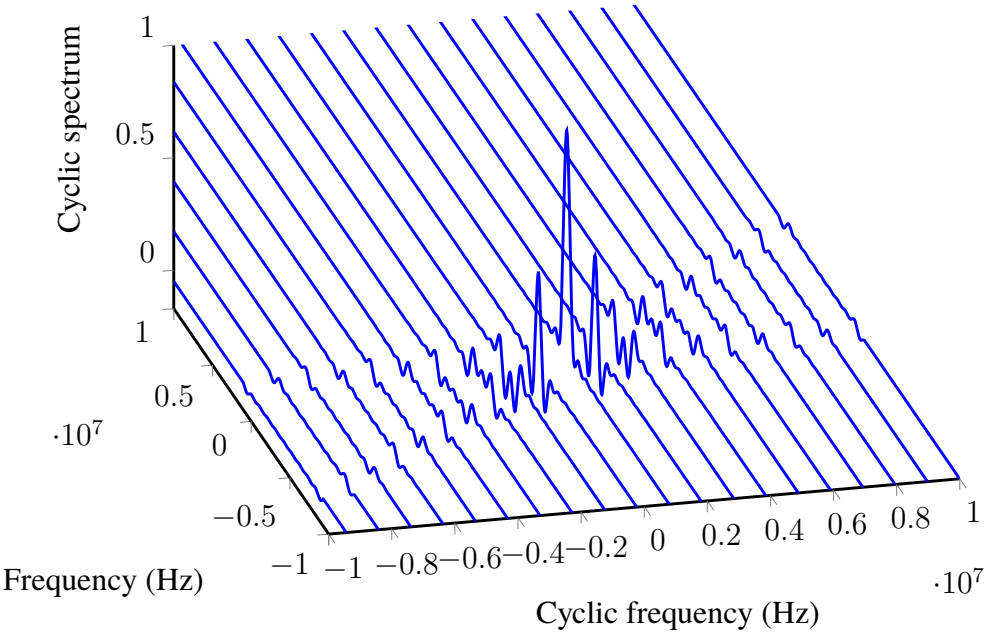

be a rectangular pulse as defined in (2.4). Fig. 3.4 shows the cyclic spectrum of such a signal, following the exact definition from Gardner (GARDNER; NAPOLITANO; PAURA, 2006). (The formalism of cyclostationary signal analysis is not used in this work, which is why we do not repeat the formal definition of the cyclic spectrum here. An excellent comprehensive overview on cyclostationary signals can be found in Gardner's book.) Note that already this idealized signal with perfect pseudorandom code exhibits features at cyclic frequencies different from zero, and therefore is not WSS. The PSD is given by the cyclic spectrum evaluated at cyclic frequency zero, but the PSD alone fails to express that the signal is *periodically correlated* (or WSCS) at multiples of T_k.

Interestingly, we observed that using the same signal with a RRC pulse leads to vanishing spectrum at all cyclic frequencies other than zero, i.e., the signal becomes WSS. This is confirmed by (G. Zang; C. Ling, 2003).

Quite different from the above idealized example, and also different from earlier works on frequency-domain CGA (VITERBI, 1995; CHO; JEONG; LEHNERT, 2000; G. Zang; C. Ling, 2003; YOON, 2002), we do not assume infinite and perfectly random (*aperiodic*) spreading code, but consider the actual PRN sequences used by the satellites. Therefore, we assume that the waveform $Q_k(f)$ does not represent a mere pulse shape, but the entire spreading waveform, and is given by

$$Q_k(f) = A_k(f)H_k(f), \tag{3.12}$$

Table 3.1 – Overview of GNSS signals L1 C/A (NAVSTAR..., 2020c) and E1-B (EUROPEAN..., 2016)

Signal	Σ_{kk}	$H_k(f)$	$A_k(f)$	N_k	T_k (ms)	C_k (dBW) [2]
E1-B	$+1$	CBOC[3]	Memory codes	20×1023	4	$[-160.0, -157.0]$
L1 C/A	-1	REC	Gold codes	4092	20	$[-158.5, -153.0]$

where $H_k(f)$ is the Fourier transform of an analog pulse (e.g., a REC or BOC pulse), and $A_k(f)$ is the deterministic code Fourier transform. The latter can be given in terms of the deterministic finite PRN code $c_k[0], \ldots, c_k[N_k - 1]$ of length N_k

$$A_k(f) = \frac{1}{\sqrt{N_k}} \sum_{n=0}^{N_k-1} c_k[n] e^{-\mathrm{j}\, 2\pi f n T_k/N_k}. \tag{3.13}$$

Taking into account that the symbols $\{b_k^{(n)}\}$ are a sequence of i.i.d. random variables with unit variance, the PSD of the kth satellite signal in (3.5) can be computed using the proof of Simon (SIMON; HINEDI; LINDSEY, 1995). For instance, for zero Doppler frequency we obtain

$$\Phi_k(f) = \frac{C_k}{T_k} \big|Q_k(f)\big|^2 = \frac{C_k}{T_k} \big|H_k(f)\big|^2 \big|A_k(f)\big|^2. \tag{3.14}$$

In (3.14), we can identify the smooth PSD as the first factor, which upon multiplication with the *code spectrum* $|A_k(f)|^2$ yields the fine PSD. Typically, the fine features are visible with a frequency resolution of a few kHz, as $1/T_1 \ll B \ll f_c$, where f_c is the signals' common carrier frequency. Exemplarily, Table 3.1 displays the above described signal and modulation paramters for L1 C/A (NAVSTAR..., 2020c) and E1 OS Data (also known as E1-B) (EUROPEAN..., 2016). The composition of their PSD is shown in Fig. 3.5. Both are transmitted at the carrier frequency $f_c = 1575.42$ MHz. Like almost all GNSS signals, both use BPSK symbol modulation and DS-CDMA, hence $|\Sigma_{kk}| = 1$.

3.3.2 Matched filter and widely linear estimators

Without loss of generality, we consider $k = 1$ as the signal of interest. We focus on coherent estimators, which require knowledge of N symbols $b_1^{(1)}, \ldots, b_1^{(N)}$ and a reasonably accurate synchronization estimate $\hat{\boldsymbol{\theta}}_1 = [\hat{\tau}_1, \hat{\nu}_1, \hat{\phi}_1]^T$. If symbols and $\hat{\phi}_1$ are unavailable, noncoherent estimators with squaring loss can be used, for which our performance analysis may serve

[2] The given interval applies only to the reference receiver with the full bandwidth $B = 10.23$ MHz (NAVSTAR..., 2020c) or $B = 12.28$ MHz (EUROPEAN..., 2016), respectively. For smaller B, parts of the PSD in Fig. 3.5 are unused, and C_k reduces accordingly.

[3] A description of the more exotic composite BOC (CBOC) pulse used by E1-B is given in (EUROPEAN..., 2016).

Figure 3.5 – (a) Smooth PSD for reference receiver bandwidth $B = 12.28\,\text{MHz}$ and maximum power C_k. (b) Code spectrum (exemplary). Multiplication of these two components yields the fine PSD $\frac{C_k}{T_k}|Q_k(f)|^2$.

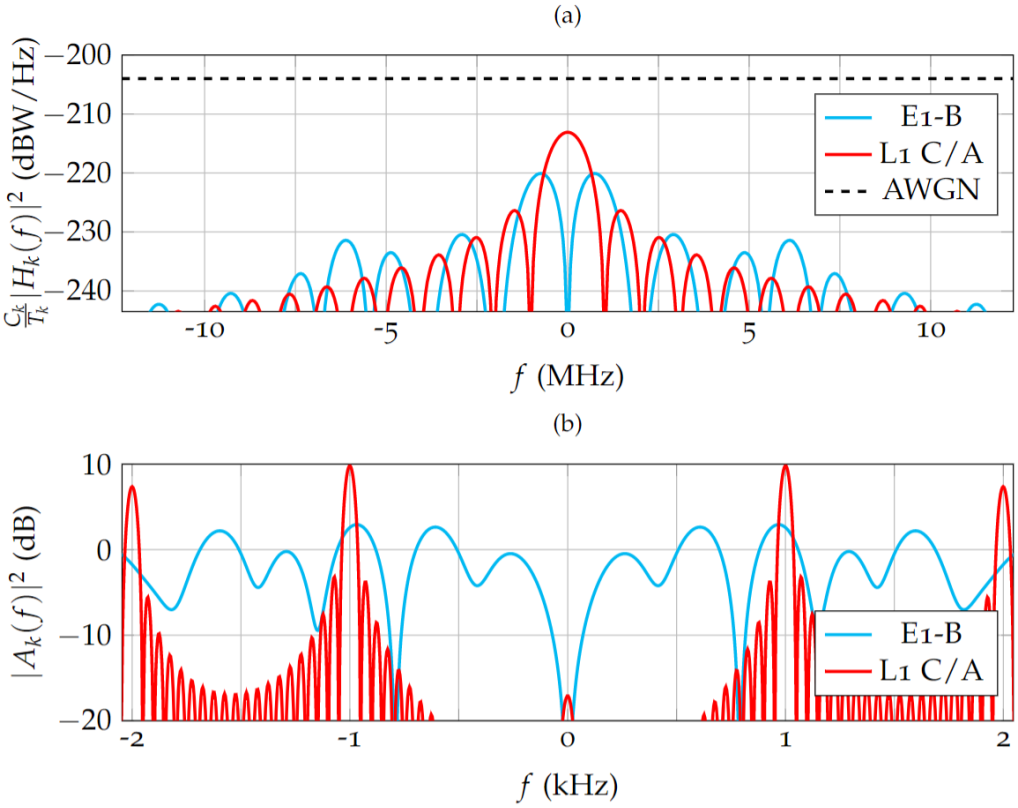

as a benchmark. Consider the bank of correlators shown in Fig. 3.6. The prompt MF output is defined as

$$\mathcal{P}_1 = \frac{1}{\sqrt{NT_1}} \sum_{n=1}^{N} \int_{-\infty}^{\infty} \left(x_1^{(n)}(t; \hat{\boldsymbol{\theta}}_1) \right)^* y(t)\, \mathrm{d}t, \tag{3.15}$$

where the expression

$$x_k^{(n)}(t; \boldsymbol{\theta}) = b_k^{(n)} e^{\mathrm{j}2\pi\nu t} e^{\mathrm{j}\phi} q_k(t - \tau - nT_k), \tag{3.16}$$

for $k \in \{1, \ldots, K\}$, is used to refer to a (energy-limited) signal replica with generic synchronization parameter $\boldsymbol{\theta} = [\tau, \nu, \phi]^T$.

The late/early outputs $\mathcal{L}_1$ and $\mathcal{E}_1$ are defined analogously to (3.15), with a delay/advance of $\hat{\tau}_1$ in (3.15) by the correlator spacing $\epsilon > 0$.

Let the relative synchronization parameters be $\Delta\boldsymbol{\theta}_k \triangleq \boldsymbol{\theta}_k - \hat{\boldsymbol{\theta}}_1$ for $k = 1, \ldots, K$. To refine the initial estimate $\hat{\boldsymbol{\theta}}_1$, the receiver produces high-resolution estimates of the unknown residuals $\Delta\phi_1$ and $\Delta\tau_1$. The coherent discriminator functions $\mathrm{Im}\{\mathcal{P}_1\}$ and $\mathrm{Re}\{\mathcal{E}_1 - \mathcal{L}_1\}$ are approximately linear in $\Delta\phi_1, \Delta\tau_1$, respectively, if $\hat{\boldsymbol{\theta}}_1 \approx \boldsymbol{\theta}_1$, and lead to the following well-known

Figure 3.6 – Correlator bank for synchronization (estimation) of code-phase and carrier-phase. The widely linear combinations of the correlator outputs are used as input to the linear estimators.

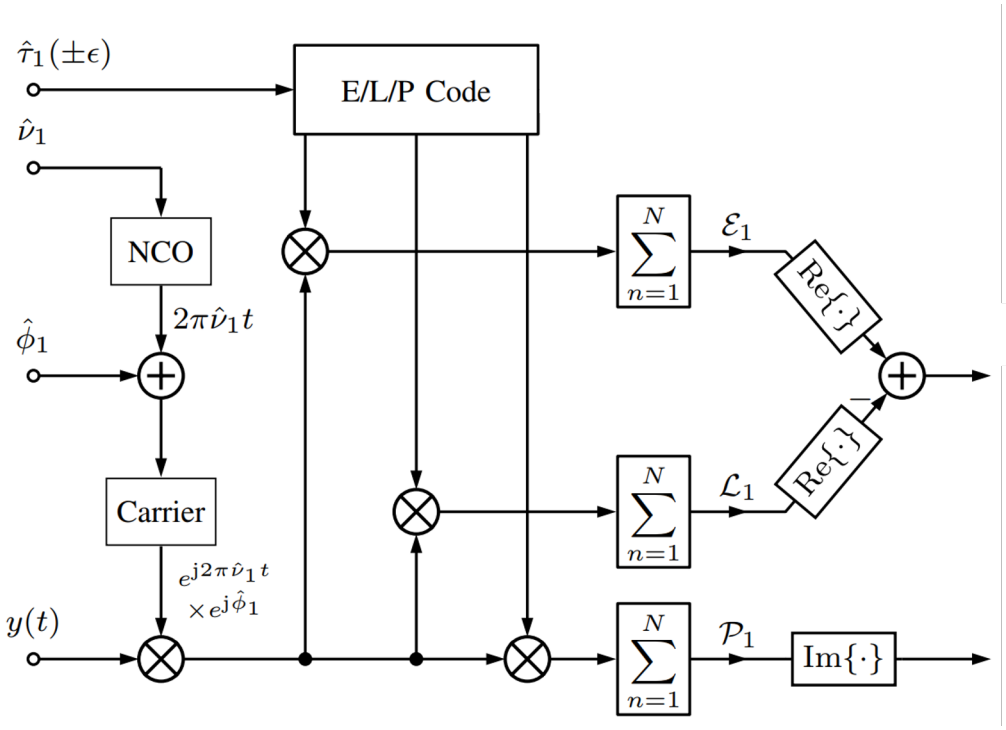

estimators realized by coherent tracking loops (HOLMES, 2007),

$$\Delta\hat{\phi}_1 = \frac{\mathrm{Im}\{\mathcal{P}_1\}}{\sqrt{NT_1C_1}} \tag{3.17}$$

$$\Delta\hat{\tau}_1 = \frac{\mathrm{Re}\{\mathcal{E}_1 - \mathcal{L}_1\}}{S_1(\epsilon)\sqrt{NT_1C_1}}. \tag{3.18}$$

Here, we used the *discriminator gain* $S_1(\epsilon) = -\frac{1}{T_1}\int_{-B}^{B} |Q_1(f)|^2 4\pi f \sin(2\pi f\epsilon)\,\mathrm{d}f$. These estimators belong to the class of widely linear estimators (SCHREIER; SCHARF, 2010; LAPIDOTH, 2017). It is easily verified that the estimators are approximately unbiased as long as the residuals are already close to zero. For instance,

$$\mathrm{E}\left[\Delta\hat{\phi}_1\right] = \Delta\phi_1\left(1 + \mathcal{O}(\Delta\tau_1^2)\right) \tag{3.19}$$

$$\mathrm{E}\left[\Delta\hat{\tau}_1\right] = \Delta\tau_1\left(1 + \mathcal{O}(\Delta\phi_1^2)\right) \tag{3.20}$$

if $\hat{\nu}_1 \approx \nu_1$. Thus, while these estimators are widely used, they only work well if coarse synchronization has already been achieved. We will focus on the estimation variance in the following.

3.4 Conditional Gaussian approximation (CGA)

For the CGA, we condition on $\mathcal{C} \triangleq (C_1, \ldots, C_K)$ and $\Theta \triangleq (\hat{\boldsymbol{\theta}}_1, \boldsymbol{\theta}_1, \ldots, \boldsymbol{\theta}_K)$, considering symbols and noise as random.

3.4.1 Variance of the carrier-phase estimator

Proposition 1. The conditional variance of the carrier-phase estimator (3.17) caused by MAI and AWGN is given by

$$\mathrm{Var}\big[\Delta\hat{\phi}_1\big] = \frac{N_0 + \sum_{k=2}^{K} C_k\big(\psi_k - \mathrm{Re}\{\tilde{\psi}_k\}\big)}{2NT_1C_1}, \tag{3.21}$$

where the (conjugate) variances due to MAI are

$$\begin{aligned}\psi_k = \frac{1}{T_1T_k}\sum_{m=-M_k}^{M_k} D_N^*\left(2\pi m\frac{T_1}{T_k}\right) \\ \times e^{\mathrm{j}2\pi m\frac{\Delta\tau_k}{T_k}}\int_{-B}^{B} Q_1(f+\Delta\nu_k)Q_k^*(f) \\ \times Q_1^*\Big(f+\Delta\nu_k-\frac{m}{T_k}\Big)Q_k\Big(f-\frac{m}{T_k}\Big)\,\mathrm{d}f,\end{aligned} \tag{3.22}$$

$$\begin{aligned}\tilde{\psi}_k = \frac{\Sigma_{11}^*\Sigma_{kk}}{T_1T_k}\,e^{\mathrm{j}4\pi\Delta\nu_k\hat{\tau}_1}e^{\mathrm{j}2\Delta\phi_k}\sum_{m=-M_k}^{M_k} D_N\left(2\pi m\frac{T_1}{T_k}+4\pi\Delta\nu_kT_1\right) \\ \times e^{-\mathrm{j}2\pi m\frac{\Delta\tau_k}{T_k}}\int_{-B}^{B} Q_1^*(f+\Delta\nu_k)Q_k(f) \\ \times Q_1^*\Big(\frac{m}{T_k}-f+\Delta\nu_k\Big)Q_k\Big(\frac{m}{T_k}-f\Big)\,\mathrm{d}f.\end{aligned} \tag{3.23}$$

Here, we used $M_k = \lfloor 2BT_k \rfloor$ and the Dirichlet kernel

$$D_N(x) \triangleq \frac{1}{N}\sum_{n=1}^{N} e^{\mathrm{j}nx} = \begin{cases} 1 & \text{if } \frac{x}{2\pi}\in\mathbb{Z} \\ \frac{\sin(Nx/2)}{N\sin(x/2)}\,e^{\mathrm{j}x(N+1)/2} & \text{otherwise.}\end{cases} \tag{3.24}$$

Proof. We first recall from (LAPIDOTH, 2017) that, for any complex random variable Y, $\mathrm{Var}[\mathrm{Im}\{Y\}] = \mathrm{Var}[Y]/2 - \mathrm{Re}\{\mathrm{Cov}[Y,Y^*]\}/2$ and apply this to the right-hand side of (3.17). Then we expand $\mathcal{P}_1$ into $K+1$ uncorrelated summands using (3.5), which represent the contributions of MAI, noise, and intersymbol interference (ISI). Variance and conjugate variance of MAI for $k \neq 1$ are given by $C_k\psi_k \triangleq \mathrm{Var}[\mathcal{P}_1]|_k$ and $C_k\tilde{\psi}_k \triangleq \mathrm{Cov}[\mathcal{P}_1,\mathcal{P}_1^*]|_k$, which are derived in Section 3.4.4. The contribution of AWGN is well-known (VITERBI, 1995), (HOLMES, 2007, Sec. 5.2.9). The ISI contributions $(C_1\psi_1, C_1\tilde{\psi}_1)$ are nonzero but negligible since $1/T_1 \ll B$ (VITERBI, 1995).

3.4.2 Variance of the code-phase estimator

Proposition 2. The conditional variance of the code-phase estimator (3.18) caused by MAI and AWGN is given by

$$\begin{aligned}\mathrm{Var}\big[\Delta\hat{\tau}_1\big] = \Bigg(N_0\Big(1 - \frac{1}{T_1}\int_{-B}^{B} |Q_1(f)|^2 \cos(4\pi f\epsilon)\,\mathrm{d}f\Big) \\ + \sum_{k=2}^{K} C_k\Big(\frac{\varepsilon_k}{2} + \frac{\lambda_k}{2} - \mathrm{Re}\left\{\chi_k\right\} + \mathrm{Re}\left\{\frac{\tilde{\varepsilon}_k}{2} + \frac{\tilde{\lambda}_k}{2} - \tilde{\chi}_k\right\}\Big)\Bigg) \\ \Big/\big(S_1^2(\epsilon) N T_1 C_1\big)\,. \end{aligned} \tag{3.25}$$

Proof. For any pair (U, V) of complex random variables,

$$\begin{aligned}\mathrm{Var}[\mathrm{Re}\{U - V\}] = \mathrm{Var}[U]/2 + \mathrm{Var}[V]/2 - \mathrm{Re}\{\mathrm{Cov}[U, V]\} \\ + \mathrm{Re}\{\mathrm{Cov}[U, U^*]/2 + \mathrm{Cov}[V, V^*]/2 - \mathrm{Cov}[U, V^*]\}\end{aligned} \tag{3.26}$$

is easy to show with (LAPIDOTH, 2017). We apply this to (3.18) and proceed as in the proof of Proposition 1; the MAI contributions $C_k\varepsilon_k \triangleq \mathrm{Var}[\mathcal{E}_1]|_k$, $C_k\tilde{\varepsilon}_k \triangleq \mathrm{Cov}[\mathcal{E}_1, \mathcal{E}_1^*]|_k$, $C_k\lambda_k \triangleq \mathrm{Var}[\mathcal{L}_1]|_k$, $C_k\tilde{\lambda}_k \triangleq \mathrm{Cov}[\mathcal{L}_1, \mathcal{L}_1^*]|_k$, $C_k\chi_k \triangleq \mathrm{Cov}[\mathcal{E}_1, \mathcal{L}_1]|_k$ and $C_k\tilde{\chi}_k \triangleq \mathrm{Cov}[\mathcal{E}_1, \mathcal{L}_1^*]|_k$ are derived in Section 3.4.4 for $k \neq 1$. The contribution of AWGN is well-known (cf., (HOLMES, 2007, Sec. 7.2.1)).

3.4.3 Signal-to-interference-plus-noise ratio (SINR)

The SINR of the prompt MF output is defined as $\mathrm{SINR} \triangleq |\,\mathrm{E}[\mathcal{P}_1]|^2/\mathrm{Var}[\mathcal{P}_1]$, where the denominator contains AWGN and MAI. It is often used as a single figure of merit, although it does not provide a full second-order characterization of $\mathcal{E}_1$, $\mathcal{L}_1$ and $\mathcal{P}_1$. Plain signal-to-noise ratio is $\mathrm{SNR} \triangleq |\,\mathrm{E}[\mathcal{P}_1]|^2/N_0$.

A useful quantity is the loss $\mathrm{SNR}\,/\,\mathrm{SINR} = 1 + \Psi$ with

$$\Psi = \sum_{k=2}^{K} \frac{C_k}{N_0}\psi_k \qquad \geq 0. \tag{3.27}$$

3.4.4 Derivation of conditional second-order moments of MAI

For a generic $\alpha \in \{-\epsilon, 0, \epsilon\}$ and $\hat{\boldsymbol{\theta}}_1(\alpha) \triangleq [\hat{\tau}_1 + \alpha, \hat{\nu}_1, \hat{\phi}_1]^T$, we consider the random contribution from the mth symbol of the kth signal to the nth MF output for unit power $C_k = 1$

$$\begin{aligned} X_{1,k}^{(n,m)}(\alpha) &\triangleq \frac{1}{\sqrt{T_1}} \int_{-\infty}^{\infty} \big(x_1^{(n)}(t; \hat{\boldsymbol{\theta}}_1(\alpha))\big)^* x_k^{(m)}(t; \boldsymbol{\theta}_k)\, \mathrm{d}t \\ &= \frac{\big(b_1^{(n)}\big)^* b_k^{(m)} e^{\mathrm{j}\Delta\phi_k}}{\sqrt{T_1}} \int_{-\infty}^{\infty} Q_1^*(f - \hat{\nu}_1) Q_k(f - \nu_k) \\ &\quad \times e^{\mathrm{j}2\pi\left((nT_1 + \hat{\tau}_1 + \alpha)(f - \hat{\nu}_1) - (mT_k + \tau_k)(f - \nu_k)\right)}\, \mathrm{d}f, \end{aligned} \tag{3.28}$$

where the equation follows with Plancherel's theorem (YOSIDA, 1995). With Poisson's summation formula (YOSIDA, 1995), we have for $k \neq 1$

$$\begin{aligned} &\mathrm{E}\left[\left(\sum_{m_1=-\infty}^{\infty} X_{1,k}^{(n,m_1)}(\alpha_1)\right)^{(*)} \sum_{m_2=-\infty}^{\infty} X_{1,k}^{(n,m_2)}(\alpha_2)\right] \\ &= \sum_{m=-\infty}^{\infty} e^{\mathrm{j}\left(\Delta\phi_k \overset{+}{(-)} \Delta\phi_k\right)} e^{\mathrm{j}2\pi(nT_1 + \hat{\tau}_1)\left(\Delta\nu_k \overset{+}{(-)} \Delta\nu_k \overset{+}{(-)} \frac{m}{T_k}\right)} e^{\overset{(+)}{-}\mathrm{j}2\pi \frac{m}{T_k}\tau_k} \\ &\quad \times \int_{-\infty}^{\infty} e^{\mathrm{j}2\pi\left(\alpha_2\left(\overset{(+)}{-} f_1 + \Delta\nu_k \overset{+}{(-)} \nu_k \overset{+}{(-)} \frac{m}{T_k}\right) \overset{+}{(-)} \alpha_1(f_1 - \hat{\nu}_1)\right)} \\ &\quad \times \big(Q_1^*(f_1 - \hat{\nu}_1) Q_k(f_1 - \nu_k)\big)^{(*)} Q_k\left(\overset{(+)}{-} f_1 \overset{+}{(-)} \nu_k \overset{+}{(-)} \frac{m}{T_k}\right) \\ &\quad \times Q_1^*\left(\overset{(+)}{-} f_1 + \Delta\nu_k \overset{+}{(-)} \nu_k \overset{+}{(-)} \frac{m}{T_k}\right) \mathrm{d}f_1\, \frac{\Sigma_{11^{(*)}}^* \Sigma_{kk^{(*)}}}{T_1 T_k}. \end{aligned} \tag{3.29}$$

We summate this result over $n = 1, \ldots, N$ as any two random variables of the form (3.28) are uncorrelated for unequal n. Finally, dividing by N and substituting $f \leftarrow f_1 - \nu_k$ yields

- the prompt (conjugate) variance $\psi_k, \tilde{\psi}_k$ for $\alpha_1 = \alpha_2 = 0$,
- the early (conjugate) variance $\varepsilon_k, \tilde{\varepsilon}_k$ for $\alpha_1 = \alpha_2 = -\epsilon$,
- the late (conjugate) variance $\lambda_k, \tilde{\lambda}_k$ for $\alpha_1 = \alpha_2 = \epsilon$,
- the early/late (conjugate) covariance $\chi_k, \tilde{\chi}_k$ for $\alpha_1 = -\alpha_2 = \epsilon$.

Conjugate variances/covariances are obtained if the operators in brackets $^{(*)}$, $\overset{+}{(-)}$, $\overset{(+)}{-}$ are ignored, and variances/covariances otherwise.

3.5 Standard Gaussian approximation (SGA)

The SGA relies on the assumption of uniformly distributed relative code-phases and carrier-phases (G. Zang; C. Ling, 2003; YOON, 2002). To obtain the SGA for any of the performance measures (3.21), (3.25) or (3.27), all conditional moments are simply replaced by

their expectations with respect to uniform $\Delta\tau_k \in [0, T_k)$ and $\Delta\phi_k \in [-\pi, \pi)$. For instance, $\mathrm{E}[\Psi]$ reduces to a weighted sum of the SSCs

$$\mathrm{E}\left[\psi_k\right] = \int_{-B}^{B} \frac{\left|Q_1(f+\Delta\nu_k)\right|^2}{T_1} \frac{\left|Q_k(f)\right|^2}{T_k} \,\mathrm{d}f. \tag{3.30}$$

Note that CGA and SGA are identical for the special case $BT_k \leq 0.5$ and $\Sigma_{kk} = 0$.

3.6 Numerical results

The CGA is conditioned on the parameters $(\mathcal{C}, \Theta)$, and also the SGA is still conditioned on $\mathcal{C}$ and the Doppler frequencies. If one is interested in performance assessment over a short period of time (on the order of seconds or less), code-phases and carrier-phases should be considered as uniformly random, while the received powers and Doppler frequencies should be kept in the conditioning. If one is interested in performance assessment over a long period of time (on the order of the satellite constellation period), code-/carrier-phases should be considered as uniformly random, while a constellation simulator can be used to remove the conditioning on received powers and Doppler frequencies. In the following, receiver performance will be investigated over both short-term and long-term periods.

3.6.1 Short-term performance

We consider a simple scenario with two satellites (one transmitting the signal component of interest, the other transmitting an interfering interplex signal consisting of multiple signal components) and negligible AWGN. In the following, all theoretical results are verified by means of Monte-Carlo simulations, using a signal generator to produce the signals in space as specified in (EUROPEAN…, 2016; NAVSTAR…, 2020a; NAVSTAR…, 2020c).

First, let the SOI be Galileo E1-C, while MAI is received either by an E1 interplex signal consisting of E1-B and E1-C (intrasystem interference), or by an L1 interplex signal consisting of L1 C/A, L1C Data, and L1C Pilot (intersystem interference). In Fig. 3.7, we show the expectation of the code-phase RMSE, where the expectation is taken over only code-phases and carrier-phases. Received power levels are the maximum power levels specified in (EUROPEAN…, 2016; NAVSTAR…, 2020a; NAVSTAR…, 2020c). No Doppler-dependency could be observed. Note that we show only the SGA here because the CGA, upon taking expectation with respect to code-/carrier-phases, reduces to the SGA. In other words, if the expected RMSE is considered as a performance measure, CGA and SGA are equivalent.

Figure 3.7 – Short-term performance in terms of code-phase estimation error (standard deviation) vs. coherent integration time, experienced by a E1-C user in the presence of either an L1 or an E1 interplex signal. Configuration of mass-market (MM) receiver: $B = 2.046$ MHz, $\epsilon = 0.25 \times 977.52$ ns; professional (PR) receiver: $B = 10.23$ MHz, $\epsilon = 0.05 \times 977.52$ ns. Lines show the standard deviation under the SGA, using the aperiodic code (AC) or periodic code (PC) assumption. Simulation results are indicated by markers.

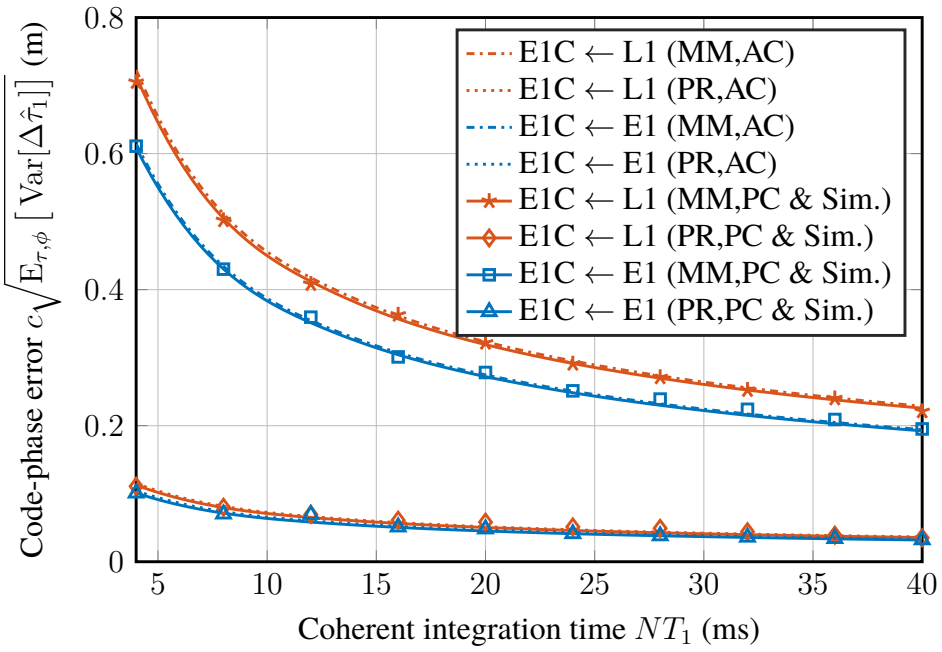

The same is true if GPS L1 C/A is considered as the SOI; results are shown in Fig. 3.8. However, a strong dependency of the RMSE on the Doppler frequency difference between the two satellites can be observed, when using simulations or the SGA with a periodic code model (i.e., not relying on the assumption of a smooth PSD). This results from the fine features of the L1 C/A code spectrum which are shown in Fig. 3.5. The MAI-A can observed to be most harmful for Doppler frequency offsets $0, \pm 1, \pm 2, \ldots$ kHz, and least harmful for Doppler frequency offsets $\pm 0.5, \pm 1.5, \ldots$ kHz.

The potential of the CGA becomes relevant if we are not only interested in the RMSE of the code-phase estimation, but rather in the error PDF. It was argued in Section 3.4 that the code-phase estimate $\Delta\hat{\tau}_1$ can be well approximated as conditonally Gaussian distributed given the relative code-phase $\delta\tau \triangleq \tau_2 - \tau_1$ and the relative carrier-phase $\delta\phi \triangleq \phi_2 - \phi_1$. Let the corresponding conditional Gaussian error PDF be denoted by $f_{\Delta\hat{\tau}_1|\delta\tau,\delta\phi}(\tau|\delta\tau,\delta\phi)$, where the dependency on the variance (3.25) is implicit. From this CGA, we can remove the conditioning on code-phase and carrier-phase by applying the law of total probability

$$f_{\Delta\hat{\tau}_1}(\tau) = \frac{1}{T_1+T_2}\frac{1}{2\pi}\int_{-(T_1+T_2)/2}^{(T_1+T_2)/2)}\int_{-\pi}^{\pi} f_{\Delta\hat{\tau}_1|\delta\tau,\delta\phi}(\tau|\delta\tau,\delta\phi)\,\mathrm{d}\delta\tau\,\mathrm{d}\delta\phi. \tag{3.31}$$

Figure 3.8 – Short-term performance in terms of code-phase estimation error (standard deviation) vs. coherent integration time, experienced by a L1 C/A user in the presence of either an L1 or an E1 interplex signal. Configuration of mass-market (MM) receiver: $B = 2.046$ MHz, $\epsilon = 0.25 \times 977.52$ ns; professional (PR) receiver: $B = 10.23$ MHz, $\epsilon = 0.05 \times 977.52$ ns. Lines show the standard deviation under the SGA, using the aperiodic code (AC) or periodic code (PC) assumption. Simulation results are indicated by markers.

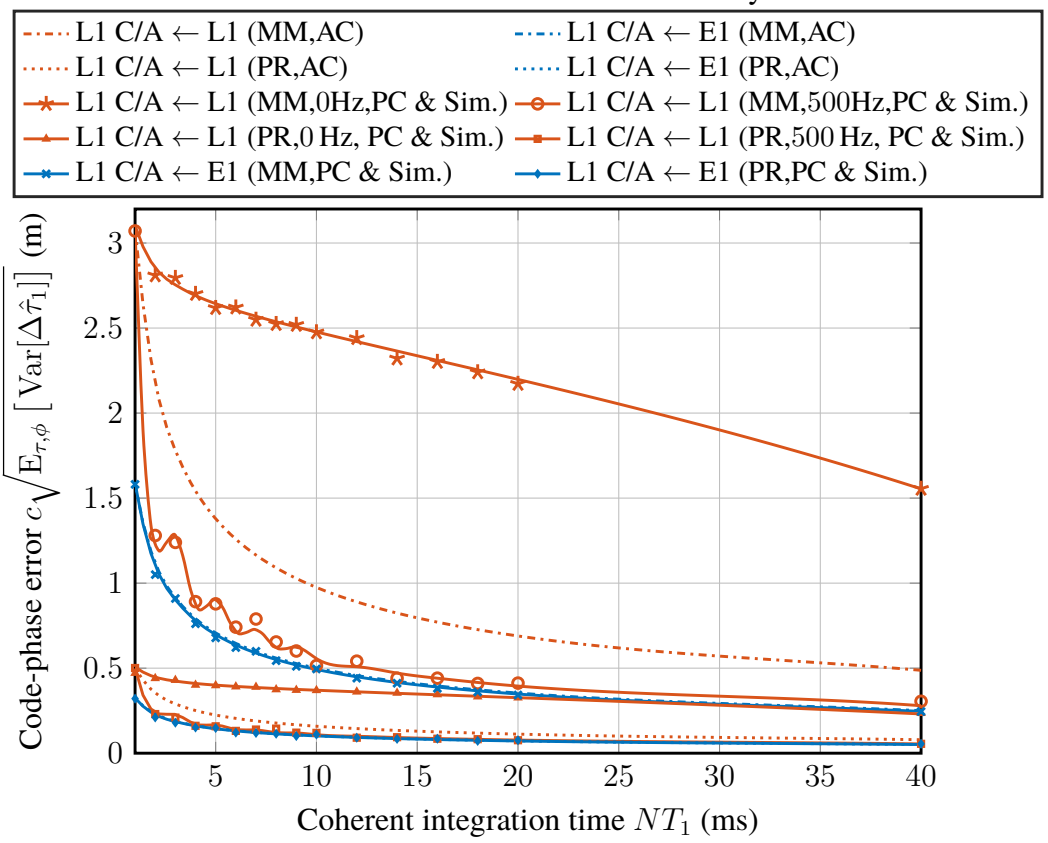

Resulting code-phase error PDFs for various scenarios are shown in Figs. 3.9-3.12. As a comparison, we show the Gaussian error PDF obtained with the SGA, which does not account for the influence of relative code- and carrier-phase. Both CGA and SGA are presented for smooth PSD modeling (aperiodic codes) and fine PSD modeling (periodic codes). It can be observed that the true error PDF does not, in general, resemble a Gaussian distribution. Rather, it decays at a much slower rate than a Gaussian PDF for large arguments, a fact which is correctly modeled by the CGA. This can even be observed if no C/A-type signals are involved, as shown in Fig. 3.12b.

The results shown in this section verify the validity of the CGA. However, the SGA can be used if one is interested only in the short-term RMSE of synchronization parameter estimation. We also observed that the CGA is already accurate for interference from a single satellite. This makes the CGA an interesting tool to evaluate performance in near-far situations (where the interfering satellite has much larger power than the SOI) or safety-critical appications.

Figure 3.9 – Code-phase error distribution experienced by an E1-C user in the presence of inter interference from one satellite transmitting the L1 interplex signal, comparing SGA vs. CGA and aperiodic code (AC) vs. periodic code (PC) spectrum assumptions. Receiver parameters: 8 ms coherent integration time, 2.046 MHz bandwidth, 0.25 chips correlator spacing.

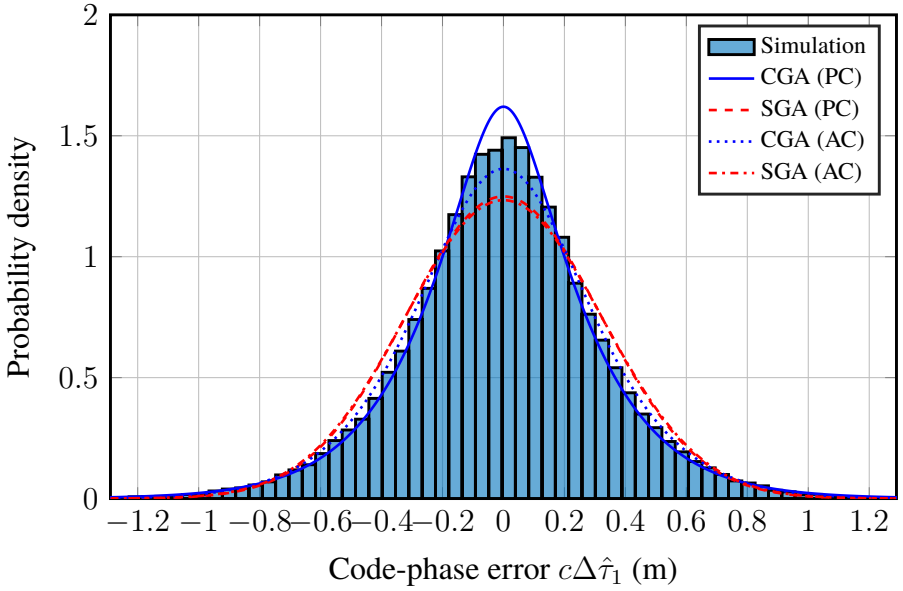

Figure 3.10 – Code-phase error distribution experienced by an L1 C/A user in the presence of inter interference from one satellite transmitting the L1 interplex signal, comparing SGA vs. CGA and aperiodic code (AC) vs. periodic code (PC) spectrum assumptions. Receiver parameters: 8 ms coherent integration time, 2.046 MHz bandwidth, 0.25 chips correlator spacing.

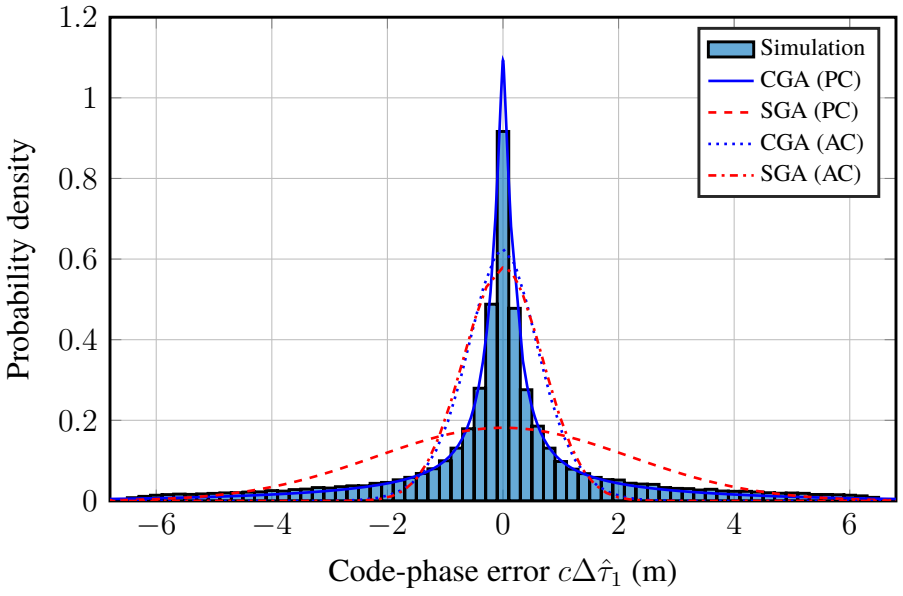

zu groß

Figure 3.11 – Code-phase error distribution experienced by an E1-C user in the presence of inter interference from one satellite transmitting the L1 interplex signal, comparing SGA vs. CGA and aperiodic code (AC) vs. periodic code (PC) spectrum assumptions. Receiver parameters: 8 ms coherent integration time, 2.046 MHz bandwidth, 0.25 chips correlator spacing.

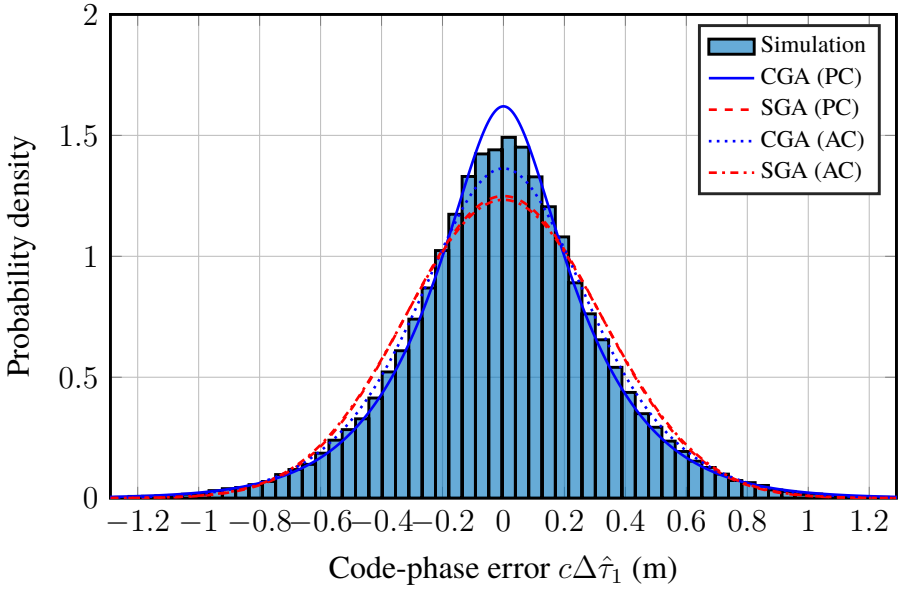

3.6.2 Long-term performance (constellation simulations)

The CGA and SGA can be used in combination with a constellation simulator to remove the conditioning on in-view satellites, received powers, and Doppler frequencies. This yields the distribution of the RMSEs $\sqrt{\mathrm{Var}[\Delta\hat{\phi}_1]}$, $\sqrt{\mathrm{Var}[\Delta\hat{\tau}_1]}$ or the SINR Ψ over a longer period of consideration. The constellation should be simulated over one full period (which is typically on the order of 1-10 days). Alternatively, only the maximum (worst-case) of these performance measures can be determined over a subset of possible constellation parameters $(\mathcal{C}, \Theta)$.

In the following, we will give two samples of this kind of RFC analysis:

- Section 3.6.2.1: intersystem interference between L1 C/A and E1-C at 1575.42 MHz;
- Section 3.6.2.2: intersystem interference between a (yet hypothetical) E1-D and the existing L1OF in the GLONASS band at 1602 MHz.

While the first scenario is an example for interference between C/A and non-C/A signals, the second scenario is an example for C/A-on-C/A intersystem interference. For both scenarios, we assess the RFC not only in terms of SINR, but also in terms of code- or carrier-phase estimation accuracy.

For the remainder of this work, we assume $N_0 = -204.0\,\frac{\mathrm{dBW}}{\mathrm{Hz}}$ (ITU-R, 2015).

Figure 3.12 – Code-phase error distribution experienced by an E1-C user in the presence of intrasystem interference from one satellite transmitting the E1 interplex signal, comparing SGA vs. improved Gaussian approximation (IGA) and aperiodic code (AC) vs. periodic code (PC) spectrum assumptions. Receiver parameters: 8 ms coherent integration time, 2.046 MHz bandwidth, 0.25 chips correlator spacing. (a) Center (b) Tail.

(a)

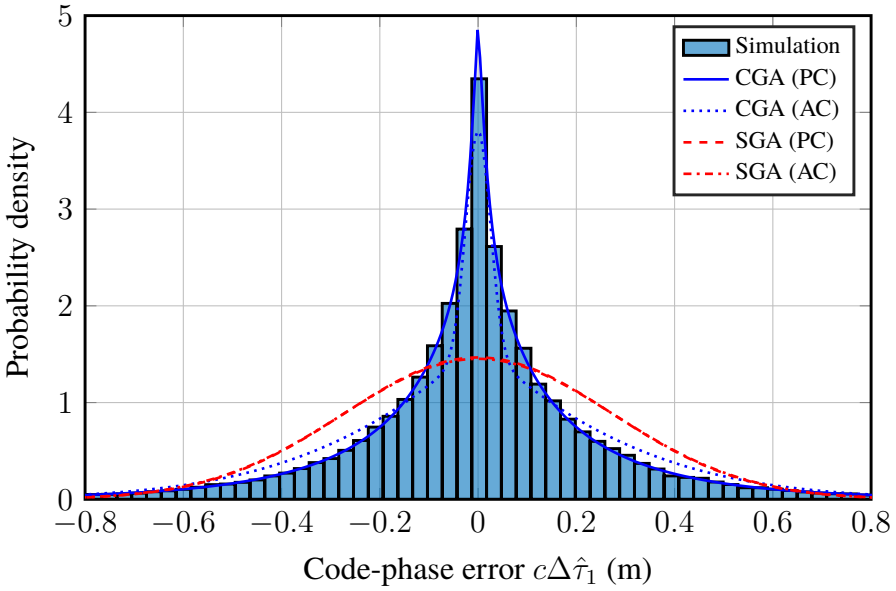

(b)

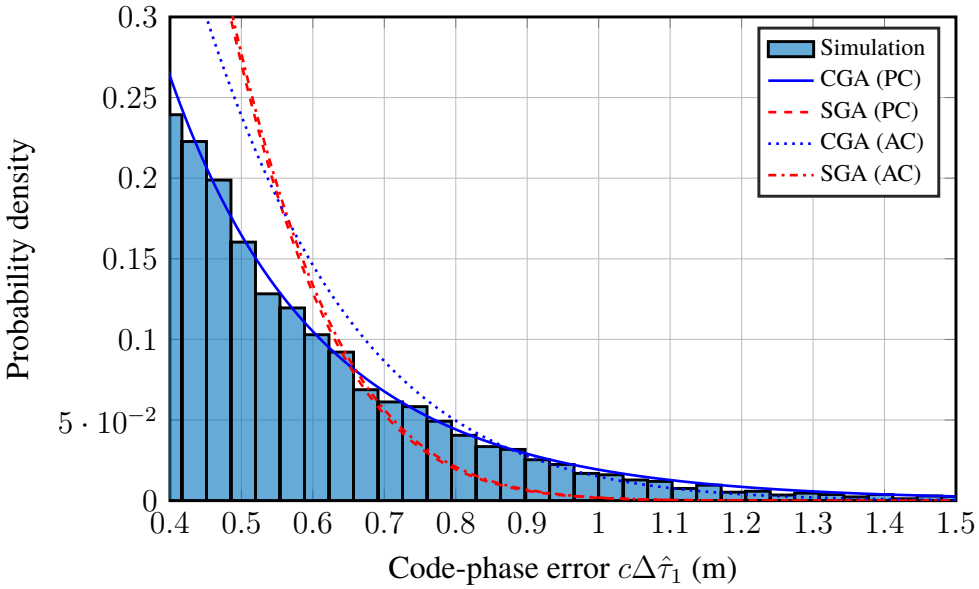

Figure 3.13 – CDF $F_\Psi(\Psi)$ of intrasystem (X←X), intersystem (X←Y), or combined (X←X+Y) MAI for $K = 55$ and $B = 2.046$ MHz.

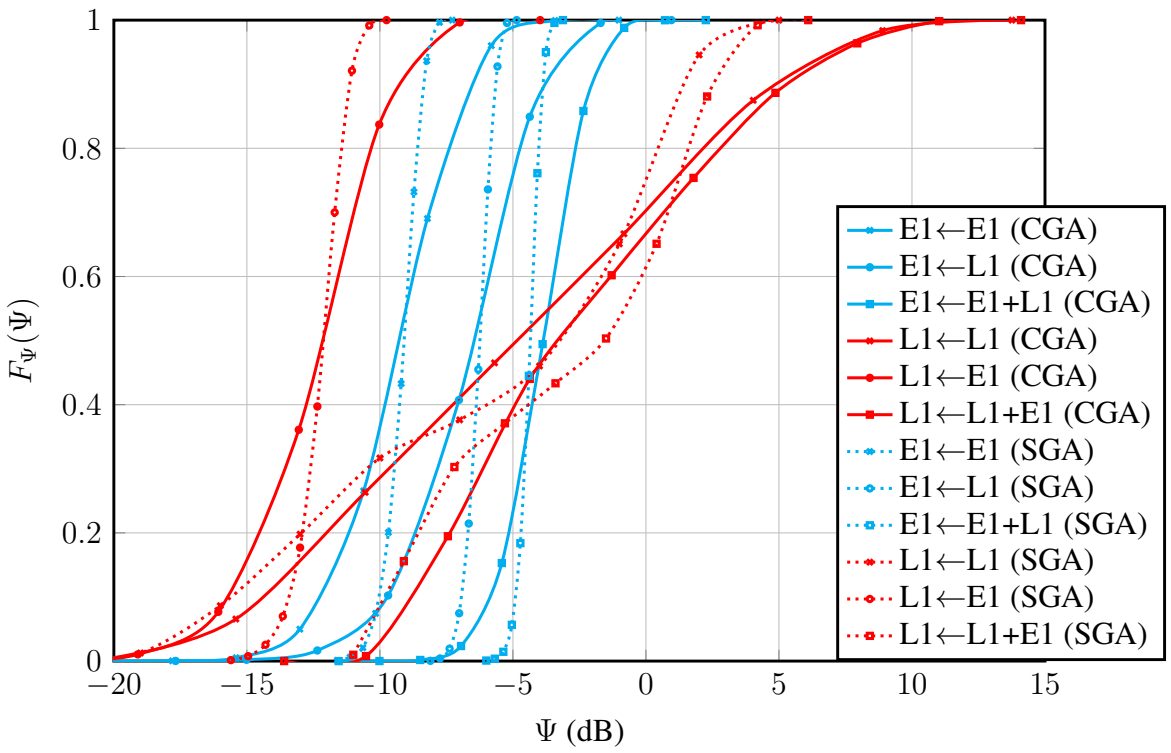

3.6.2.1 RFC of L1 C/A and E1 OS

We consider 31 GPS satellites and 24 Galileo satellites to determine the cumulative density function (CDF) $F_\Psi(\Psi)$, using reference constellations (NAVSTAR…, 2020c; EUROPEAN…, 2019). With L1 C/A and E1-B, there are $K = 55$ potentially active signals. For the power profile $\mathcal{C}$, we assume the maximum C_k from Table 3.1 whenever the corresponding satellite appears with at least $5°$ elevation, and zero otherwise. Whenever $k = 1$ is active, we compute CGA and SGA for each constellation point $(\mathcal{C}, \Theta)$ in time with a resolution of 6.5 Hz, and approximate $F_\Psi(\Psi)$ by their cumulative histograms. We consider ten sidereal days, as this is the least common multiple of the GPS and Galileo constellation periods. The receiver is located at $52°$ northern lattitude (Central Europe). The results in Fig. 3.13 reveal that the SGA tends to underestimate the tails of $F_\Psi(\Psi)$ by 4-8 dB. Moreover, L1 C/A SINR is dominated by L1 C/A (intrasystem) MAI rather than by AWGN 30% of the time. Meanwhile, E1-B SINR is barely affected by E1-B MAI, which is due to better spreading waveforms, fewer satellites but also lower power: if maximum E1-B received power is increased by 6 dB, for instance, intrasystem MAI will exceed AWGN 5% of the time.

A worst-case analysis is less useful for a full constellation analysis, but can be useful to study MAI for a single interferer ($K = 2$) as a function of the receiver configuration (N, B, ϵ),

Figure 3.14 – Carrier-phase standard deviation vs. coherent integration time for $B = 2.046$ MHz. Contributions of AWGN and worst-case intrasystem (X←X) or intersystem (X←Y) MAI for $K = 2$.

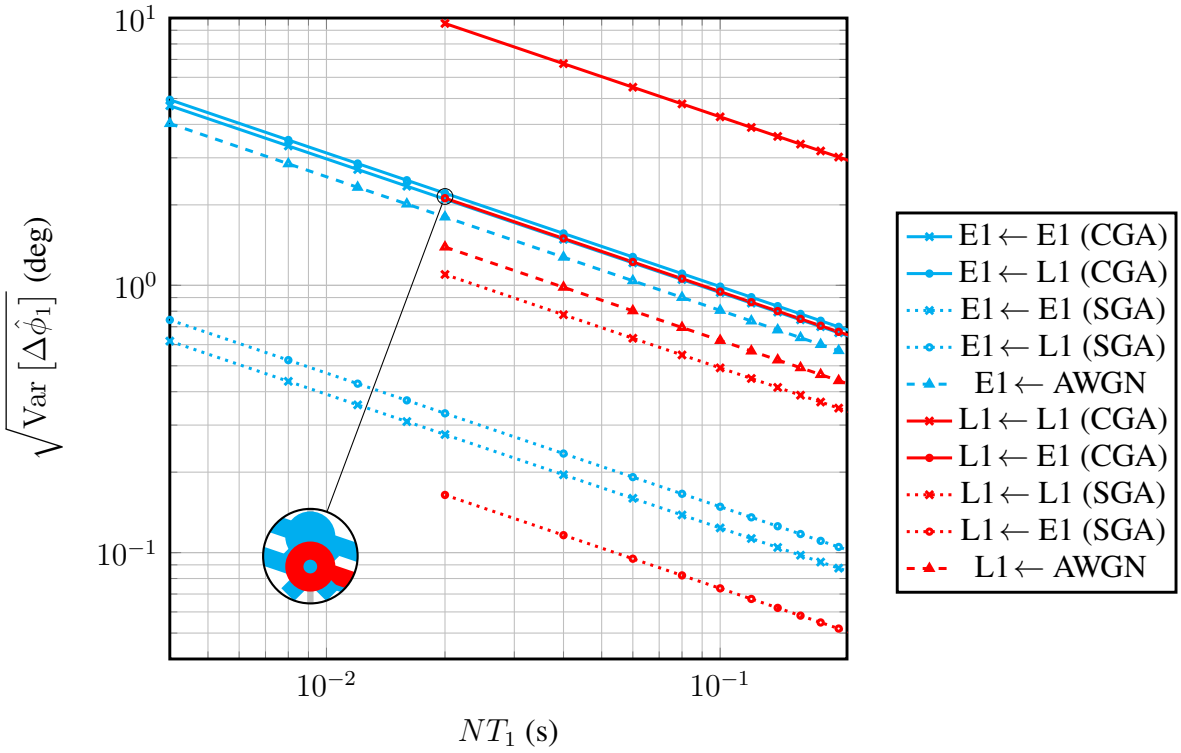

interferer-to-signal ratio C_2/C_1, or signal-to-noise-density ratio C_1/N_0, without the need to simulate full constellations. For the powers $\mathcal{C}$, we use the minimum C_k from Table 3.1 for $k = 1$ and the maximum C_k for $k = 2$. The range of possible synchronization parameters Θ can simply be described by $0 \leq \tau_k \leq T_k$, $|\phi_k| \leq \pi$ and $|\nu_k| \leq 4$ kHz, $k = 1, 2$. Results in Figs. 3.14 and 3.15 show that MAI may exceed the impact of thermal noise even for $K = 2$. While longer coherent integration times NT_1 can only improve the overall performance, small correlator spacings ϵ can effectively suppress MAI for code-phase estimation.

3.6.2.2 RFC of L1OF and (forthcoming) E1-D

Assessing the RFC between two C/A-type signals is particularly challenging, as both exhibit strong spectral lines in their PSD and are prone to MAI. An example for such a scenario is considered in the following.

There is currently discussion at which carrier frequency to transmit the forthcoming Galileo E1 C/A signal, which we will refer to as E1-D. While transmission in the already congested frequency band around 1575.42 MHz is unlikely (WALLNER *et al.*, 2020), it is one option to

Figure 3.15 – Code-phase standard deviation vs. bandwidth and correlator spacing with E1-B for $NT_1 = 80$ ms. (a) CGA for worst-case intrasystem MAI ($K = 2, C_2/C_1 = 3$ dB). (b) Contribution of AWGN ($C_1/N_0 \approx 44$ dB-Hz). Speed of light is given by $c = 2.998 \times 10^8$ m/s.

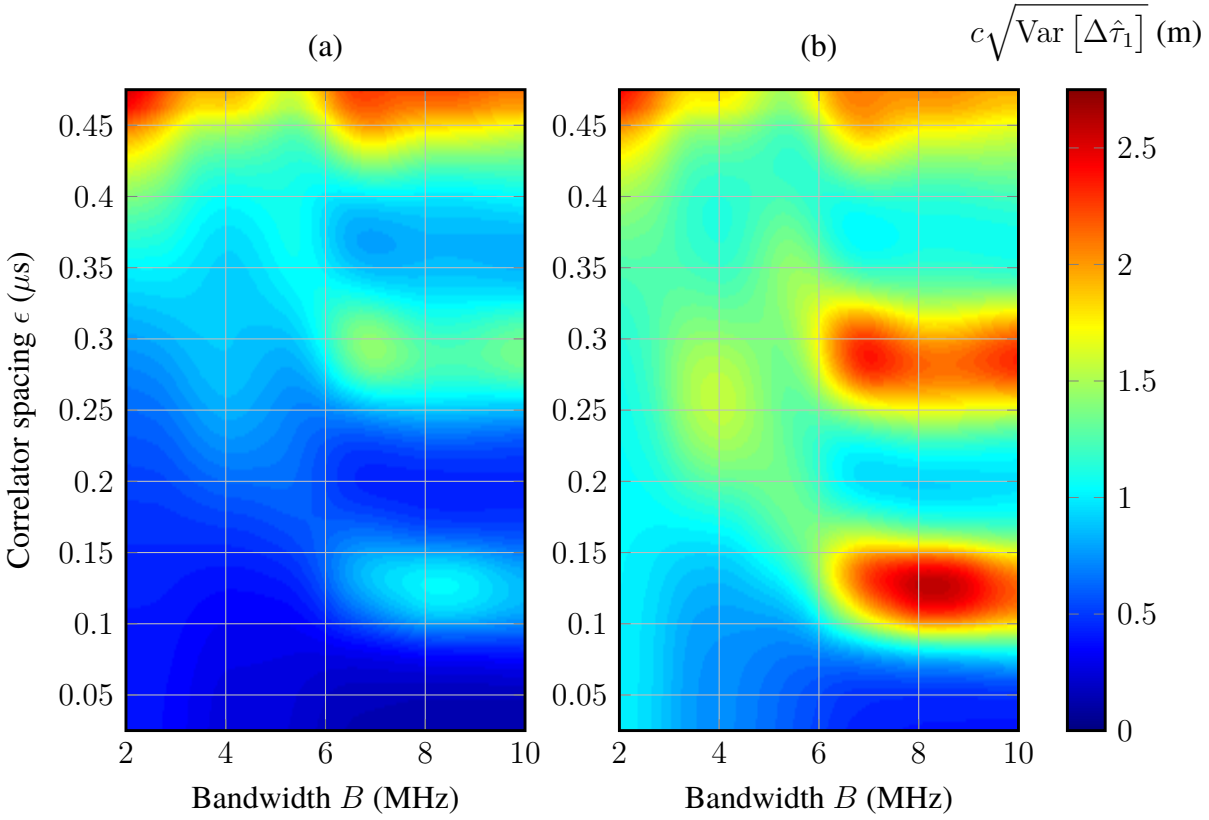

transmit E1-D at a higher carrier frequency

$$f_c = 1575.42\,\text{MHz} + m \times 1.023\,\text{MHz}, \tag{3.32}$$

with $m \in \{20, 21, \ldots, 30\}$ considered as possible offset factors. However, these possible carrier frequencies are near the legacy GLONASS L1OF signal, which uses FDMA and is therefore distributed to multiple frequency channels spanning either side of 1602 MHz. For the E1-D candidate signal, we assume a BPSK symbol modulation and a REC pulse with one of the possible chipping rates $1/T_c = z \times 1.023$ MHz, $z \in \{0.5, 1, 5\}$. We refer to these various design options by OBPSK(m, z). The smooth PSDs of these signal options, as well as the smooth PSD of L1OF, are shown in Fig. 3.16.

An additional degree of freedom is the choice of the symbol rate, which does not affect the smooth PSD but the fine features. While the L1OF symbol rate is fixed at 100 Hz (resulting from a 50 Hz navigation message encoded by a Manchester scheme), options for E1-D include symbol rates $1/T_b \in \{25, 50, 100, 1000\}$ Hz. The resulting code spectra are shown in

Figure 3.16 – Smooth PSDs of GLONASS L1OF and design options for a Galileo E1 C/A signal.

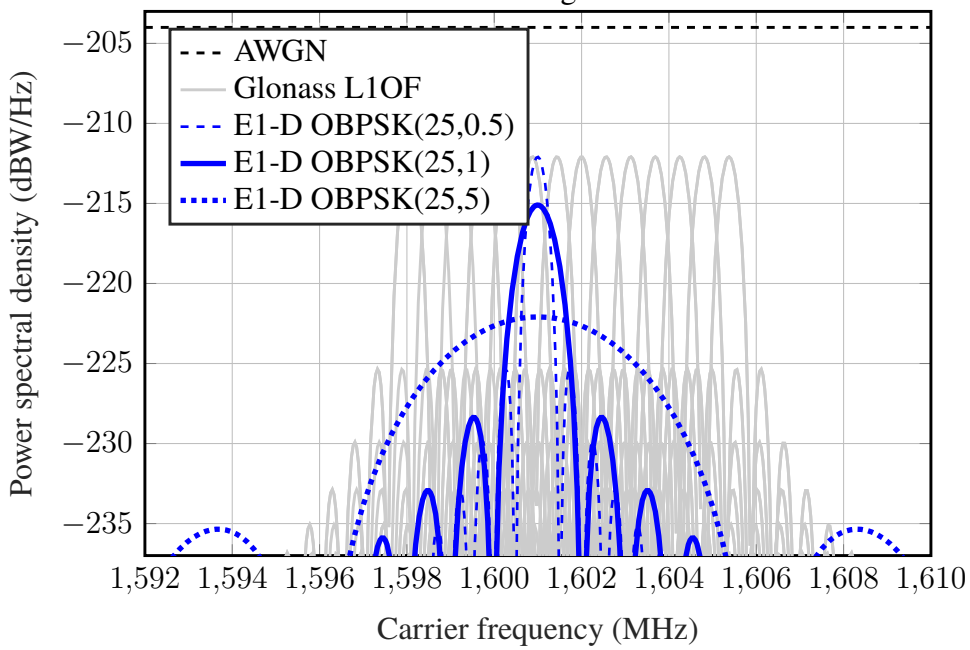

Figure 3.17 – Code spectrum of L1OF signal (exemplary selection of PRN and frequency range).

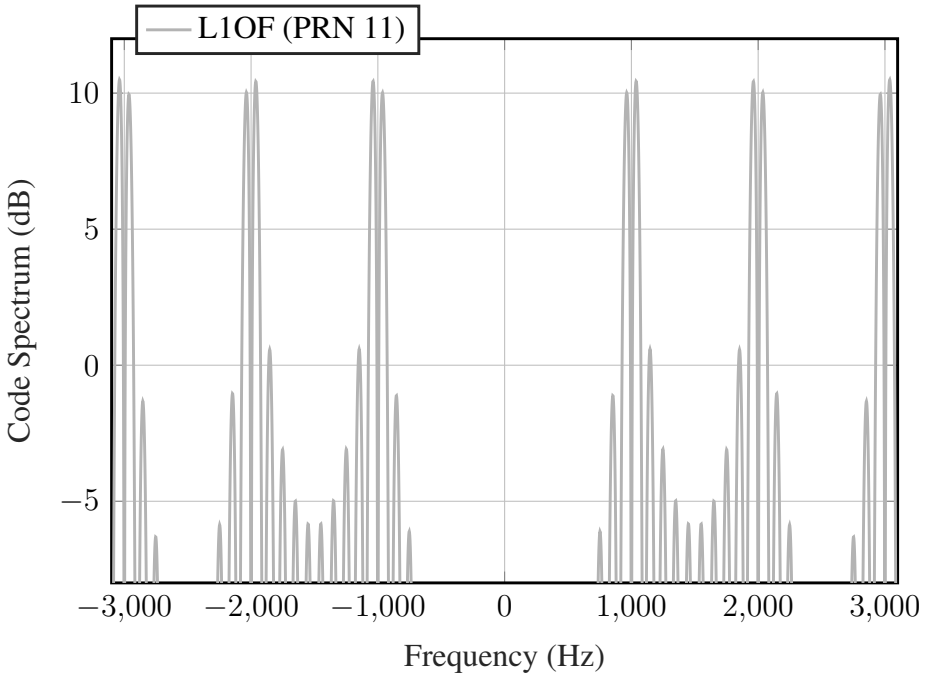

Figs. 3.17 and 3.18, respectively. As PRN codes for E1-D are yet unknown, a finite random code was assumed (AVILA-RODRIGUEZ, 2008); therefore, we show the expectation $\mathrm{E}[|A_k(f)|^2]$.

In the first step, we consider the SSC (3.30) obtained with and without taking into account the code spectrum. The results are shown in Fig. 3.19 for E1-D MAI-A, and in Fig. 3.20 for the intersystem MAI between E1-D and a GLONASS L1OF signal, if both are transmitted at the same carrier frequency. Note that a CGA approach cannot be used here, since the deterministic

Figure 3.18 – Code spectrum of E1-D (assuming random finite codes), for various symbol durations T_b.

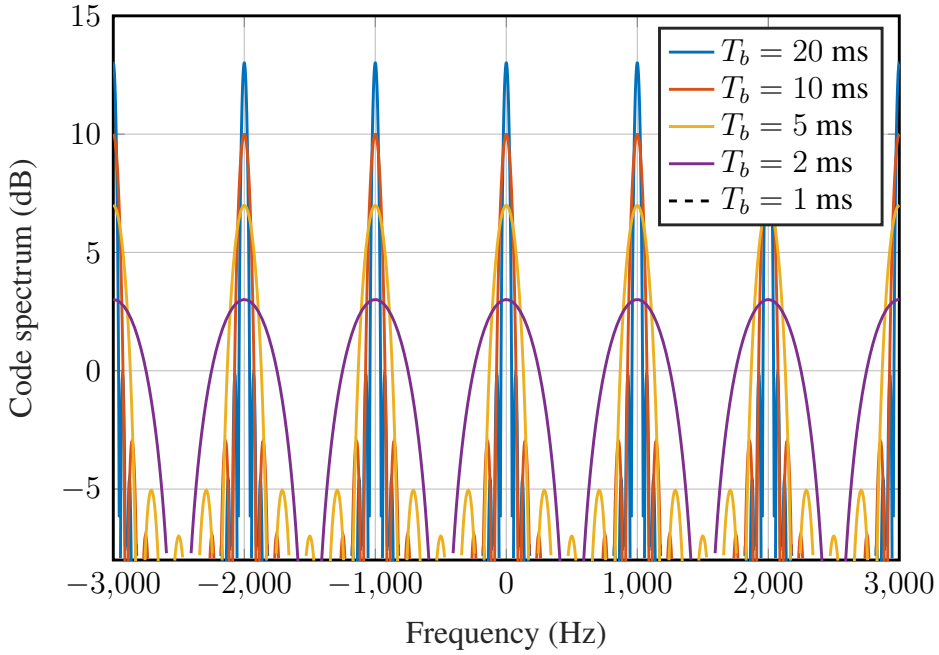

Figure 3.19 – SSC for E1-D MAI-A, for various E1-D symbol duration candidates T_b. The thick solid line is also obtained when neglecting the code spectrum features.

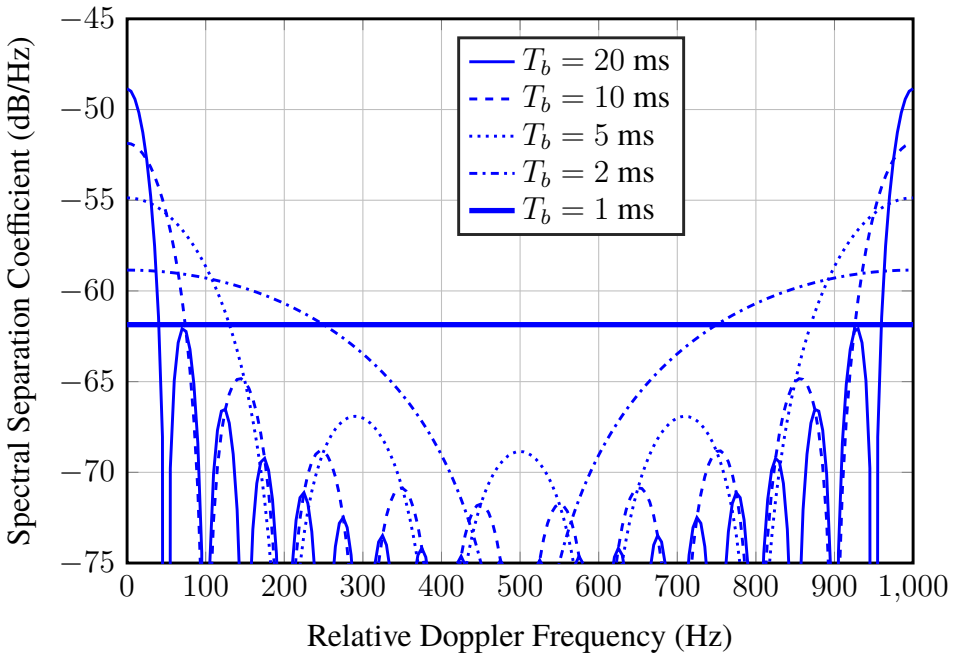

E1-D PRN code would have to be known for the computation of $Q_k(f)$.

In the next step, we perform a constellation simulation to determine the distribution of the SINR loss Ψ (3.27) due to MAI-A and intersystem MAI from the point of view of a E1-D receiver. Since the constellation period is 10 sidereal days for Galileo and 8 sideral days for GLONASS, we use a total simulation time of 40 sidereal days (least common multiple) and compute (3.27) every 60 seconds. Let the set of Galileo satellites be denoted by $\mathcal{K}_A = \{1, \ldots, 24\}$

Figure 3.20 – SSC for intersystem MAI between E1-D and L1OF, for various E1-D symbol duration candidates T_b. The thick solid line is also obtained when neglecting the code spectrum features.

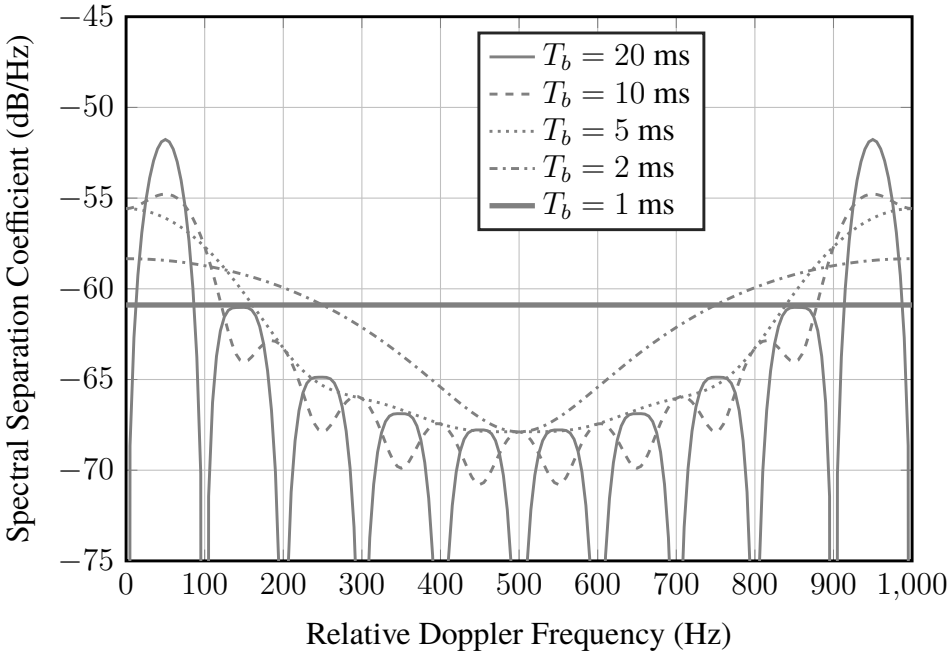

(nominal Walker constellation (EUROPEAN…, 2019)), and the set of GLONASS satellites by $\mathcal{K}_B = \{25, \ldots, 49\}$ (Almanac data (GLONASS…, 2016) from January 2018), and let the SOI be given by the satellite from Galileo satellite $k = 1$. For simplicity, we assume that the received powers are uniform $C_1 = \ldots = C_{49} \triangleq C$ for every satellite that is visible under at least $5°$ elevation (isoflux pattern assumption), and that the antenna gain is zero otherwise. Then, the SINR loss is simply given by

$$\Psi = \frac{C}{N_0}\Bigg(\underbrace{\sum_{\substack{k\in\mathcal{K}_A\\k\neq 1}}\psi_k}_{\mathrm{SSC}_A} + \underbrace{\sum_{k\in\mathcal{K}_B}\psi_k}_{\mathrm{SSC}_B}\Bigg). \tag{3.33}$$

The distributions of the individual contributions SSC_A and SSC_B are shown in Fig. 3.21 for the offset BPSK (OBPSK)$(25, 5)$ option. From experience, values larger than -60 dB/Hz begin to affect GNSS receiver performance (ITU-R, 2015; HEGARTY, 2020). While SSC_A and SSC_B are below this value on average, they exceed by several dB/Hz in worst-case constellations. In Fig. 3.22, we show the average, 95%-quantile, and worst case values of SSC_A and SSC_B for the OBPSK$(m, 1)$ option as a function of m (carrier frequency). Not surprisingly, carrier frequencies which lead to less intersystem interference from L1OF can be found further away from the L1OF center at 1602 MHz. Notably, however, the average SSCs are not a meaningful quantity when assessing MAI for signals with long symbol durations.

Figure 3.21 – Distribution of contributions to SINR loss caused by E1-D self-interference and L1OF intersystem interference, for E1-D OBPSK$(25, 5)$. Period under consideration: 40 sideral days.

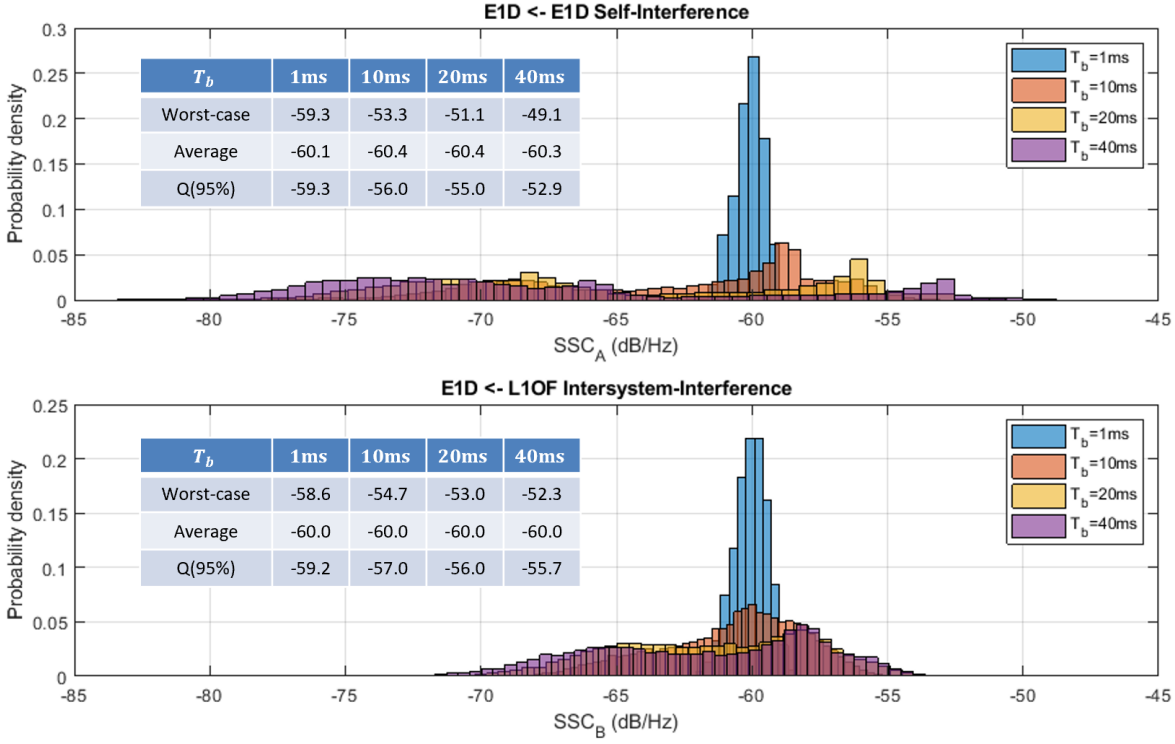

T_b	1ms	10ms	20ms	40ms
Worst-case	-59.3	-53.3	-51.1	-49.1
Average	-60.1	-60.4	-60.4	-60.3
Q(95%)	-59.3	-56.0	-55.0	-52.9

T_b	1ms	10ms	20ms	40ms
Worst-case	-58.6	-54.7	-53.0	-52.3
Average	-60.0	-60.0	-60.0	-60.0
Q(95%)	-59.2	-57.0	-56.0	-55.7

Furthermore, the distribution of $\sqrt{\mathrm{Var}[\Delta\hat{\tau}_1]}$ (3.25) under the SGA is shown in Figs. 3.23-3.25 for the three OBPSK$(25, z)$ options with $z = 5, 1, 0.5$, respectively. While the code-phase estimation accuracy may be a more intuitive performance measure, some assumptions had to be placed on received power levels and setup of the code-phase estimator. We assumed $C = -155\,\mathrm{dBW}$ received power from all satellites, $B = 12.28$ MHz front-end bandwidth, $\epsilon = 0.25 \times 977.52$ ns correlator spacing, and smoothing of the code-phase estimate with a 1 Hz first-order loop filter (KAPLAN; HEGARTY, 2005). It can be observed that the wideband option $z = 5$ is more robust to MAI.

Figure 3.22 – Total SSC contributions to SINR loss caused by E1-D self-interference (SSC_A) and by L1OF intersystem interference (SSC_B), as a function of the carrier frequency of E1-D OBPSK$(m, 1)$. Period under consideration: 40 sideral days.

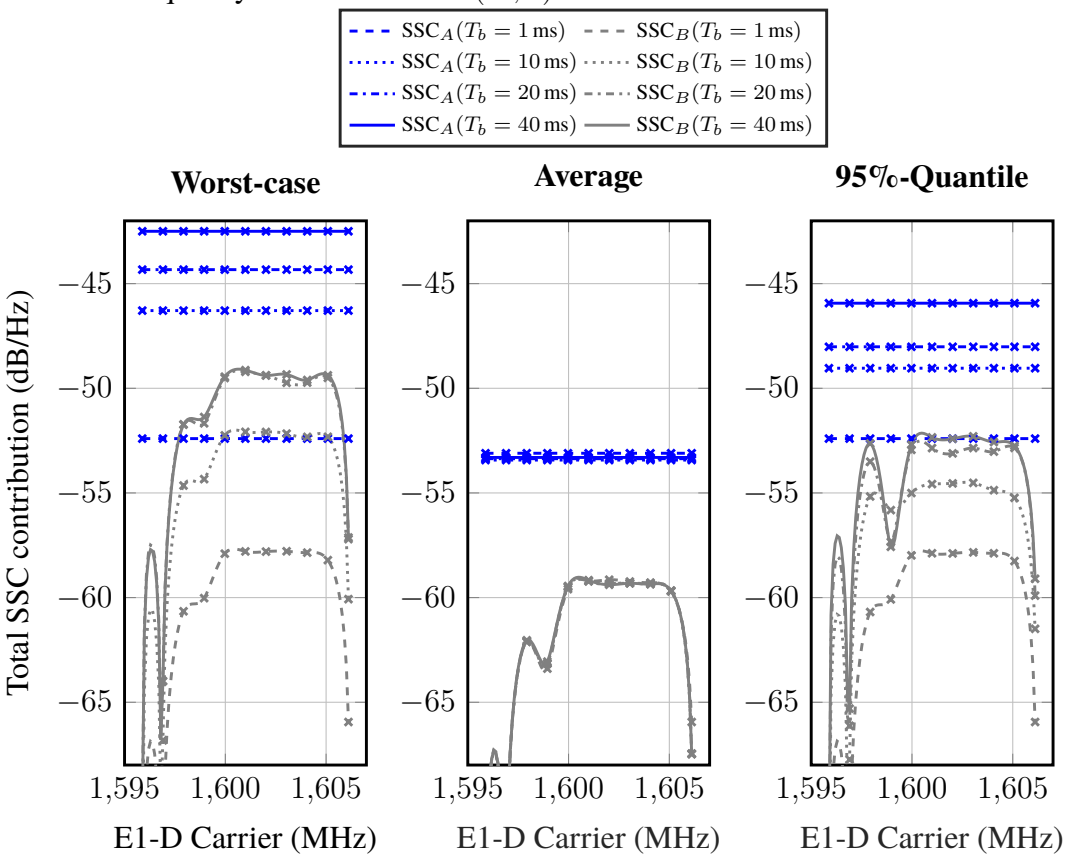

Figure 3.23 – Distribution of code-phase RMSE (in meters) caused by E1-D self-interference and L1OF intersystem interference, for E1-D OBPSK$(25, 5)$. Period under consideration: 40 sideral days.

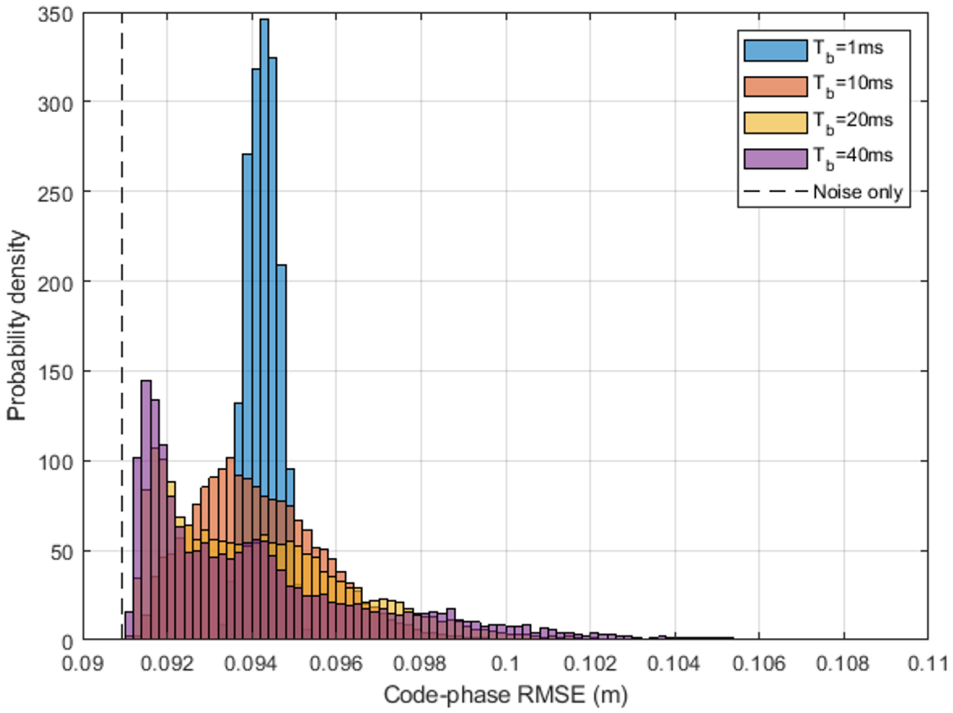

Figure 3.24 – Distribution of code-phase RMSE (in meters) caused by E1-D self-interference and L1OF intersystem interference, for E1-D OBPSK$(25, 1)$. Period under consideration: 40 sideral days.

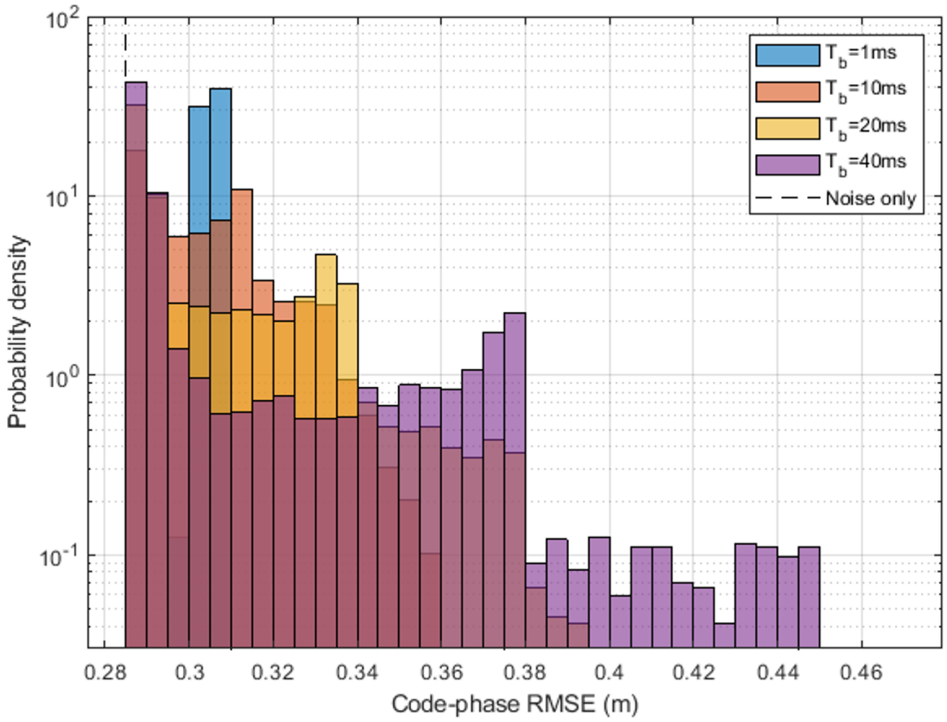

Figure 3.25 – Distribution of code-phase RMSE (in meters) caused by E1-D self-interference and L1OF intersystem interference, for E1-D OBPSK$(25, 0.5)$. Period under consideration: 40 sideral days.

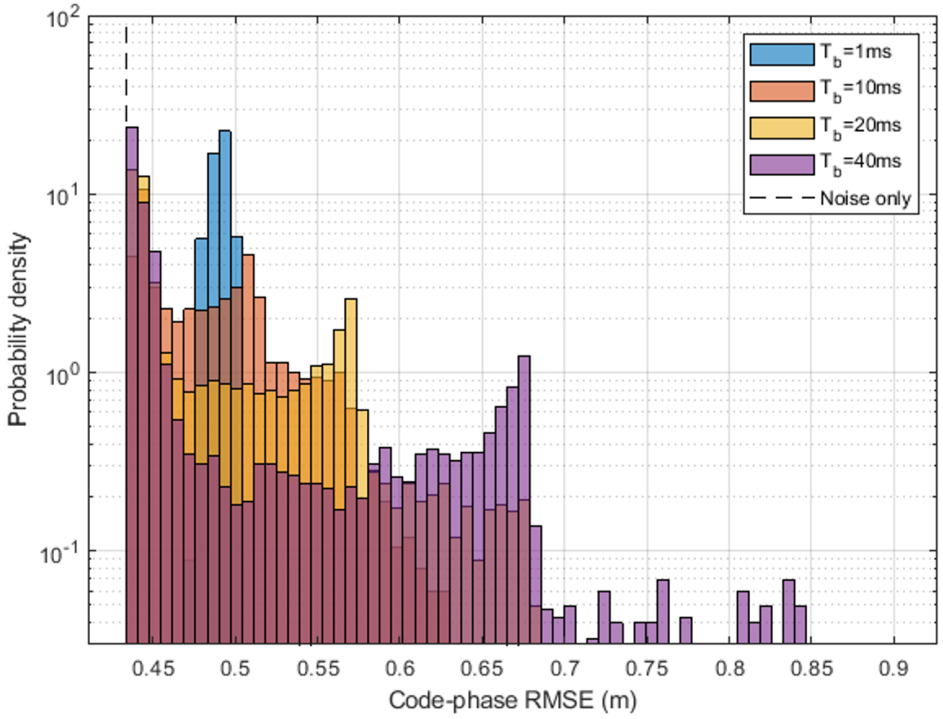

4 CONCLUSION

The present thesis discussed the problem of MAI in satellite navigation between signals of one GNSS and between signals of different GNSSs. This was done with a focus on the transmitter (system operator) side, targeting the design of novel acquisition-aiding GNSS signals and the coordination and assessment of interference between newly introduced and existing signals in a shared frequency band.

We argued that C/A signals with short PRN code and low symbol/data rate are still an attractive option to facilitate rapid, low-energy acquisition − even 43 years after the first transmission of the GPS L1 C/A signal. With regard to the huge group of mass-market GNSS-enabled electronic devices, each GNSS may eventually introduce a new C/A signal to their portfolio, or (in the case of GPS and GLONASS) re-design their existing legacy C/A signals. Interestingly, many of the C/A features that facilitate acquisition (short PRN code, low symbol rate, low bandwidth, high transmit power) are precisely the features which strain the GNSS's DS-CDMA scheme by increasing MAI-A. While considerable research has been performed on the topic of MAI-A between L1 C/A signals, its effect on the 2-D signal acquisition in the code/Doppler domain has not yet been investigated systematically. We demonstrated that some few Doppler search bins can be severely affected by C/A-on-C/A interference, and are thus more likely to lead to a global false alarm in the acquisition search. We proposed the randomized SSC-R approach that can be used to assess the acquisition reliability in terms of the ROC curve (GPD plotted vs. GPF). Compared with state-of-the-art methods, the SSC-R achieves a trade-off between the accurate but computationally costly SSC-D and the overly simplistic standard SSC. While it is based on the simplifying assumption of randomized i.i.d. MAI-A across search bins, we retain the accuracy of the SSC-D, its key element being the Doppler-dependency of MAI-A. Owing to its accuracy and simplicity, the SSC-R is suitable not only for performance evaluation but also for system optimization, where PRN code length, symbol rate, and other signal characteristics are flexible parameters to be selected. With regard to the (re-)design of C/A signals with short PRN codes, the developed methodology allows us to draw the following conclusions (in answer to Q1):

- The PRN code length needs to be chosen with great attention to the modeling of the receiver's acquisition reliability. In particular, if the PRN code is too short, the user may not be able to acquire signals reliably due to MAI-A.
- The PRN code length can be minimized down to the order of 300-700 without excessive

loss of acquisition reliability, considering typical constraints on the available received power, number of in-view satellites, and coherent integration times.

- Reduction of the symbol rate has opposite effects on the acquisition performance. On the one hand, higher levels of MAI-A can be observed, as the decorrelating effect of symbol modulation ceases (cf. Fig. 2.5); on the other hand, symbol transitions are less likely to occur during the receiver's coherent integration time. Overall, the latter effect was observed to outweigh the previous, so that best results in terms of reliability and sensitivity were achieved by signals with zero symbol rate.

This minimum PRN code length could be used by a future Galileo C/A signal, which would reduce the size of the acquisition search grid by a factor of 18-36 as compared with the current Galileo E1 OS, and still by a factor of 1.5-3 as compared with GPS L1 C/A. Beyond the scope of this thesis, however, such a "pure pilot" signal may lead to an ambiguity resolution problem during the handover to other signal components or during the pseudorange computation (WALLNER *et al.*, 2020).

Furthermore, we addressed the question how the RFC of these and other newly launched GNSS signals with existing GNSS signals can be ensured. Signals are said to be radio frequency compatible if they can coexist in a shared frequency band without harming receiver functionalities; this includes the SINR measure (and derivatives thereof), but also more palpable performance measures such as code-/carrier-phase synchronization accuracy. Intra- and intersystem interference are already affecting the receiver's synchronization parameter estimation, and may become a more important nuisance in the future with the introduction of more C/A-type signals and/or with the further increase of transmit power levels. In such a future multi-constellation scenario with interference-limited receiver performance, it would be important to model MAI with a higher level of detail to be able to assess RFC accurately. We reviewed conventional and state-of-the-art RFC modeling, and proposed a way forward for the case that GNSSs continue their transformation from noise-limited to interference-limited DS-CDMA systems (in answer to Q2):

- We identified a number of mismatched assumptions on the statistical properties of GNSS signals. We pointed out that the currently used WSS/proper approximation is not fulfilled by any of today's GNSS signals. Instead, we argued that they are more accurately modeled as being WSCS/improper, owing to the effects of periodic PRN code, pulse shape, and BPSK (or non-circular interplexing of multiple BPSK) symbol alphabets.
- The MAI from such a signal after correlation is not, in general, CSG distributed. However,

it is well approximated as Gaussian distributed when conditioned on channel parameters (Doppler frequency, code-phase, carrier-phase). Based on a detailed review of state of the art research in the context of GNSS (which has focused on the effect of Doppler frequency) and in the context of terrestrial communications (which has focused on the effect of code- and carrier-phase), we derived a generalized CGA for MAI, which takes into account the effect of all three channel parameters; moreover, the generalization to improper symbol alphabets is unique to our refined MAI model. Further, this model can take into account unique symbol/chipping rates, pulse shapes, and deterministic PRN codes for each signal.

- Based on a WSCS/improper signal model with conditionally Gaussian distributed correlator outputs, we derived a full second-order characterization of MAI after correlation. This consists of the (co-)variances and conjugate (co-)variances of an early, prompt, and late correlator output. Based on that, we derived accurate receiver-specific expressions for performance in terms of SINR, carrier-phase estimation accuracy, and code-phase estimation accuracy.

Simulation results demonstrated that the proposed methodology allows for a more accurate evaluation of the receiver's SINR, code-phase and carrier-phase estimation accuracy. The proper/WSS/CSG approximations lead to overoptimistic results, especially when we investigated the intersystem interference between the C/A-type signals L1OF and E1-D.

In sum, this thesis identified a variety of problems related to intra- and intersystem interference, which are expected to be encountered by GNSS signal designers and system operators in the near future. We argued that the current trend towards more navigation satellites, more navigation signals transmitted per satellite, less signal complexity, and higher signal power, requires a better understanding of estimation and detection performance of DS-CDMA in the presence of MAI from satellites. We developed mathematical methodologies to assess the impact of MAI on receiver performance in terms of acquisition reliability and synchronization accuracy. While we have focused on the GNSSs (GPS, GLONASS, Galileo, and Beidou), the results may also be useful and applicable to satellite constellations other than MEO such as mega-constellation networks, which are very prone to interference (HÖYHTYÄ *et al.*, 2017). In general, the proposed methodologies can be utilized for the analysis and design of next-generation satellite navigation signals whose performance is limited by MAI rather than noise.

REFERENCES

AGREEMENT on the promotion, provision and use of Galileo and GPS satellite-based navigation systems and related applications. Dromoland Castle, Ireland: Council of the European Union, 2004.

ANGHILERI, M. *et al.* FUNTIMES - Future Navigation and Timing Evolved Signals. In: **Proceedings of the 31st International Technical Meeting of the Satellite Division of The Institute of Navigation (ION GNSS+ 2018)**. Miami, Florida: [s.n.], 2018. p. 876–912.

ANTREICH, F.; NOSSEK, J. A. Optimum chip pulse shape design for timing synchronization. In: **2011 IEEE international conference on acoustics, speech and signal processing (ICASSP)**. [S.l.: s.n.], 2011. p. 3524–3527.

AVILA-RODRIGUEZ, J.-A. **On Generalized Signal Waveforms for Satellite Navigation**. jun. 2008. Tese (Doutorado) — University of the Federal Armed Forces (UFAF) Munich.

BeiDou Navigation Satellite System Signal In Space Interface Control Document: Open Service Signal B1C. [S.l.]: China Satellite Navigation Office, 2017.

BeiDou Navigation Satellite System Signal In Space Interface Control Document: Open Service Signal B2a. [S.l.]: China Satellite Navigation Office, 2017.

BeiDou Navigation Satellite System Signal In Space Interface Control Document: Open Service Signal B2b. [S.l.]: China Satellite Navigation Office, 2020.

BeiDou Navigation Satellite System Signal In Space Interface Control Document: Open Service Signal B3I. [S.l.]: China Satellite Navigation Office, 2018.

BETZ, J. W. Effect of Narrowband Interference on GPS Code Tracking Accuracy. In: **Proceedings of the 2000 National Technical Meeting of The Institute of Navigation**. Anaheim, CA: [s.n.], 2000. p. 16–27.

BETZ, J. W. Binary offset carrier modulations for radionavigation. **NAVIGATION, Journal of The Institute of Navigation**, v. 48, n. 4, p. 227–246, dez. 2001.

BETZ, J. W. Effect of Partial-Band Interference on Receiver Estimation of C/N0: Theory. In: **Proceedings of the 2001 National Technical Meeting of The Institute of Navigation**. Long Beach, CA: [s.n.], 2001. p. 817–828.

BETZ, J. W.; KOLODZIEJSKI, K. R. Generalized theory of code tracking with an early-late discriminator part I: Lower bound and coherent processing. **IEEE Transactions on Aerospace and Electronic Systems**, v. 45, n. 4, p. 1538–1556, out. 2009.

BETZ, J. W.; KOLODZIEJSKI, K. R. Generalized theory of code tracking with an early-late discriminator part II: Noncoherent processing and numerical results. **IEEE Transactions on Aerospace and Electronic Systems**, v. 45, n. 4, p. 1557–1564, out. 2009.

BONNOR, N. A Brief History of Global Navigation Satellite Systems. **The Journal of Navigation**, v. 65, n. 1, p. 1–14, jan. 2012.

BORIO, D. **A Statistical Theory for GNSS Signal Acquisition**. 2008. Tese (Doutorado) — Politecnico di Torino.

BORIO, D.; CAMORIANO, L.; PRESTI, L. L. Impact of GPS acquisition strategy on decision probabilities. **IEEE Transactions on Aerospace and Electronic Systems**, v. 44, n. 3, p. 996–1011, jul. 2008. ISSN 0018-9251.

CHEN, K. *et al.* Modeling and Improving the Energy Performance of GPS Receivers for Location Services. **IEEE Sensors Journal**, v. 20, n. 8, p. 4512–4523, abr. 2020. ISSN 1530-437X, 1558-1748, 2379-9153.

CHENG, U.; HURD, W.; STATMAN, J. Spread-spectrum code acquisition in the presence of Doppler shift and data modulation. **IEEE Transactions on Communications**, v. 38, n. 2, p. 241–250, fev. 1990. ISSN 00906778.

CHO, J. H.; JEONG, Y. K.; LEHNERT, J. S. A closed-form BER expression for band-limited DS/SSMA communications. In: **Proc. IEEE military commun. Conf. 2000**. Los Angeles, CA: [s.n.], 2000.

CHO, J. H.; LEHNERT, J. S. An optimal signal design for band-limited asynchronous DS-CDMA communications. **IEEE Transactions on Information Theory**, v. 48, n. 5, p. 1172–1185, maio 2002.

COENEN, A.; VAN NEE, D. Novel fast GPS/GLONASS code-acquisition technique using low update rate FFT. **Electronics Letters**, v. 28, n. 9, p. 863, 1992. ISSN 00135194.

COLBURN, R. Global Positioning System Status and Modernization. In: **Proceedings of the 33rd International Technical Meeting of the Satellite Division of The Institute of Navigation (ION GNSS+ 2020)**. St. Louis, Missouri: [s.n.], 2020. p. 929–937.

CORAZZA, G. On the MAX/TC criterion for code acquisition and its application to DS-SSMA systems. **IEEE Transactions on Communications**, v. 44, n. 9, p. 1173–1182, set. 1996. ISSN 00906778.

DAFESH, P. A.; CAHN, C. R. Phase-optimized constant-envelope transmission (POCET) modulation method for GNSS signals. In: **Proceedings of the 22nd International Technical Meeting of the Satellite Division of The Institute of Navigation (ION GNSS 2009)**. Savannah, GA: [s.n.], 2009. p. 2860– 2866.

DAUTERMANN, T. *et al.* Non-Gaussian error modeling for GBAS integrity assessment. **IEEE Transactions on Aerospace and Electronic Systems**, v. 48, n. 1, p. 693–706, jan. 2012.

DICARLO, D.; WEBER, C. Multiple Dwell Serial Search: Performance and Application to Direct Sequence Code Acquisition. **IEEE Transactions on Communications**, v. 31, n. 5, p. 650–659, maio 1983. ISSN 0096-2244. Disponível em: ⟨http://ieeexplore.ieee.org/document/1095867/⟩.

EASTON, R.; BUISSON, J.; MCCASKILL, T. **Initial results of the NAVSTAR GPS NTS-2 satellite**. Washington, D. C., 1978. Disponível em: ⟨https://books.google.de/books?id=WsmPugEACAAJ⟩.

ENNEKING, C.; ANTREICH, F.; ALMEIDA, A. L. F. de. GNSS Acquisition Performance of Short Spreading Codes. In: **33rd International Technical Meeting of the Satellite Division of The Institute of Navigation (ION GNSS+ 2020)**. [S.l.: s.n.], 2020. p. 1238–1260.

ENNEKING, C. *et al.* Pure Pilot Signals: How Short can we Choose GNSS Spreading Codes? In: **2019 International Technical Meeting of The Institute of Navigation**. Reston, Virginia: [s.n.], 2019. p. 925–935.

ENNEKING, C. *et al.* Gaussian Approximations for Intra- and Intersystem Interference in RNSS. **IEEE Communications Letters**, v. 23, n. 7, p. 1198–1201, jul. 2019.

ENNEKING, C. *et al.* Multi-satellite time-delay estimation for reliable high-resolution GNSS receivers. In: **Proceedings of the 2012 IEEE/ION position, location and navigation symposium**. [S.l.: s.n.], 2012. p. 488–494.

ESPLUGA, L. O. *et al.* New Solutions on the Design of a Galileo Acquisition-Aiding Signal to Improve the TTFF and the Sensitivity. In: **Proceedings of the 2018 International Technical Meeting of The Institute of Navigation**. Reston, Virginia: [s.n.], 2018. p. 810–825.

EUROPEAN GNSS (Galileo) Open Service: Service Definition Document. In: . [S.l.]: European Union, 2019.

EUROPEAN GNSS (Galileo) Open Service: Signal-in-Space Interface Control Document. European Union, OS SIS ICD Issue 1.3, Interface Specification: [s.n.], 2016.

EUROPEAN GNSS SUPERVISORY AUTHORITY. **GNSS market report**. LU: Publications Office, 2019. Disponível em: ⟨https://data.europa.eu/doi/10.2878/031762⟩.

FONTANA, R. D. *et al.* The New L2 Civil Signal. In: **Proceedings of the 14th International Technical Meeting of the Satellite Division of The Institute of Navigation (ION GPS 2001)**. Salt Lake City, UT: [s.n.], 2001. p. 617–631.

FOUCRAS, M. *et al.* Probability of detection for GNSS signals with sign transitions. **IEEE Transactions on Aerospace and Electronic Systems**, v. 52, n. 3, p. 1296–1308, jun. 2016.

G. Zang; C. Ling. Performance evaluation for band-limited DS-CDMA systems based on simplified improved Gaussian approximation. **IEEE Transactions on Communications**, v. 51, n. 7, p. 1204–1213, jul. 2003. ISSN 0090-6778.

GARDNER, W. A.; NAPOLITANO, A.; PAURA, L. Cyclostationarity: Half a century of research. **Signal Processing**, v. 86, n. 4, p. 639–697, abr. 2006. ISSN 0165-1684. Number of pages: 59 Publisher: Elsevier North-Holland, Inc. tex.acmid: 1139726 tex.address: Amsterdam, The Netherlands, The Netherlands tex.issue_date: April 2006. Disponível em: ⟨http://dx.doi.org/10.1016/j.sigpro.2005.06.016⟩.

GEIGER, B. C.; VOGEL, C. Influence of Doppler Bin Width on GPS Acquisition Probabilities. **IEEE Transactions on Aerospace and Electronic Systems**, v. 49, n. 4, p. 2570–2584, out. 2014. ISSN 0018-9251. ArXiv: 1107.1972. Disponível em: ⟨http://arxiv.org/abs/1107.1972⟩.

GEIGER, B. C.; VOGEL, C.; SOUDAN, M. Comparison Between Ratio Detection and Threshold Comparison for GNSS Acquisition. **IEEE Transactions on Aerospace and Electronic Systems**, v. 48, n. 2, p. 1772–1779, 2012. ISSN 0018-9251.

GLOBAL Positioning System Standard Positioning Service Signal Specification. National Coordination Office for Space-Based Positioning, Navigation, and Timing., 1993. Disponível em: ⟨https://www.gps.gov/technical/ps/1993-SPS-signal-specification.pdf⟩.

GLONASS Interface Control Document. Montreal, Canada: International Civil Aviation Organization (ICAO), 1995.

GLONASS Interface Control Document, General Description of Code Division Multiple Access Signal System. Moscow: Russian Space Systems, 2016.

GOLD, R. Optimal binary sequences for spread spectrum multiplexing. **IEEE Transactions on Information Theory**, v. 13, n. 4, p. 619–621, out. 1967.

GOLSHAN, R. *et al.* Implications of C/A-on-C/A Interference on Carrier Tracking Loop Performance. In: **Proceedings of the 27th International Technical Meeting of The Satellite Division of the Institute of Navigation (ION GNSS+ 2014)**. Tampa, Florida: [s.n.], 2014. p. 3510–3525.

GSA. **Power-efficient positioning for the Internet of Things: merging GNSS with low power connectivity solutions: white paper.** [S.l.]: European GNSS Agency (GSA), Publications Office, 2020.

HEGARTY, C. J. A simple model for GPS C/A-code self-interference. **NAVIGATION**, v. 67, n. 2, p. 319–331, jun. 2020.

HEIN, G. W. *et al.* MBOC: The new optimized spreading modulation recommended for GALILEO L1 OS and GPS L1C. In: **2006 IEEE/ION position, location, and navigation symposium**. [S.l.: s.n.], 2006. p. 883–892.

HEIN, G. W. *et al.* The GALILEO Frequency Structure and Signal Design. In: **Proceedings of the 14th International Technical Meeting of the Satellite Division of The Institute of Navigation (ION GPS 2001)**. Salt Lake City, UT: [s.n.], 2001. p. 1273 – 1282.

HOLMES, J. K. **Spread spectrum systems for GNSS and wireless communications**. [S.l.]: Artech House, 2007.

HUDNUT, K. W.; TITUS, B. GPS L1 Civil Signal Modernization (L1C). In: **Stewardship Project 204: The L1C Project**. [S.l.]: Interagency GPS Executive Board, 2004.

HÖYHTYÄ, M. *et al.* Database-assisted spectrum sharing in satellite communications: A survey. **IEEE Access**, v. 5, p. 25322–25341, 2017.

ITU. **Final Acts of the World Radiocommunication Conference (WRC-2000)**. Istanbul, Turkey: International Telecommunication Union Library & Archives Service, 2000. 560–563 p.

ITU-R. **A coordination methodology for radionavigation-satellite service intersystem interference estimation**. [S.l.: s.n.], 2015. (Recommend., M.1831-1).

KANIUTH, R. *et al.* A snap-shot positioning approach for a high integrated GPS/Galileo chipset. In: **Proceedings of the 18th International Technical Meeting of the Satellite Division of the Institute of Navigation (ION GNSS 2005)**. Long Beach, CA: [s.n.], 2005. p. 1153–1159.

KAPLAN, E.; HEGARTY, C. **Understanding GPS: Principles and applications**. [S.l.]: Artech House, 2005. (Artech House mobile communications series).

LAPIDOTH, A. **A Foundation in Digital Communication**. 2. ed. Cambridge: Cambridge University Press, 2017. ISBN 978-1-316-82270-8. Disponível em: ⟨http://ebooks.cambridge.org/ref/id/CBO9781316822708⟩.

LOK, T. M.; LEHNERT, J. S. An asymptotic analysis of DS/SSMA communication systems with general linear modulation and error control coding. **IEEE Transactions on Information Theory**, v. 44, n. 2, p. 870–881, mar. 1998.

LOPEZ-RISUENO, G.; SECO-GRANADOS, G. CN0 estimation and near-far mitigation for GNSS. In: **2005 IEEE 61st Vehicular Technology Conference**. [S.l.: s.n.], 2005.

MARCUM, J. A statistical theory of target detection by pulsed radar. **IRE Transactions on Information Theory**, v. 6, n. 2, p. 59–267, 1960.

MISRA, P.; ENGE, P. **Global Positioning System: Signals, Measurements, and Performance**. Rev. 2. ed. Lincoln, MA: Ganga-Jamuna Press, 2011.

NAGLE, J.; VAN DIERENDONCK, A. J.; HUA, Q. Inmarsat-3 navigation signal C/A code selection and interference analysis. **NAVIGATION, Journal of The Institute of Navigation**, v. 39, n. 4, p. 445–462, 1992.

NAVSTAR GPS Space Segment/ User Segment L1C Interfaces. El Segundo, CA: GPS Enterprise, 2020. (IS-GPS-800, Rev. G).

NAVSTAR GPS Space Segment/ User Segment L5 Interfaces. El Segundo, CA: GPS Enterprise, 2020. (IS-GPS-705, Rev. G).

NAVSTAR GPS Space Segment/Navigation User Interfaces. El Segundo, CA: GPS Enterprise, 2020. (IS-GPS-200, Rev. L).

O'DRISCOLL, C. **Performance analysis of the parallel acquisition of weak GPS signals**. 2007. Tese (Doutorado) — University College Cork.

O'DRISCOLL, C.; FORTUNY-GUASCH, J. On the Determination of C/A Code Self-Interference with Application to RFC Analysis and Pseudolite Systems. In: **Proceedings of the 25th International Technical Meeting of The Satellite Division of the Institute of Navigation (ION GNSS 2012)**. Nashville, TN: [s.n.], 2012. p. 3620–3631.

PAONNI, M. *et al.* Quasi-Pilot Signals: Improving Sensitivity and TTFF without Compromises. In: **Proceedings of the 24th International Technical Meeting of the Satellite Division of The Institute of Navigation (ION GNSS 2011)**. Portland, Oregon: [s.n.], 2011. p. 1254–1263.

PAONNI, M.; BAVARO, M. On the Design of a GNSS Acquisition Aiding Signal. In: **Proceedings of the 26th International Technical Meeting of the Satellite Division of The Institute of Navigation (ION GNSS+ 2013)**. Nashville, Tennessee: [s.n.], 2013. p. 1445–1456.

PARKINSON, B. W.; POWERS, S. T. The origins of GPS: Part I. **GPS World**, v. 21, n. 5, p. 30–41, maio 2010.

POLYDOROS, A.; WEBER, C. A Unified Approach to Serial Search Spread-Spectrum Code Acquisition–Part I: General Theory. **IEEE Transactions on Communications**, v. 32, n. 5, p. 542–549, 1984. ISSN 0090-6778.

POLYDOROS, A.; WEBER, C. A Unified Approach to Serial Search Spread-Spectrum Code Acquisition–Part II: A Matched-Filter Receiver. **IEEE Transactions on Communications**, v. 32, n. 5, p. 550–560, 1984. ISSN 0090-6778.

PROAKIS, J. **Digital communications**. [S.l.]: McGraw-Hill, 2001. (Electrical engineering series).

PURSLEY, M. Performance evaluation for phase-coded spread-spectrum multiple-access communication - part I: System analysis. **IEEE Transactions on Communications**, v. 25, n. 8, p. 795–799, ago. 1977.

QAISAR, S.; DEMPSTER, A. Cross-correlation performance assessment of global positioning system (GPS) L1 and L2 civil codes for signal acquisition. **IET Radar, Sonar & Navigation**, v. 5, n. 3, p. 195, 2011. ISSN 17518784.

QUINLAN, M. *et al.* Validation of novel navigation signal structures for future GNSS systems. In: **Position location and navigation symposium (PLANS)**. [S.l.: s.n.], 2004. p. 389–398.

RIES, L. *et al.* Tracking and Multipath Performance Assessments of BOC Signals Using a Bit-Level Signal Processing Simulator. In: **Proceedings of the 16th International Technical Meeting of the Satellite Division of The Institute of Navigation (ION GPS/GNSS 2003)**. Portland, OR: [s.n.], 2003. p. 1996 – 2010.

RTCA, Inc. **Assessment of Radio Frequency Interference Relevant to the GNSS L1 Frequency Band**. 2008. (DO-235).

SCHREIER, P. J.; SCHARF, L. L. **Statistical signal processing of complex-valued data: the theory of improper and noncircular signals**. Cambridge: Cambridge University Press, 2010.

SCHWEIKERT, R.; WOERZ, T. Signal Design and Transmission Performance Study for GNSS-2. In: **ESA Contract No. 12182/96/NL/JSC Final Report**. [S.l.: s.n.], 1998.

SCHWEIKERT, R. *et al.* On signal structures for GNSS-2. **International Journal of Satellite Communications**, v. 18, n. 4-5, p. 271–291, 2000.

SHAFRAN, S. V.; GIZATULOVA, E. A.; KUDRYAVTSEV, I. A. Snapshot technology in GNSS receivers. In: **2018 25th Saint Petersburg International Conference on Integrated Navigation Systems (ICINS)**. St. Petersburg: IEEE, 2018.

SHANMUGAM, S. K. *et al.* Design of Short Synchronization Codes for Use in Future GNSS System. **International Journal of Navigation and Observation**, v. 2008, p. 1–14, 2008.

SIMON, M.; HINEDI, S.; LINDSEY, W. **Digital communication techniques: Signal design and detection**. [S.l.]: PTR Prentice Hall, 1995. (Digital communication techniques, Bd. 1).

SPILKER, J. J. GPS signal structure and performance characteristics. **NAVIGATION, Journal of The Institute of Navigation**, v. 25, n. 2, p. 121–146, 1978.

SPILKER, J. J.; NATALI, F. D.; FITZGERALD, P. M. Defense Navigation Satellite Special Study. In: **Final Report Contract No. F04701-74-C-0053**. Los Angeles, CA: Stanford Telecommunications, Inc., 1974.

SPILKER, J. J.; ORR, R. S. Code multiplexing via majority logic for GPS modernization. In: **Proc. ION GNSS 11th Int. Tech. Meeting Satellite Div.** Nashville, TN: [s.n.], 1998. p. 265–273.

STANSELL, T. A. *et al.* Proposed Evolution of the C/A Signal. In: **Proceedings of the 28th International Technical Meeting of the Satellite Division of The Institute of Navigation (ION GNSS+ 2015)**. Tampa, Florida: [s.n.], 2015. p. 1807–1825.

SUNDARARAJAN, D. **A practical approach to signals and systems**. Singapore: John Wiley & Sons (Asia), 2008.

TANG, K.; SIEGEL, P.; MILSTEIN, L. A comparison of long versus short spreading sequences in coded asynchronous DS-CDMA systems. **IEEE Journal on Selected Areas in Communications**, v. 19, n. 8, p. 1614–1624, ago. 2001.

TEUNISSEN, P. J.; MONTENBRUCK, O. (Ed.). **Springer Handbook of Global Navigation Satellite Systems**. Cham: Springer International Publishing, 2017.

THOELERT, S. *et al.* GNSS Nominal Signal Distortions - Estimation, Validation and Impact on Receiver Performance. In: **Proceedings of the 28th International Technical Meeting of the Satellite Division of The Institute of Navigation (ION GNSS+ 2015)**. Tampa, Florida: [s.n.], 2015. p. 1902–1923.

TITUS, B. M. *et al.* Intersystem and Intrasystem Interference Analysis Methodology. In: **Proceedings of the 16th International Technical Meeting of the Satellite Division of The Institute of Navigation (ION GPS/GNSS 2003)**. Portland, OR: [s.n.], 2003. p. 2061–2069.

VAN DIERENDONCK, A. *et al.* A More Accurate Evaluation of GPS C/A Code Self-Interference Considering Critical Satellites. In: . Monterey, California: [s.n.], 2017. p. 671–680.

VAN DIERENDONCK, A. J. *et al.* Determination of C/A Code Self-Interference Using Cross-Correlation Simulations and Receiver Bench Tests. In: **Proceedings of the 15th International Technical Meeting of the Satellite Division of The Institute of Navigation (ION GPS 2002)**. Portland, OR: [s.n.], 2002. p. 630–642.

VAN DIERENDONCK, A. J. *et al.* Cross-Correlation of C/A Codes in GPS/WAAS Receivers. In: **Proceedings of the 12th International Technical Meeting of the Satellite Division of The Institute of Navigation (ION GPS 1999)**. Nashville, TN: [s.n.], 1999. p. 581–596.

VAN DIGGELEN, F. Who's Your Daddy? Why GPS Will Continue to Dominate Consumer GNSS. **Inside GNSS**, v. 9, n. 2, mar. 2014.

VAN DIGGELEN, F. Redoing GNSS from Scratch - The Perfect System. In: . St. Louis, Missouri: [s.n.], 2020. p. 3199–3209.

VAN DIGGELEN, F. S. T. **A-GPS: Assisted GPS, GNSS, and SBAS**. [S.l.]: Artech House, 2009.

VITERBI, A. **CDMA: Principles of spread spectrum communication**. [S.l.]: Addison-Wesley Publishing Company, 1995. (Addison-Wesley wireless communications series).

WALES, B.; TARAZONA, L.; BAVARO, M. Snapshot positioning for low-power miniaturised spaceborne GNSS receivers. In: **5th ESA Workshop on Satellite Navigation Technologies and European Workshop on GNSS Signals and Signal Processing (NAVITEC)**. Netherlands: IEEE, 2010.

WALLNER, S. **Galileo System and Signal Evolution**. International Technical Symposium on Navigation and Timing, Toulouse, France: [s.n.], 2017.

WALLNER, S. *et al.* Galileo E1 OS and GPS L1C Pseudo Random Noise Codes - Requirements, Generation, Optimization and Comparison. In: **Proceedings of the 20th International Technical Meeting of the Satellite Division of The Institute of Navigation (ION GNSS 2007)**. Fort Worth, TX: [s.n.], 2007. p. 1549 – 1563.

WALLNER, S. *et al.* Revised PRN Code Structures for Galileo E1 OS. In: **Proceedings of the 21st International Technical Meeting of the Satellite Division of The Institute of Navigation (ION GNSS 2008)**. Savannah, GA: [s.n.], 2008. p. 887 – 899.

WALLNER, S. *et al.* Novel Concepts on GNSS Signal Design serving Emerging GNSS User Categories: Quasi-Pilot Signal. In: **European Navigation Conference (ENC) 2020**. Dresden, Germany: DGON, 2020.

YAO, Z.; LU, M.; FENG, Z. Spreading code phase measurement technique for snapshot GNSS receiver. **IEEE Transactions on Consumer Electronics**, v. 56, n. 3, p. 1275–1282, ago. 2010.

YAO, Z.; LU, M.; FENG, Z. M. Quadrature multiplexed BOC modulation for interoperable GNSS signals. **Electronics Letters**, v. 46, n. 17, p. 1234 –1236, ago. 2010.

YAO, Z.; ZHANG, J.; LU, M. ACE-BOC: dual-frequency constant envelope multiplexing for satellite navigation. **IEEE Transactions on Aerospace and Electronic Systems**, v. 52, n. 1, p. 466–485, fev. 2016.

YOON, Y. C. A simple and accurate method of probability of bit error analysis for asynchronous band-limited DS-CDMA systems. **IEEE Transactions on Communications**, v. 50, n. 4, p. 656–663, abr. 2002.

YOSIDA, K. **Functional Analysis**. [S.l.]: Springer-Verlag Berlin Heidelberg, 1995. (Classics in Mathematics, 6th ed.). CitationKey: Yosida.

ZIEDAN, N. **GNSS receivers for weak signals**. Boston, Lodon: Artech House, 2006.